Univerzita Karlova
Přírodovědecká fakulta

Studijní program: Biologie
Studijní obor: Buněčná a Vývojová biologie – Fyziologie buňky

Bc. Ondřej Pácalt

Analýza strumpellinu, podjednotky WASH komplexu
Analysis of WASH complex member strumpellin

Diplomová práce

Školitel: RNDr. Lenka Libusová, PhD.

Praha, 2019

Prohlášení

Prohlašuji, že jsem závěrečnou práci zpracoval samostatně a že jsem uvedl všechny použité informační zdroje a literaturu. Tato práce ani její podstatná část nebyla předložena k získání jiného nebo stejného akademického titulu.

V Praze, 2. 1. 2019

_____

Ondřej Pácalt

Table of contents

Abstract

Actin polymerization facilitated by the Arp2/3 complex plays a critical role in a wide range of cellular processes such as motility, endocytosis and cargo recycling. Activation and appropriate localization of the Arp2/3 complex is mediated by an interaction with the nucleation-promoting factor (NPF). WASH complex is the major endosomal NPF which plays a crucial role in the cargo recycling back to the trans-Golgi network (TGN) or plasma membrane. It is composed of five subunits: WASH1, SWIP, FAM21, CCDC53 and strumpellin. While WASH1 and FAM21 have been extensively studied, much less is known about strumpellin, a protein causally implicated in the onset of hereditary spastic paraplegia (HSP). This work focuses on strumpellin function in the cells, showing that only full-length protein incorporates into the WASH complex. In a strumpellin knock out cell line, we demonstrated that loss of strumpellin resulted in destabilization of the other WASH complex subunits. Still, an incomplete WASH complex without strumpellin was assembled. Cells also displayed enlarged endosomal subdomains and WASH complex nucleation activity on endosomes was largely diminished as assessed by loss of the actin patches. Finally, the absence of strumpellin was also accompanied by the accumulation of glucose transporter 1 (GLUT1) and transferrin receptor (TfR) in the early endosomal compartment. Importantly, it remains to be uncovered whether the observed phenotypes resulted entirely from the strumpellin absence or they could be attributed to the overall reduction of the WASH complex.

Abstrakt

Polymerizace aktinu zprostředkovaná komplexem Arp2/3 je zásadní pro řadu buněčných procesů, jako je například pohyb, endocytóza či recyklace nákladu. Lokalizace a vazba komplexu Arp2/3 je závislá na tzv. faktorech zahajujících nukleaci (NPF). WASH komplex je hlavním NPF na membráně endozómů a hraje zde zásadní roli v recyklaci nákladu zpět do trans-Golgi (TGN) nebo na plasmatickou membránu. WASH komplex se skládá z pěti podjednotek: WASH1, SWIP, FAM21, CCDC53 a strumpellinu. V minulosti byly studovány především podjednotky WASH1 a FAM21. Naopak o strumpellinu není mnoho známo, a to i přesto, že souvisí se vznikem dědičné spastické paraplegie (HSP). Tato práce se zaměřuje na roli strumpellinu v buňce. Ukazuje, že pro úspěšné začlenění strumpellinu do WASH komplexu jsou potřeba všechny jeho části. Pomocí buněčné linie zbavené strumpellinu jsme dále ukázali, že ztráta strumpellinu vede k destabilizaci ostatních podjednotek WASH komplexu. To však nebrání sestavování částečného WASH komplexu v nepřítomnosti strumpellinu. Delece strumpellinu také vedla ke zvětšení endozomálních subdomén a ke snížení aktivity WASH komplexu, pozorovatelné jako úbytek aktinových teček. V buňkách zbavených strumpellinu navíc docházelo k akumulaci glukózového přenašeče 1 (GLUT1) a transferinového receptoru (TfR) v oblasti časných endozómů. Do budoucna je potřeba ověřit, zdali pozorované efekty jsou důsledkem pouhé ztráty strumpellinu, nebo celkového snížení množství WASH komplexu v buňkách.

1. Theoretical background

1.1. Vesicular trafficking

Vesicular trafficking is process securing essential events in every eukaryotic cell including a nutrition uptake, cell signalling, protein/membrane production/secretion/turnover. How does the vesicular trafficking facilitate all these events? The answer is based upon small membrane vesicles travelling from one destination to another carrying specific protein cargo between the membrane compartments of the cell. In more detail, cargo/receptor protein is recognised by the proteins called coat proteins, which induce membrane curvature and vesicle budding. Newly generated and loaded vesicle is cut off its maternal membrane with the dynamin GTPase and further transported by the interplay of molecular motor proteins and cytoskeletal tracks. Before reaching the appropriate destination, vesicle needs to be recognised. This is facilitated by the binding between specific tethering proteins on the vesicle and the destination membrane. This bond is further strengthened by the addition of specific soluble NSF attachment protein receptor (SNARE) proteins, which finally promotes fusion between the vesicle and the destination membrane [Jovic et al., 2010].

Vesicular trafficking is usually divided into two fundamental parts – the secretory pathway, facilitating protein modification and secretion, and the endocytic pathway, responsible for protein turnover, and recycling. Although both secretory and endocytic pathways are interesting and important, this work will further focus on the endocytic pathway.

1.1.1. Endocytic pathway

During endocytosis, various cargoes are enclosed into the small membrane vesicles and transported from the plasmatic membrane (PM) towards the interior of the cell. These vesicles then fuse with a sorting station of early endosome, where the decision about the fate of the incoming cargoes is made. There are three main pathways, which the cargo can undertake once it reaches the early endosome. The first one leads to the recycling of the cargo back to the plasmatic membrane. Alternatively, cargo is recycled to the trans-Golgi network (TGN), and in the last case, cargo proceeds forth through the endosomal pathway, ending with the degradation in the lysosome [Cullen, 2008].

1.1.2. Early endosome, sorting, and recycling

As mentioned above, there are numerous cargoes arriving to the early endosome, waiting for recycling back to the PM or the TGN. Protein sorting and recycling machinery plays a pivotal role in their subsequent transport. Nowadays the best-known sorting and recycling complex is retromer. Retromer

has two functionally different subcomplexes, a cargo-selective complex (CSC), composed of vacuolar protein sorting 26 (VPS26), VPS29 and VPS35, and a sorting nexin (SNX) heterodimer, comprised of proteins SNX 1 or 2 and 5 or 6. The Bin-Amphyphisin-Rvs (BAR) domain is critical for the function of SNX proteins, granting them an ability to bind and shape the membranes. This ability of the SNX heterodimer is needed for the formation of so-called membrane tubules - tubulovesicular structures emanating from the body of the early endosome. Those structures serve as a cargo sorting platform before the new vesicle buds away for recycling to the particular destination. Nevertheless, this platform is not responsible for cargo selection. Therefore the retromer CSC is needed. CSC binds to the membrane of the early endosome through the direct interaction with the Ras-associated in brain 7a (Rab7a) protein. Another anchor for CSC is a protein SNX3, which mediates a binding between the CSC and the membrane lipid phosphatidylinositol-3-phosphate through its phox homology (PX) domain. Importantly, CSC also binds directly to the SNX heterodimer and number of cargo proteins. This secures tight interplay between the creation and the loading of the membrane tubule platforms, often described as endosomal microdomains. To give an example of cargo the retromer recycles from the early endosome back to the TGN, a cation independent mannose-6-phosphate receptor (CIMPR) can be mention [Anitei et al., 2011; Seaman, 2012; Seaman et al., 2013].

Above described retromer could be thought of as a canonical retromer, which is proposed to recycle cargo from the early endosomes back to the TGN. Several papers have already shown that retromer also has a particular role in recycling of cargo back to the PM while binding additional proteins. Essential protein of this recycling pathway is SNX27, which serves as cargo adaptor for recycling of β2-adrenergic receptor (β2AR) and glucose transporter 1 (GLUT1) back to the PM [Temkin et al., 2011; Steinberg et al., 2013].
In reality, SNX heterodimer force to shape the membrane into the membrane tubules is not the only force which drives the tubule formation [Anitei et al., 2011]. It was shown that small actin patches on the membrane of early endosome are fundamental for the recycling of some cargoes [Puthenveedu et al., 2010]. Therefore, the cytoskeleton is needed not only for the motion of the whole vesicles but also for the proper sorting and recycling of the cargoes.

1.2. Actin cytoskeleton

Actin microfilaments are a very prominent part of the cytoskeleton in the matter of vesicular trafficking. They are made up of G-actin, small ATP/ADP binding globular protein, which possesses an ability to assemble into long actin fibres known as F-actin. Every single actin fibre is polarised, giving rise to two different ends, barbed and pointed, which both vary in their biochemical properties.

Those properties are closely related to the ability of actin to undergo cycles of assembly, elongation, and depolymerisation. The elongation occurs mostly at the barbed end of actin fibres. Compare to the elongation, the process of assembly is more energetically demanding. Successful *de novo* formation of the actin fibre needs to overcome the energetically unfavourable state of 3 actin monomers composed together. There are two possibilities how to bypass this point. The first one is the severing of the already existing filament/fibre and thus creating two barbed ends for the further elongation. Another option is the intervention of proteins that facilitate the formation of a nucleation seed for a new actin fibre. These proteins are called actin nucleators and will be discussed below [Pollard, 2016].

1.2.1. Actin nucleators

There are two types of actin nucleators. The first group comprises of the formins, whereas the second group contains only a single member - Actin-related protein 2/3 (Arp2/3) complex. While formins mainly facilitate the elongation and the nucleation of the straight actin fibres, which are widely present in the cytoplasm, the Arp2/3 complex is strictly responsible for the formation of more compact Y-branched actin network (**Figure 1**) on various locations throughout the cell. The Arp2/3 complex is a multiprotein complex which binds on the side of already assembled actin fibre and creates new actin nucleation seed under an angle of circa 70 degrees. This new seed leads to the establishment of new Y-branched actin filament. Such activity must be precisely regulated. Indeed, the Arp2/3 complex is intrinsically inactive until it binds one of the proteins classified as a nucleation-promoting factor (NPF; **Figure 1**). It is the variability between particular NPFs, which is responsible for the location-specific activation of Arp2/3 complex and subsequent generation of a Y-branched actin network at the proper place [Campellone et al., 2010; Anitei et al., 2011].

Figure 1 - Schematic mechanism of NPF class I dependent Arp2/3 complex activation. Adapted from [Campellone et al., 2010]

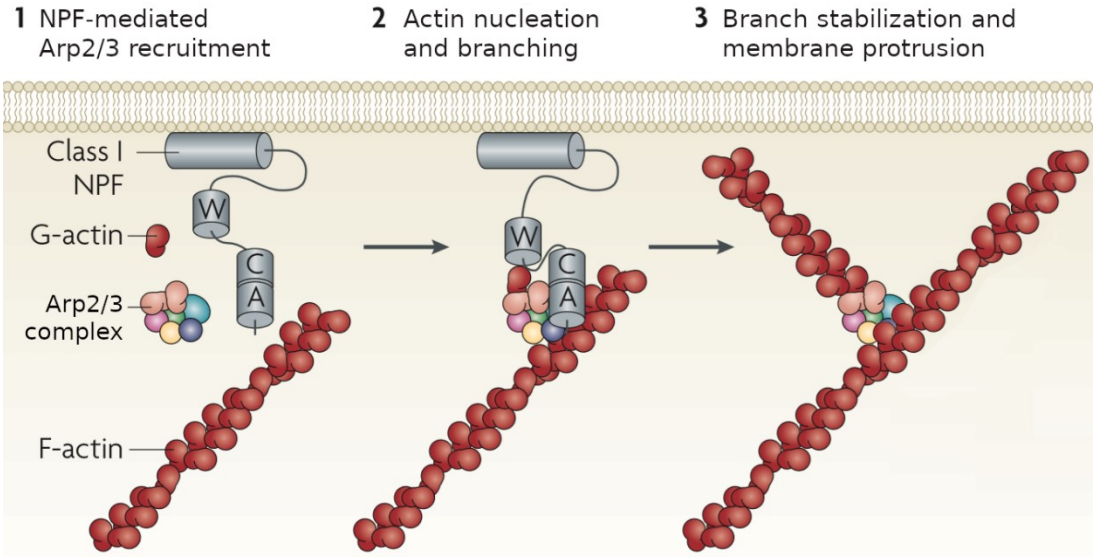

1.3. Nucleation promoting factors

NPFs are usually divided into the two groups – the NPF class I and II. In this work, the NPF class I will be discussed.

Different NPF I activate Arp2/3 complex at a different site in the cell. This is enabled by the general structure of NPFs, which encompasses some common domains for the Arp2/3 complex activation and unique domains for NPF targeting. Among the common domains, there is a proline-rich region and a WCA domain for the Arp2/3 complex activation itself. More precisely, the WCA domain consists from the Wiskott-Aldrich syndrome protein (WASP) homology domain 2 (W) for monomer actin binding and connector (C) and acidic (A) regions facilitating recognition and binding of the Arp2/3 complex [Campellone et al., 2010; Insall et al., 2010].

Nowadays, 5 NPFs of the class I are known to be present in mammalian cells (**Figure 2**). The WASP, WASP family Verprolin-homologous protein (WAVE), WASP homolog associated with actin, membranes, and microtubules (WHAMM), junction-mediating and regulatory protein (JMY) and finally WASP and Scar homolog (WASH). Every single NPF, as far as we know, has its own discreet function in the cell (**Figure 2**). In brief, WASP is responsible for the early steps of endocytosis. WAVE is needed for pseudopodia and lamellipodia formation. JMY operates as a regulator of gene expression, WHAMM act as an Arp2/3 complex activator in the secretory pathway and finally, WASH is vital for the proper recycling of cargoes from the endocytic pathway [Campellone et al., 2010; Rottner et al., 2010; Alekhina et al., 2017].

Figure 2 – Overview of events known to be driven by the NPF class I dependent activation of the Arp2/3 complex and subsequent actin polymerization on the various intracellular locations. Adapted from [Campellone et al., 2010].

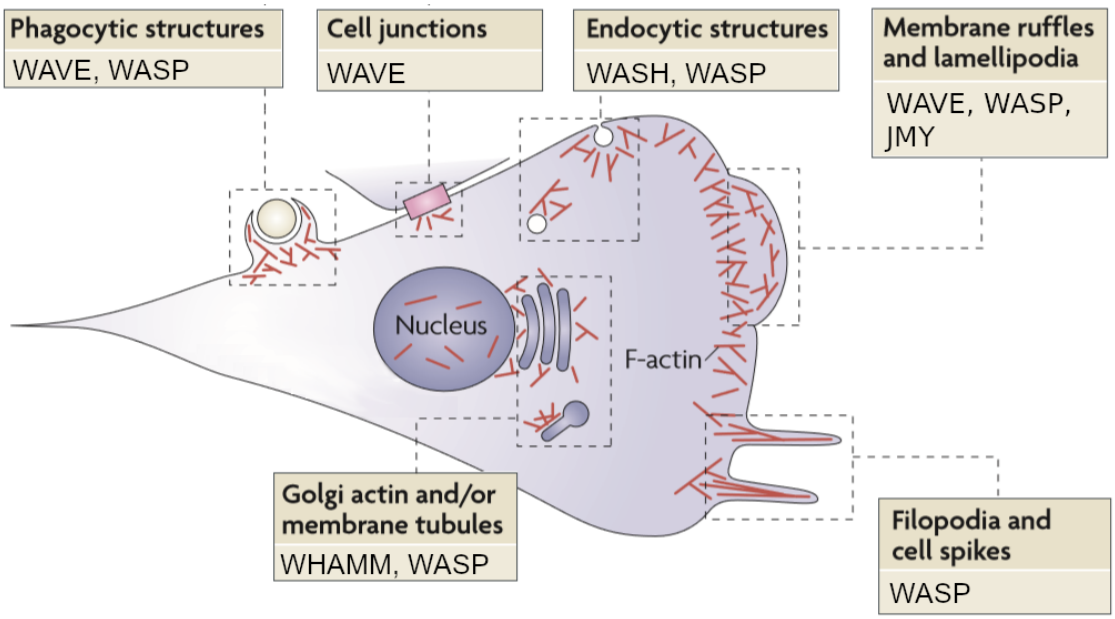

This work is further focused mainly on endosomal transport, sorting and recycling, as it is the place of the WASH complex action.

1.4. WASH complex

Initially, only WASH1 subunit was discovered as a gene located in the sub-telomeric region of the human genome in 2007 [Linardopoulou et al., 2007]. Two years later, the rest of the WASH complex was identified (**Figure 3**) [Derivery et al., 2009; Gomez et al., 2009]. WASH complex is composed of 5 subunits – WASH1, a family with sequence similarity 21 protein (FAM21), strumpellin, strumpellin and WASH1 interacting protein (SWIP) and finally coiled-coil domain containing protein 53 (CCDC53)[Derivery et al., 2009; Jia et al., 2010].

Figure 3 – Schematic representation of the pentameric WASH complex, which depicts particular subunits and bonds between them. Adapted from [Jia et al., 2010].

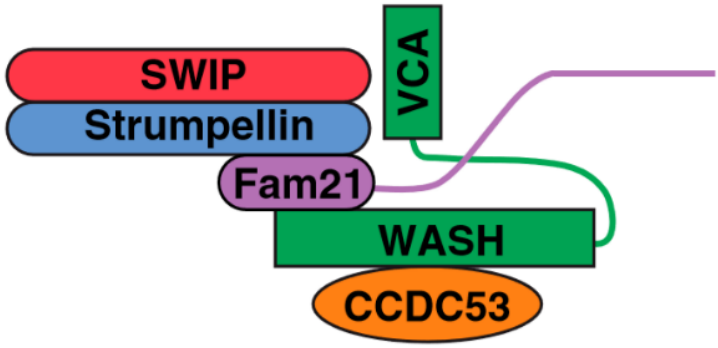

WASH complex is an ancient protein complex, well conserved across eukaryotic phyla, present in vertebrates, *D. melanogaster*, *C. elegans* or *D. discoideum*, but missing in others, e. g. yeasts. Insall et al. showed that if one subunit of the WASH complex is present in the organism, others are also there/nearby with few exceptions. In *C. elegans*, FAM21 subunit was not detected, and in marine phytoplankton *Thalassiosira,* the only subunit absent is WASH1 itself [Derivery et al., 2010; Insall et al., 2010]. The strikingly different situation is within the plant kingdom. Some plants have intact WASH complex (*Ostreococcus)*, some have only a few subunits of the WASH complex (*Sorghum),* and some does not have WASH complex at all (*Arabidopsis)* [Insall et al., 2010].

Each subunit of the WASH complex plays a crucial role in its stability [Derivery et al., 2009; Jia et al., 2010]. It was proposed that the WASH complex has a stable core, created from its subunits - FAM21, SWIP, strumpellin, and CCDC53, called WASH regulatory complex (SHRC) [Jia et al., 2010]. From the beginning, it was known that WASH1 alone is very potent and intrinsically

active NPF [Linardopoulou et al., 2007; Derivery et al., 2009; Duleh et al., 2010]. Later, it was shown that SHRC inhibits WASH1 ability to activate the Arp2/3 complex [Jia et al., 2010]. This finding was followed by the paper presenting WASH complex mediated activation of the Arp2/3 complex dependent on WASH1 lysin 220 K63-ubiquitination by the E3 RING (really interesting new gene) ubiquitin ligase complex MAGE-L2-TRIM27 (melanoma antigen family l2; tripartite motif containing 27) [Hao et al., 2013]. Interestingly, the WASH complex interacts, through the FAM21 subunit, with the heterodimer of the capping protein Z band α and β (CapZ α/β) [Derivery et al., 2009; Jia et al., 2010]. The CapZ α/β heterodimer is known to regulate actin cytoskeleton but in the opposite manner as do the NPFs. It binds to the free barbed end of the actin fibre and suppresses its further elongation [Pollard, 2016]. The WASH complex promotes Y-branched actin network assembly, but also attract the negative regulator of this process the CapZ α/β heterodimer.

In 2009 two independent groups declared WASH complex as a major early endosomal NPF [Derivery et al., 2009; Gomez et al., 2009]. Shortly after that, a lot of new articles describing the interaction between the WASH complex and the recycling complex retromer appeared [Harbour et al., 2010, 2012; Jia et al., 2012]. This, together with the already mentioned need for the actin patches in cargo recycling [Puthenveedu et al., 2010], established the WASH complex as a part of the recycling machinery (**Figure 4**). Based on knockdown (KD) experiment evidence, WASH complex was proposed to contribute to the scission of the membrane tubule intermediates [Derivery et al., 2009; Gomez et al., 2009; Harbour et al., 2010]. However, in further studies, the different phenotype was observed in knockout (KO) cells. No excessive tubular structures were present in the WASH1 KO cells, but rather enlarged early endosomal and lysosomal compartments clustered in the perinuclear region [Gomez et al., 2012]. At first sight, phenotypes are contradictory, but in more detail, it seems that the WASH complex is needed not only for the resolution of membrane tubule intermediates but also for their formation. In line with this claim, KD and KO of WASH complex subunits lead to the disruption of cargoes recycling. Therefore, the WASH complex is proposed to contribute to the recycling of many cargoes for example CIMPR to the TGN [Gomez et al., 2009] and GLUT1 [Piotrowski et al., 2013], transferrin receptor (TfR) [Derivery et al., 2009], α5β1 integrin [Zech et al., 2011] or β2AR [Puthenveedu et al., 2010; Temkin et al., 2011] to the PM. The WASH complex also interacts with the BLOC1 complex and together participate in the recycling of ATPase 7A (ATP7A) and vesicle-associated membrane protein 7 (VAMP7) [Ryder et al., 2013]. Importantly, there is not complete consensus, whether all of the cargoes mentioned above, namely TfR and GLUT1, are dependent with their recycling on the WASH complex [Duleh et al., 2010; Steinberg et al., 2013; McGough et al., 2014].

Figure 4 – WASH complex driven activation of Arp2/3 complex leads to the actin polymerization and formation of membrane tubules, tubular structures used for cargo sorting. WASH complex is proposed to contribute on the recycling of cargoes from the early endosome to the TGN as CIMPR or to the PM as β2AR. Adapted from [Seaman et al., 2013].

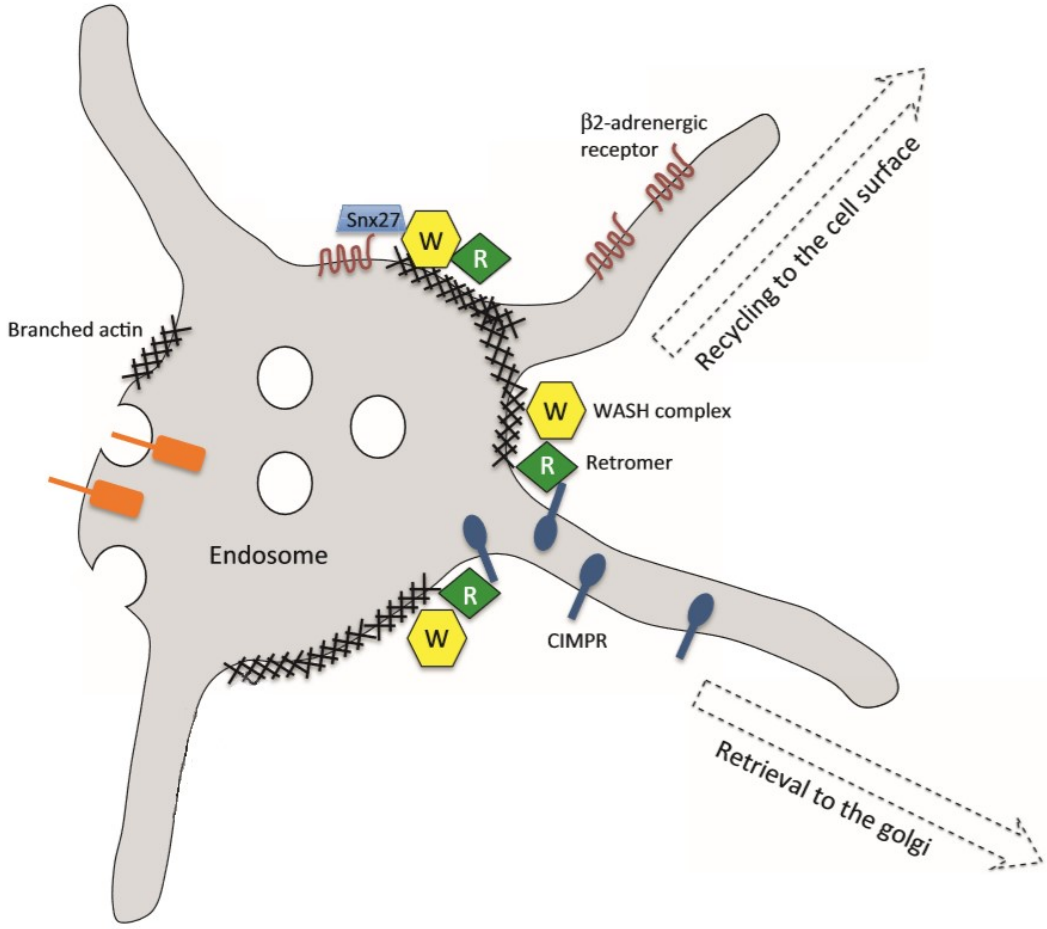

In the *D. discoideum*, the WASH complex is responsible for the retrieval of V-ATPase from the lysosomal compartment [Carnell et al., 2011; Song et al., 2018]. This phenotype was also observed in the subset of immune cells in *D. melanogaster* [Nagel et al., 2017]. Moreover, perturbation of the WASH complex leads to the defective delivery of the hydrolases from the post-lysosomal compartments back to the late endosomes/lysosomes and phagosomes, resulting in the inability to efficiently digest proteins and lipids [King et al., 2013].

Interestingly, many cargoes are dependent on the interaction between the WASH complex subunit FAM21 and retromer subunit VPS35 (**Figure 5**) [Zavodszky et al., 2014]. This observation, together with the substantial dissociation of WASH complex from the membrane of the early endosome after overexpression of FAM21, contributed to the prevailing opinion that retromer alone is required for the WASH complex binding to the membrane of the early endosome [Harbour et al., 2012;

Jia et al., 2012; Helfer et al., 2013]. Nevertheless, the purified recombinant WASH complex was able to bind artificially generated vesicles in vitro [Derivery et al., 2009] and knockout of FAM21 in *D. discoideum* did not alter the vesicle localisation of SWIP, strumpellin or WASH1 [Park et al., 2013]. Moreover, McNally et al. saw membrane-bounded FAM21 upon VPS35 KO in HeLa cells [McNally et al., 2017]. All this indicates that there could be another protein, which is involved in the WASH complex membrane anchorage.

Figure 5 – WASH complex is recruited to the endosomal membrane via FAM21-VPS35 interaction. Together facilitate membrane tubule formation, sorting of cargoes and its subsequent recycling. Adapted from [Seaman et al., 2013].

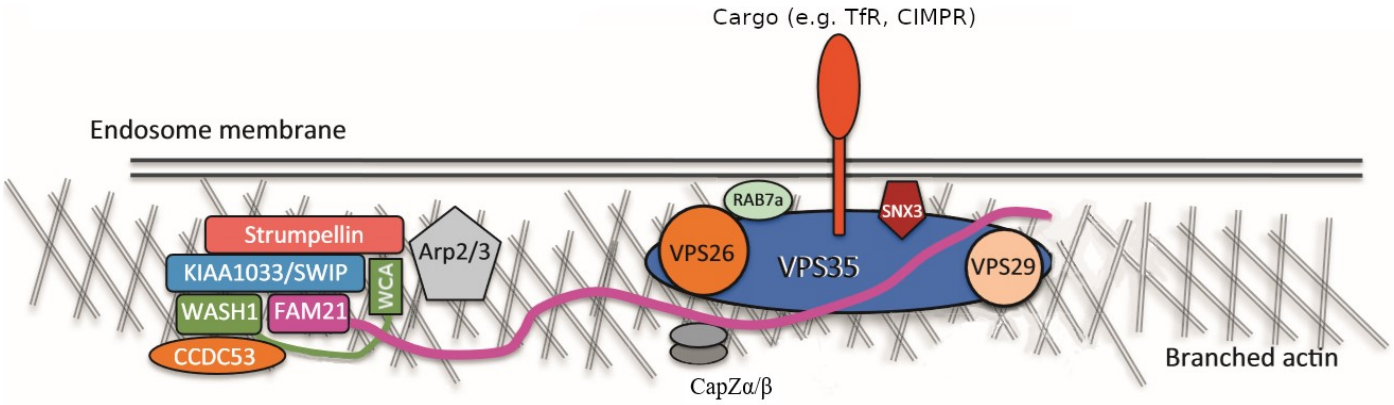

Besides the retromer, WASH complex interacts through FAM21 subunit with other recycling machinery - the CCC complex composed of the coiled-coil domain containing protein 22 (CCDC22), CCDC93 and copper metabolism MURR1 domain-containing 1 protein (COMMD1). It was proposed that both the CCC complex and the WASH complex, are together responsible for the recycling of ATP7A and low-density lipoprotein receptor (LDLR) [Phillips-Krawczak et al., 2015; Bartuzi et al., 2016]. CCC complex further facilitates connection of the WASH complex to the recently described retriever complex, which together with SNX17 cargo adaptor, mediate recycling of retromer independent cargoes as α5β1 [McNally et al., 2017].

1.4.1. WASH1

WASH1 protein is composed of 465 aa and has a well-defined domain structure. The C-terminal part of the protein shares common motifs with other NPFs as Proline-rich region (303-330) and WCA domain (349-465), already described above. The N-terminal part of the WASH1 protein is unlike the C-terminal part unique and has two distinguishable domains – WASH homology domain 1 (WAHD1) and WAHD2 (lately renamed to the tubulin-binding region – TBR, to avoid confusion). It was

proposed that part of WAHD1 domain facilitates binding of the WASH1 to the WASH complex [Jia et al., 2010] and therefore to the endosomal membrane. Interestingly, recombinant WASH1 possess an ability to bundle actin and microtubule fibres in vitro [Liu et al., 2009], which is in line with the ability of TBR domain to bind tubulin dimers [Gomez et al., 2009]. Thus, the N-terminal part of WASH1 makes from the WASH complex interesting actin regulator at the crossroad of two major cytoskeletal components and the vesicular trafficking.

Often, NPF of class I has an upstream regulator as for example WAVE complex is regulated by small Ras-related C3 botulinum toxin substrate 1 (Rac1) GTPase [Eden et al., 2002]. In *D. melanogaster* WASH1 was proposed to genetically interact with Ras homolog family member A (RhoA) GTPase [Liu et al., 2009]. Subsequent GST-pulldown of *D. melanogaster's* RhoA was genuinely able to detect an interaction between WASH1 and RhoA, but this bond was not observed in the mammalian cell lysates [Liu et al., 2009; Jia et al., 2010]. Therefore, an upstream regulator of the mammalian WASH complex is still not known. The difference between the results from mammalian cells and *D. melanogaster* could be easily caused by the relatively mild evolutionary conservation of WASH1 between those organisms [Derivery et al., 2010].

1.4.2. FAM21

FAM21 is the best-described subunit of the WASH complex. FAM21 is a 1341 aa large protein, structurally divided into two parts. The first part, the N-terminal part of FAM21, spanning from the aa 1 to 220 is mainly of globular character and facilitate incorporation of FAM21 to the WASH complex [Gomez et al., 2009; Jia et al., 2010; Harbour et al., 2012]. The second part, the C-terminal part of FAM21, spanning from the aa 220 to 1341 has no recognisable domain and is usually described as an unstructured "tail" of FAM21. This part is specific with the presence of 21 repeating $LF(D/E)_{3\text{-}10}LF$ amino acid motifs, so-called LF motifs.

It was shown that those motifs are crucial for the binding of the WASH complex to the retromer subunit CSC/VPS35. This interaction is important for WASH complex binding to the early endosome [Harbour et al., 2010; Jia et al., 2012]. Interestingly, it was shown, that VPS35 D620N mutation associated with the onset of Parkinson´s disease (PD) leads to the impaired bond between FAM21 and VPS35, further disrupting cargo recycling from early endosome. Such cargo is, for example, autophagy-related protein 9A (ATG9A), which is needed for early steps in autophagy pathway [McGough et al., 2014; Zavodszky et al., 2014]. Therefore, D620N mutation is responsible for the impairment of autophagy which is tightly connected to the inability to digest aberrant proteins, resulting in the formation of cytotoxic, undigested protein aggregates, typical for PD [Zavodszky et al., 2014].

Besides the FAM21-VPS35 link, there is a lot of other proteins which interacts with the WASH complex through the FAM21 tail domain (CapZ α/β [Jia et al., 2010], CCDC22 and 93 [Phillips-Krawczak et al., 2015], protein required for receptor-mediated endocytosis 8 (RME-8) [Freeman et al., 2014] and WASP and FKBP like protein (WAFL) [Harbour et al., 2012]). Therefore, FAM21 serves as a main interaction platform of the WASH complex.

In *D. discoideum*, it was shown that FAM21 together with CapZα/β heterodimer stands behind the WASH complex recirculation from post-lysosomal compartment before the exocytic vesicle is formed, which release the WASH complex for the further use [Park et al., 2013]. One paper also described a nuclear role for FAM21. They demonstrated that FAM21 has nuclear localisation signal as well as a nuclear export signal within its sequence and interacts with the protein p50 and p65, components of the NF-κB (nuclear factor kappa-light-chain-enhancer of activated B cells) signalling. Therefore, it is possible that FAM21 tune NF-κB dependent gene transcription [Deng et al., 2015].

1.4.3. SWIP

SWIP is probably the worst characterised protein of the WASH complex. SWIP has about 1172 aa in length and no recognisable domain. According to in silico analysis, SWIP is predicted to be mainly helical [Humhalova, 2017]. SWIP is able to directly bind FAM21, WASH1 and strumpellin [Jia et al., 2010; Harbour et al., 2012]. The whole SWIP is needed for the proper incorporation to the WASH complex, albeit region spanning from the aa 704 to the end possess an ability to bind strumpellin exclusively [Jia et al., 2010]. Additionally, Freeman and colleagues were not able to efficiently immunoprecipitate other members of the WASH complex bonded together upon SWIP KD. Above mentioned imply, that SWIP is more integral for the WASH complex assembly than for example strumpellin [Freeman et al., 2014]. Importantly, point mutation P1019X in SWIP leads to the autosomal recessive intellectual disability (ARID) [Ropers et al., 2011]. Cells harbouring this mutation has substantially lowered amounts of the strumpellin and the WASH1 [Ropers et al., 2011], indicating, that single mutation in the SWIP can destabilise the whole complex and result in a severe defect in the organism. In the *D. discoideum*, Park et al. revealed, that SWIP KO, in contrast with KO of other WASH complex subunits, led to the substantial loss of strumpellin and WASH1 from the endosomal membrane [Park et al., 2013].

1.4.4. CCDC53

CCDC53 is protein about 194 aa in length and probably the most elusive subunit of the WASH complex. CCDC53 is needed for stability of the WASH complex [Derivery et al., 2009; Jia et al., 2010] but its evolutionary conservation substantially decreases with the increasing distance from the

Mus musculus homolog, much faster than for other subunits of the WASH complex [Derivery et al., 2010]. An essential part of CCDC53 for the binding to the WASH complex is a helical part spanning from the aa 24 to 72 [Jia et al., 2010]. Recently it was shown that CCDC53 and its interaction partner heat shock factor binding protein 1 (HSBP1) is responsible for the assembly of the WASH complex at the centrosome [Visweshwaran et al., 2018].

1.4.5. Strumpellin

Strumpellin is protein about 1159 aa in length. It has no recognizable domains except for spectrin-like domain repeat spanning from the aa 241 to aa 791, which is often associated with binding to the cytoskeleton [Valdmanis et al., 2007; Clemen et al., 2010]. Almost the whole protein is predicted to be helical [Harbour et al., 2010]. With the set of initial immunoprecipitation experiments, Jia et al. couldn't identify any other part of the strumpellin than full-length strumpellin which facilitate binding to the WASH complex. This binding is most probably promoted by the N-terminal part of SWIP [Jia et al., 2010].

Evolutionary conservation of strumpellin is extensive. In fact, strumpellin is very well conserved subunits of the WASH complex across phyla [Derivery et al., 2010]. Strumpellin is present in all organism which possesses other WASH complex subunits [Derivery et al., 2010; Insall et al., 2010].

1.4.5.1. Cellular effect of strumpellin deprivation

Strumpellin KO was shown to affect substantially other WASH complex subunits levels in the cell as well as the structure of the early endosomal compartment, which is enlarged and clustered in the perinuclear region as in the case of the WASH1 KO [Tyrrell et al., 2016]. Interestingly, residual truncated WASH complex still localises on the early endosomes in strumpellin KO cells [Park et al., 2013; Tyrrell et al., 2016]. Tyrrell et al. further shows, that deletion of strumpellin does not affect the migration of melanocytes as does the WASH1 KD in the A2780 cells. Additionally, strumpellin KO had only a mild effect on actin accumulation on the early endosomes [Tyrrell et al., 2016]. Thus, Tyrrell et al. speculate that the residual WASH complex in the absence of strumpellin is impaired but possibly still active and able to traffic cargo needed for the cell motility as α5β1 integrin [Zech et al., 2011; Tyrrell et al., 2016]. Discovery of the WASH complex without strumpellin in the wt and strumpellin KO melanocyte cell line with the blue native electrophoresis gave arising to additional questions [Tyrrell et al., 2016]. There are two possible explanations: the existence of two WASH complexes in the cell, one with and one without strumpellin or weaker association of strumpellin with the WASH complex during the blue-native polyacrylamide gel

electrophoresis (PAGE) procedure [Tyrrell et al., 2016]. It looks like the strumpellin is more weakly associated with the WASH complex than for example SWIP or FAM21. Importance of the strumpellin is further underlined by the embryonic lethality of the mice deprived of it. More on, lethality took place in very early embryonic stages, as no signs of terminated development were present in the uteri [Jahic et al., 2015].

1.4.5.2. Strumpellin is associated with diseases

In 2007, Valdmanis et al. showed, that there is a direct link between hereditary spastic paraplegia (HSP) and particular point mutations in the SPG8 (spastic paraplegia gene 8) locus, specifically in the strumpellin gene itself [Valdmanis et al., 2007]. HSP is a human disease known for the degeneration of long corticospinal neurons, more precisely, their axons [Salinas et al., 2008; Blackstone et al., 2011]. Freeman et al. speculate, that such a long axon has special and much bigger demand on proper vesicular traffic, including protein sorting and recycling and even a small disturbance of this system, leads to its disruption after a modest period of time (20-30 years)[Freeman et al., 2013]. Until this day, 11 point mutations are known in the strumpellin that leads, each alone, to the onset of the HSP. Those mutations are E83K [Song et al., 2018; secondary citation], I226T [Bettencourt et al., 2013], N471D [Valdmanis et al., 2007], R583S [Ishiura et al., 2014], S591P [Wang et al., 2014], L619F [Valdmanis et al., 2007], V620A [Jahic et al., 2014], V626F [Valdmanis et al., 2007], G696A [De Bot et al., 2013] E713K [Ichinose et al., 2016], R1035C [Neveling et al., 2013]. It is of the major interest that 3 of those mutations are in the predicted helix spanning from aa 608 to 628 and 7 of the mutations are somehow in the middle region of the protein. Interestingly, Valdmanis et al. presented, that depletion of strumpellin during the *D. rerio* development leads to the curly-tail phenotype, which is rescued by the intact human strumpellin, but not the mutated one [Valdmanis et al., 2007]. Nevertheless, it is not clear, what causes the HSP onset in human patients. It was shown that mutations N471D, L619F, and V626F have no deleterious effect on the stability nor the localisation of the WASH complex upon expression in wild-type cells [Jia et al., 2010; Freeman et al., 2013]. Recently in *D. discoideum* Song et al. were able to observe a clear defect in the exocytosis of post-lysosomes upon re-expression of N471D strumpellin in KO cells [Song et al., 2018]. Importantly post-lysosomes were already neutralised, if strumpellin N471D was present and thus the defect occurred upstream of previously described inability to neutralise lysosome prior exocytosis upon WASH1 KO in *D. discoideum* [Carnell et al., 2011; Song et al., 2018]. Interestingly, mutation N471D also resulted in the loss of 43 previously unknown interactions [Song et al., 2018]. Therefore, undescribed strumpellin function/interaction most probably play an essential role in the phenotype mentioned above.

Unfortunately, results were acquired using *D. discoideum*, which is evolutionarily distant from a human. Further verification of those results in mammalian cells is needed.
It was shown, that mammalian strumpellin interacts with another two proteins, spartin and valosin-containing protein (VCP) which are implicated in the HSP onset if they are mutated [Clemen et al., 2010; De Bot et al., 2012; Zhao et al., 2015]. Thus, there are at least three proteins in close proximity connected to this pathology. Still, we could only speculate about the functional link which connects all of the mentioned candidates with the HSP.
Furthermore, there is another pathology associated with mutated strumpellin. 3-point mutations, c.3335+2T>A, c.3335+4C>A, c.3335+8A>G, were identified as a cause of Ritscher–Schinzel/3C syndrome. These mutations lead to the skipping of the exon 27 and the eightfold decrease in the strumpellin mRNA levels resulting in the 60% decrease in the protein level [Elliott et al., 2013].

Strumpellin role in the cell is elusive. It is one of the five subunits of the WASH complex, but its role in it is almost unknown. KO of strumpellin was proved to be embryonically lethal in mice and two pathologies, HSP and 3C syndrome, are associated with particular point mutations in strumpellin. All this indicates, that strumpellin is an important protein for the cell and development of the organism. Moreover, the effect of strumpellin deprivation from the cell was not studied much. Thus, I have decided to take an interest in the role of strumpellin in the cell.

2. Goals

WASH complex plays a crucial role at the crossroad of the cargo recycling and vesicle formation. The role of FAM21 or WASH1 subunits of the WASH complex in this process has been studied in detail. On the other hand, strumpellin has been largely neglected despite the fact that its mutations lead to the HSP or 3C syndrome in humans. To characterise the role of strumpellin within the WASH complex and its impact on endosomal recycling, I have decided to:

1. Establish strumpellin KO cell line
2. Produce truncated fragments of strumpellin and analyse their subcellular localisation
3. Analyse the role/function of incomplete WASH complex in strumpellin KO cell line

3. Reagents

3.1. Solutions and buffers

Lysogeny broth (LB)

- Bacto™ Trypton (Becton, Dickinson and Company, France): 10 g
- Yeast extract BioChemica (AppliChem, Germany): 5 g
- NaCl (Penta, Czech Republic): 10 g
- ddH_2O to 1 L

Mammalian cell growth medium (DMEM++)

- Dulbecco's Modified Eagle Medium (DMEM) with GlutaMAX-I, 4.5 g/L, D-glucose and pyruvate (Gibco, USA)
- 10% fetal bovine serum (Gibco, USA), inactivated for 45 min in 50 °C and filtered through 0.2 μm filter (TPP, Switzerland)
- 1% penicillin/streptomycin 100x solution (Biowest, USA)

Running buffer SDS PAGE

- 25 mM Tris base (Sigma-Aldrich, USA)
- 192 mM glycine (Lach-Ner, Czech Republic)
- 0.1% sodium dodecyl sulfate (SDS; Sigma-Aldrich, USA)

4x Laemmli buffer

- 62.2 mM Tris base (Sigma-Aldrich, USA)
- 2% SDS (w/v; SDS; Sigma-Aldrich, USA)
- 10% glycerol (v/v; Penta, Czech Republic)
- 5% mercaptoethanol (v/v; SERVA, Germany)
- traces of bromphenol blue (SERVA, Germany)

1x Phosphate buffer saline (PBS)

- 137 mM NaCl (Penta, Czech Republic)
- 2.7 mM KCl (Lachema, Czech Republic)
- 10 mM Na_2HPO_4 (Lachema, Czech Republic)
- 1.8 mM KH_2PO_4 (Sigma-Aldrich, USA)

pH adjusted to 7.4, autoclaved

Tris-acetate EDTA (TAE) buffer

- 40 mM Tris base (Sigma-Aldrich, USA)
- 20 mM CH_3COOH (Penta, Czech Republic)
- 1 mM ethylenediaminetetraacetic acid (EDTA; Lach-Ner, Czech Republic)

Tris-buffer saline Tween 20 (TBST) buffer

- 10 mM Tris-HCl (Carl Roth, Germany)
- 150 mM NaCl (Penta, Czech Republic)
- 0.05% Tween 20 (SERVA, Germany)

pH adjusted to 7.4

Blocking buffer

- 3% Skim milk (Becton, Dickinson and Company, France) in 1x TBST (w/v)

Blotting buffer

- 25 mM TRIS base (Sigma-Aldrich, USA)
- 192 mM glycine (Lach-Ner, Czech Republic)
- 20% methanol (v/v; Penta, Czech Republic)

10x PFU buffer

- 200 mM Tris-HCl (Carl Roth, Germany)
- 100 mM KCl (Lachema, Czech Republic)
- 100 mM $(NH_4)_2SO_4$ (Sigma-Aldrich, USA)
- 20 mM $MgSO_4$ (Sigma-Aldrich, USA)
- 1% Triton X-100 (Sigma-Aldrich, USA)
- 1mg/mL bovine serum albumin (BSA; Sigma-Aldrich, USA)

pH adjusted to 8.8 (25°C)

2xHEPES buffer

- 50 mM HEPES (Sigma-Aldrich, USA)
- 280 mM NaCl (Penta, Czech Republic)
- 1.5 mM Na_2HPO_4 (Lachema, Czech Republic)

pH adjusted to 7.01-7.04, filtered

Mowiol

- 2.4 g Mowiol ($m_w \sim 31\,000$; Sigma-Aldrich, USA)
- 6 ml ddH_2O
- 12 ml of 0.2M Tris (pH 8.5)
- traces of NaN_3 (0.02%) (Sigma-Aldrich, USA)

3.2. Antibodies and fluorescent probes

Table 1: Primary antibodies

Specificity	Type	Species	Company	Cat. No.	WB dilution	IMF dilution
strumpellin	polyclonal	rabbit	Abcam	ab101222	1:1000	1:400
SWIP	polyclonal	rabbit	Bethyl Lab., Inc.	A304-919-A-M	1:1000	1:1000
FAM21	polyclonal	rabbit	Santa Cruz	sc-137995	1:1000	1:200
WASH1	polyclonal	rabbit	Atlas	HPA002689	1:1000	-
VPS35	polyclonal	goat	Abcam	ab10099	1:1000	1:200
EEA1	monoclonal	rabbit	Cell signalling	3288	-	1:800
Rab11	polyclonal	rabbit	Cell signalling	2413	-	1:150
LAMP1	monoclonal	rabbit	Cell signalling	9091	-	1:300
Glut1	monoclonal	rabbit	Abcam	ab115730	-	1:400
TfR	polyclonal	mouse	Gift Horejsi	-	-	1:100
myc	monoclonal	mouse	Exbio	11-433-C100	1:1000	1:1000
flag	monoclonal	mouse	Sigma	F1804	1:1000	1:1000
ARP2	monoclonal	mouse	Sigma, Gift Schwarzerova	A6104	-	1:10

Table 2: Secondary antibodies

Specificity	Species	Conjugated probe	Company	Cat. No.	Dilution
mouse	goat	horseradish peroxidase	Jackson Immunoresearch	115-035-146	1:10 000
rabbit	goat	horseradish peroxidase	Jackson Immunoresearch	111-035-045	1:10 000
goat	bovine	horseradish peroxidase	Jackson Immunoresearch	805-035-180	1:10 000
rabbit	donkey	Cy5	Jackson Immunoresearch	711-175-152	1:500
mouse	donkey	DyLight488	Jackson Immunoresearch	715-485-150	1:500
mouse	goat	Alexa488	ThermoFisher Scientific	A11001	1:500
goat	donkey	Cy5	Jackson ImmunoResearch	705-175-147	1:500
goat	donkey	Alexa594	Jackson ImmunoResearch	A11058	1:500

Table 3: Fluorescent probes

Name	Conjugated stain	Company	Cat. No.	Dilution
Phalloidin	Alexa488	Invitrogen	A12379	1:100
Phalloidin	Alexa594	Invitrogen	A12381	1:100

4. Methods

4.1. Polymerase chain reaction

Polymerase chain reaction (PCR) was done according to the following protocol (**Table 4** and **5**).

Table 4: PCR reaction mixture

Reagents	Volume
ddH2O	15.25 µL
10x PFU buffer	2.00 µL
Primer F	0.50 µL
Primer R	0.50 µL
dNTPs	0.50 µL
PFU pol	0.25 µL
Template	1.00 µL
Total volume	20.00 µL

Table 5: PCR thermocycler program for amplification of strumpellin fragments

	Str_F/NM/MC/M		Str_N/C	
Step	**Duration**	**Loop**	**Duration**	**Loop**
Initial denaturation	2 min	1x	2 min	1x
Denaturation	40 s	30x	40 s	30x
Annealing	40 s		40 s	
Elongation	3.5 min		1 min	
Final elongation	5 min	1x	5 min	1x

4.2. Molecular cloning

4.2.1. Restriction cloning

Firstly, specific primers with flanking ends for the cloning of the human strumpellin gene (GenBank: BC026951.1) and its fragments into the plasmid pcDNA4-myc/his-TO (myc) and pTripleFLAG (flag) were designed. Altogether, it was necessary to design 12 different primers (**Table 6**).

PCR from the HeLa cells cDNA was done using pairs of the degenerated primers (**Table 6**). Obtained DNA was separated and cleared on 1% agarose 1x TAE gel electrophoresis and gel-extracted with Gel/PCR DNA Fragments Extraction Kit (Geneaid, USA). Next, the amount of isolated DNA was measured, and up to 2 µg were used for the restriction enzyme digest reaction. Appropriate restriction enzymes and buffers were used according to **Table 6** and manufacturer instructions (Thermo Fisher Scientific, USA) for the strumpellin fragments as well as for the plasmid's backbones.

Table 6: Primers used for restriction cloning

Primer name	Sequence	Restriction enzyme	Generated fragment	Cloned vector
Strump_F_KpnI	tcaggtaccatgttggactttctagccgag	KpnI	F/NM/N	Str_F/NM/N_myc
Strump_R_Spe	gcaactagtcagcactgttctgaactcatc	SpeI	F/MC/C	Str_F/MC/C_myc
hStrumpellin-C_F	ttgagctcgattctaaacatctggcagc	SacI	C	Str_C_flag
hStrumpellin-C_R	ttgggcccttacagcactgttctgaactcatc	ApaI	F/MC/C	Str_F/MC/C_flag
hStrumpellin-M_F	ttgagctctatcctttgccggagcatc	SacI	MC/M	Str_MC/M_flag
hStrumpellin-M_R	ttgggcccttaaaaccgacaagaataatttaat	ApaI	NM/M	Str_NM/M_flag
hStrumpellin-N_F	ttgagctcttggactttctagccgagaac	SacI	F/NM/N	Str_F/NM/N_flag
hStrumpellin-N_R	tggggcccttacgctgagacctggttgtaaatatc	ApaI	N	Str_N_flag
hStrumpellinC_F2	cgaggtaccatggattctaaacatctggcagc	SpeI	C	Str_C_myc
hStrumpellinM_F2	ttcggtaccatgtatcctttgccggagcatc	KpnI	NM/M	Str_NM/M_myc
hStrumpellinM_R2	gcactagtaaaccgacaagaataatttaat	SpeI	MC/M	Str_MC/M_myc
hStrumpellinN_R2	taactagtcgctgagacctggttgtaaatatc	KpnI	N	Str_N_myc

Digested DNA was cleared with 1% 1xTAE gel electrophoresis. Bands of the correct size were excised and DNA within was extracted with High-Speed Plasmid Mini Kit (Geneaid, USA). Amount of the isolated DNA was measured on the NanoDrop ND-1000 (Thermo Fisher Scientific, USA) and ligation reaction with T4 DNA ligase (Thermo Fisher Scientific, USA) was set according to **Table 7**.

Table 7: The digest reaction mixture

Reagents	Amount
Digested backbone DNA	1.00 µg
Digested fragment DNA	3.00 µg
10x T4 DNA ligase buffer	2.00 µl
T4 DNA ligase	0.25 µl
ddH_2O	to 20.00 µl

The reaction was incubated at room temperature overnight. Next day, the ligation reaction was transformed to the bacterial cells using Bacterial heat shock transformation protocol (see **4.3.**), seed to the LB agarose plates with appropriate antibiotics and cultivated overnight at 37 °C. Usually, 5-8 distinct colonies were then tested using colony PCR, and positive clones were then inoculated to the media with appropriate antibiotics and harvested for the DNA the next day (see **4.4.**). Successful completion of the cloning procedure was tested using control digest reaction and gel electrophoresis followed by the Sanger sequencing of the positive samples (Sequencing unit, Charles University, Faculty of Science).

4.2.2. Gibson assembly cloning

First, primers for Gibson assembly cloning were designed (**Table 8**).

Table 8: Primers for Gibson assembly cloning

Primer name	Sequence	Generated fragment	Cloned vector
pcDNA4_pgk_GFP_vect_for	atccagcacagtggcgg	backbone	GFP_Strumpellin
pcDNA4_pgk_GFP_vect_rev	cattagctcgtccatgccgaga	backbone	GFP_Strumpellin
3xF_Str_to_pgk_GFP_for	ccgccgggatcactctcggcatggacgagctaatgttggactttctagccgagaac	insert	GFP_Strumpellin
3xF_Str_to_pgk_GFP_rev	ccctctagactcgagcggccgccactgtgctggatttacagcactgttctgaactcatc	insert	GFP_Strumpellin

Insert from Str_F_flag vector and backbone from PGK_GFP_FAM45 vector were amplified with primers depicted above (**Table 8**) via PCR. Subsequently, the reaction mixture was prepared (**Table 9**).

Table 9: Gibson assembly cloning mixture

Reagents	Volume
Amplified insert	2 µl
Amplified backbone	3 µl
Gibson assembly mastermix	15 µl

The reaction mixture was incubated in a thermocycler for 1 h at 50 °C. Next, the reaction mixture was transformed into the bacterial cells using Bacterial heat shock transformation protocol (see **4.3.**) and single colonies were further used for vector DNA isolation, using Isolation of the DNA from the bacterial cultures protocol (see **4.4.**). Successful completion of the cloning procedure was tested using control digest reaction and gel electrophoresis followed by the Sanger sequencing of the positive samples (Sequencing unit, Charles University, Faculty of Science).

4.3. Bacterial heat shock transformation

Competent bacterial cells, DH5α, were thawed on ice. Next, a ligation mixture/plasmid (3-5 µl) was added. After 30 minutes on ice, bacterial cells were heat-shocked at 42°C for 60-90 seconds, cooled on ice for 5 minutes and followed by the addition of at least 500 µl of LB medium. After 1h incubation at 37°C, bacteria were plated on LB agar plate with appropriate antibiotics. Usually, the plates were incubated at 37°C overnight and then stored at 4-8°C.

4.4. Isolation of the DNA from the bacterial cultures

Bacterial cells were inoculated to the 4 ml of LB medium with appropriate antibiotics and cultured overnight at 37°C. For the isolation of recombinant DNA from the bacterial cells commercial kit High-Speed Plasmid Mini Kit (Geneaid, USA) was used according to the manufacturer's instructions. The concentration of the obtained DNA was measured on NanoDrop ND-1000 (Thermo Fisher Scientific, USA) and DNA solution was then stored at -20°C.

4.5. Cell cultures

4.5.1. Cell culture cultivation

Cell cultures (see **Table 10**) were cultivated in the DMEM++ growth medium, 37°C and 4% CO_2 atmosphere. Upon reaching confluence, cells were subcultured – washed with sterile 1x PBS (GE Healthcare Life Sciences, USA), trypsinized with 1x Trypsin-EDTA solution (Biowest, USA) to detach them from the surface, centrifuged at 160g/25°C for 5 min, diluted in the DMEM++ growth media and then seeded as needed for subsequent experiments on the plate, flask or well plate (TPP, Switzerland).

Table 10: All cell line cultures of human origin used in this work:

Cell line	Tissue of origin	Genetical manipulation	Provided by
HEK293_wt	Embryonic kidney	-	-
U2OS_wt	Bone osteosarcoma	-	-
U2OS_Str_KO	Bone osteosarcome	Strumpellin KO - CRISPR/Cas9	own
U2OS_Str_KO_rescue	Bone osteosarcome	GFP_strumpellin rescue	own
U2OS_SWIP_KO	Bone osteosarcoma	SWIP KO - CRISPR/Cas9	Tereza Humhalova
U2OS_VPS35_KO	Bone osteosarcome	VPS35 KO - CRISPR/Cas9	Tereza Humhalova
MDA_wt	Breast cancer	Plain CRISPR/Cas9	Ben Tyrrell; Beatson Institute for Cancer Research, UK
MDA_Str_KO	Breast cancer	Strumpellin KO - CRISPR/Cas9	Ben Tyrrell; Beatson Institute for Cancer Research, UK

4.5.2. Transient transfection of cell cultures

For the transfection of HEK293 cells calcium phosphate method was used, according to the following protocol (**Table 11**).

Table 11: Calcium phosphate method reaction mixture

Reagents	Amount
Plasmid DNA	5 µg
$CaCl_2$	25 µL
ddH_2O	to 160 µL
2xHEPES buffer	160 µL
Total volume	320 µL

The mixture was prepared in the following order: 1) ddH_2O, 2) $CaCl_2$, 3) DNA. Immediately followed by addition of 2xHEPES buffer by single drops and incubation for 5-20 minutes, RT. The solution was then carefully poured on cells.

Other cell lines (**Table 10**) than HEK293 were transfected with commercial transfection reagent – X-tremeGENE HP DNA Transfection Reagent (Roche, Germany), according to the following protocol (**Table 12**).

Table 12: X-tremeGENE HP DNA Transfection Reagent transfection reaction mixture

Reagents	Amount
DMEM	to 100 µL
Plasmid DNA	1 µg
X-tremeGENE HP DNA Transfection Reagent	1 µL

The mixture was prepared in the microcentrifuge vial in the following order: 1) DMEM without antibiotics and sera, 2) plasmid DNA, 3) X-tremeGENE HP DNA Transfection Reagent (added carefully into the volume of the liquid). The transfection mixture was further incubated at RT for 30 minutes and then poured on cells.

4.5.3. Stable expression cell line generations

U2OS_Str_KO cells were seeded onto 6-well plate (TPP, Switzerland) and three wells were transiently transfected with GFP_Strumpellin expression vector as described above (see **4.5.2.**). After two days, hygromycin B was added to final concentration 300/500/700 µg/ml into the transfected wells. Additionally, 500 µg/ml of hygromycin B in total were added to the well with untransfected cells. Media with antibiotics were changed every two days. Untransfected cells were all dead before 6-day passed. Surviving cells from transfected wells were harvested and seeded as polyclonal stable expression rescue cell line. For this study, only U2OS_Str_KO_rescue cell line cultured with 500 µg/ml hygromycin B was used.

4.5.4. Knock-out cell line generation

DNA oligos were designed according to the Addgene gRNA sequence library (Addgene, USA; https://www.addgene.org/pooled-library/zhang-human-gecko-v2/) for KIAA0196/strumpellin gene targeting exon 6/29 (**Table 13**). Obtained DNA oligos were annealed, phosphorylated and subsequently inserted via BpiI restriction site into the plasmid pSpCas9(BB)-2A-Puro_(PX459)V2.0 (Addgene, USA).

Table 13: DNA oligos designed for KO cell line generation

DNA oligo name	Sequence	Cloned vector
Str_pSpCas9_sgDNA_F	CACCGCAACGAATCCTTCATCAGTA	pSpCas9(BB)-2A-Puro (PX459) V2.0-gStrumpellin
Str_pSpCas9_sgDNA_R	AAACTACTGATGAAGGATTCGTTGC	

Sequence of pSpCas9(BB)-2A-Puro_(PX459) V2.0-gStrumpellin was verified by Sanger sequencing (Sequencing unit, Charles University, Faculty of Science) followed by the transfection of 1 µg of the vector DNA with X-tremeGENE HP DNA Transfection Reagent (Roche, Germany) to the U2OS_wt cells (see **4.5.2.**). Next day, puromycin at a final concentration of 2.5µg/ml was added to the cell culture. Cells were exposed to the antibiotic treatment for three days and then washed with fresh DMEM++ and left for a one week to recover from treatment. No cells survived treatment in control antibiotic-treated well (without transfection). Polyclonal U2OS str KO cells were harvested, diluted and seeded single cell per well on two 96-well plates (VWR, China), thus generating monoclonal cell lines of U2OS_str_KO. Three potential clones were then tested using western blot and those which lacked strumpellin signal were selected for further work.

4.6. Lysate preparation

Cells were washed three times with 1x PBS, 37°C for 5 minutes. PBS was discarded, the dish was laid on ice and cells were immediately lysed adding 4x Laemmli buffer. The scraper was used to detach cells from the dish surface, and the lysate was transferred to the 1.5ml tube on ice. Lysates were sonicated two times, 10 pulses (0.8 s per pulse), 60% amplitude with Compact Lab Homogenizer (Hielscher, Germany) and then incubated at 75°C for 5 minutes, in a heat block (Eppendorf, Germany). Next, samples were centrifuged 10 minutes, 38000 RCF. The supernatant was transferred to the new 1,5ml tubes and used as sample/lysate. If needed, samples were freeze and stored at -80°C.

4.7. Polyacrylamide gel electrophoresis (PAGE)

Optimal separation gel percentage was produced according to the **table 14**.

Table 14: Separation gel mixture

Reagents	6%	7%	8%	9%	10%
ddH_2O	2.7 mL	2.55 mL	2.35 mL	2.2 mL	2.05 mL
Tris 1.5 M; pH 8.8	1.25 mL	1.25 mL	1.25 mL	1.25 mL	1.25 mL
Acryl/Bis-acrylamide 30%	1 mL	1.15 mL	1.35 mL	1.5 mL	1.65 mL
10% SDS	0.05 mL	0.05 mL	0.05 mL	0.05 mL	0.05 mL
Adenosinpersulphate	0.05 mL	0.05 mL	0.05 mL	0.05 mL	0.05 mL
TEMED	0.004 mL	0.004 mL	0.004 mL	0.004 mL	0.004 mL
Total volume	5 mL	5 mL	5 mL	5 mL	5 mL

Optimal stacking gel percentage was produced according to the **table 15**.

Table 15: Stacking gel mixture

Reagents	5%
ddH_2O	1.4 mL
Tris 1 M pH 6.8	0.25 mL
Acryl/Bis-acrylamide 30%	0.33 mL
10% SDS	0.02 mL
Adenosinpersulphate	0.02 mL
TEMED	0.002 mL
Total volume	2 mL

The source was set to constant voltage – 100 V. Voltage was then increased to the 130 V after samples got focused.

4.8. Western blot

Proteins from the PAGE gel were transferred on the 0,2 μm nitrocellulose membrane (GE Healthcare Life Sciences, USA) using semi-dry blotting equipment set (Hoefer, USA) to the 0.9mA per cm^2 of PAGE gel, for 1 hour or wet blotting aperture set (Labnet International), to the 120mV per PAGE gel, for 2 hours. After that, the membrane was blocked in blocking buffer for 1 hour and then stained with primary antibody dissolved in blocking buffer overnight in cold room. Next day, the membrane was three times washed with 1x TBST for 5 minutes and then stained with appropriate secondary antibody horseradish peroxidase conjugate dissolved in blocking buffer for 45-90 minutes. Afterwards, the membrane was washed three times with 1x TBST for 5 minutes.

Washed membrane was put on Saran (Dow Chemical, USA) and soaked with peroxidase substrate Immobilon® ECL Ultra Western HRP Substrate (1 : 1, ECL1 : ECL2; Merck KGaA, Germany) for 5 minutes. Excess substrate was dried out with filtration paper and membrane was wrapped in Saran. Darkroom exposure or LAS4000CCD camera (GE Healthcare, Great Britain) was used for image acquisition.

4.8.1. Western blot analysis

Western blot images were analysed using the ImageStudio Lite™ Software (LI-COR, USA). A rectangle of one size was used to choose a band of the interest and count total signal amount in the selected region. The background of the membrane was quantified from the amount of signal in the 3-pixel wide surrounding of the particular rectangle and subtracted from the total signal value. Obtained values were afterwards used for the normalisation and quantification of the relative protein amount.

4.9. *In silico* structure prediction

Domain and secondary structure *in silico* predictions were done using DomPred/PsiPred software respectively with the preset basic setup [Bryson et al., 2007; Buchan et al., 2013]. The sequence of strumpellin for analysis was obtained from UniProt, query UniProtKB - Q12768 (https://www.uniprot.org/uniprot/Q12768)[Bateman et al., 2017]. Results of PsiPred secondary structure prediction were than manually visualised using Inkscape software (https://inkscape.org/cs/).

4.10. Microscopy cell fixation and permeabilisation

Cells on coverslip were washed three times 5 minutes in 1x PBS (37 °C), followed by incubation in 3% paraformaldehyde solution in 1x PBS for 10 minutes. Fixed cells were washed three times for 5 minutes in 1x PBS and afterwards incubated with 0.01% Triton x-100 in 1x PBS for 5 minutes followed by three more washes in 1x PBS. If needed fixed and permeabilised cells were stored at 4°C after the addition of NaN_3 (0,02%).

4.11. Immunofluorescence

Fixed and permeabilised cells were stained with primary antibody (**Table 1**) dissolved in DMEM ++ for 45 minutes. Sequential staining was used if more than one primary antibody were used (with three wash steps between each staining). Samples were washed three times 5 minutes in 1x PBS and stained for 45 minutes in secondary antibodies (**Table 2**) diluted in DMEM++ (not sequential). Samples were rewashed three times in 1x PBS for 5 minutes, briefly cleared in ddH_2O and fixed in Mowiol with DAPI (1µg/ml). Samples were stored at least overnight at 8 °C before taken to the microscope.

In some applications, cell polymerised actin was stained with phalloidin-fluorescence dye conjugate. Usually, actin staining was connected with standard immunofluorescence procedure. Thus, immunofluorescence procedure took place with the addition of fluorescently labelled phalloidin to the diluted secondary antibody in DMEM++. The further procedure was the same as for immunofluorescence.

4.12. Confocal microscopy

Images acquired with laser scanning confocal microscope Leica TSC SP2:
For acquisition of images were used 63x objective with NA 1.4 made up for oil immersion and proper excitation and emission filters (depending on secondary antibodies). Despite the possibility of variable pixel size most of the images were acquired with pixel size 43.88 nm (in x and y) with overall resolution 2048x2048 pixels.
Images acquired with laser scanning confocal microscope Zeiss LSM800:
For acquisition of images were used 63x objective with NA 1.4 made up for oil immersion. Excitation and emission filter were set according to the used antibodies. Images were acquired with pixel size 47.05 nm (in x and y) with overall resolution 2868x2868 pixels.

For image acquisition with both confocal microscopes, we performed control for secondary antibody bleed-through and set appropriate emission filters to avoid it.

4.13. Fluorescence microscopy

In some application (VPS35 positive subdomain analysis), images were acquired with classical inverted fluorescence microscope Olympus Cell-R (Cell-R). For acquisition of images, 60x objective with NA 1.35 made up for oil immersion was used. Image resolution 1344x1024 pixels. Images had a fixed pixel size of 107.5 nm (in x and y). Multiple focal planes (33) were captured and z-projected with 25 nm step size.

4.14. Image processing and automated particle/nuclei counting

Images from both confocal microscopes were processed to the image panels using Fiji software [Schindelin et al., 2012, 2015] with FigureJ plugin [Mutterer et al., 2013]. Regions of interest were selected and additionally zoomed in the insets. For the purpose of this thesis, the intensity of the images was uniformly increased.
Images from Cell-R microscope were deconvolved using “Classic Maximum Likelihood Estimation” function of Hyugens compute engine (4. 3. Lp3 64b) and further processed with Fiji software.

VPS35 positive subdomains counting:

Images were in the form of z-stack and thus, “z-project” function of Fiji, set to maximal intensity, was applied to acquire an image of maximal intensity projection. Next, “background subtraction” function of Fiji, set to rolling ball with a radius of 20 pixels, was used to subtract background. Mask of the image was created with the intensity threshold “Otsu dark”. VPS35 positive subdomains were

then analysed using “analyze particle” function of Fiji, used to count particles and their respective area. The whole process was automated using “batch” function of Fiji with this macro:

```
run("Set Measurements...", "area mean standard modal min skewness kurtosis area_fraction limit display nan
redirect=None decimal=3");
if (nSlices>1) run("Z Project...", "projection=[Max Intensity]");
run("Properties...", "unit=µm pixel_width=0.1075000 pixel_height=0.1075000 voxel_depth=0.2500000");
run("Subtract Background...", "rolling=20");
setAutoThreshold("Otsu dark");
run("Analyze Particles...", "size=1-Infinity pixel display summarize");
```

Cell/Nucleus counting:

Average intensity projection images were used for nuclei counting. Signal of the nuclei channel was blurred. Next, threshold named “IsoData dark” was set. Function “Find Maxima” of Fiji was then used to identify and count nuclei. Whole process was automated using batch function of Fiji and following macro:

```
if (nSlices>1) run("Z Project...", "projection=[Average Intensity]");
run("Mean...", "radius=15");
run("Gaussian Blur...", "sigma=20");
setAutoThreshold("IsoData dark");
run("Find Maxima...", "noise=10 output=Count above");
```

4.15. Statistical analysis of images/particles

Statistical analysis was done using R software (version 3.5.1) [R Core Team 2014] with attached libraries bbmle [Bolker et al. 2016] and truncnorm [Trautmann et al. 2014]. Data acquired with particle counting had the threshold set to 0.012 from left. A classic statistical approach, using parametric tests was improper, as no prerequisites/assumptions were fulfilled. Thus, we performed a permutation test. Area values of analysed subdomains were randomised between two groups (wt/KO), pooled and followed by the free sampling with 99 repeats. To estimate area means of allotted datasets we called maximal likelihood function with Nealder-Mead optimisation. Difference between the estimated area means of every couple of the two groups (original and permutated) was then recorded and compared to the original difference. Thus, receiving p-value (what number of the area mean differences is larger or equivale to the original difference). R software was also used for boxplot graph generation. A code used for the statistical analysis in R software is depicted on the next page.

The code used for the statistical analysis of VPS35 positive subdomains:

```
library(bbmle)
library(truncnorm)
library(vioplot)
endoz <- read.table("MDA_Endosomes_Otsu.csv",header=T,sep=";",dec=".")
endoz$Slip <- as.factor(endoz$Slip)
endoz$Image <- as.factor(endoz$Image)
endoz$log10Area <- log(endoz$Area, 10)
ko <- endoz$Area[endoz$Type=="KO"]
wt <- endoz$Area[endoz$Type=="WT"]
ko <- endoz$log10Area[endoz$Type=="KO"]
wt <- endoz$log10Area[endoz$Type=="WT"]
ntruncNLL <- function(x,xmean,xsd){ -
sum(log(dtruncnorm(x,a=log(0.012,10),b=Inf,mean=xmean,sd=xsd))) }
estim.mean <- function(data){
+ estimate <- mle2(minuslogl=ntruncNLL,start=list(xmean=-1, xsd=1),data=list(x=data))
+ return(coef(estimate)[1])}
pertype <- tapply(endoz$log10Area, endoz$Type, estim.mean)
labels <- endoz$Type
xxx <- rep(NA,999)
for (ii in 1:999){newlabels <- sample(labels)
+ npertype <-tapply(endoz$log10Area, newlabels, estim.mean)
+ xxx[ii] <- npertype["KO"] - npertype["WT"]}
puvodni.rozdil <- pertype["KO"] - pertype["WT"]
vse <- c(xxx, puvodni.rozdil )
p <- length(which(vse>=puvodni.rozdil))/length(vse)
p
[1] 0.001
perimage <- tapply(endoz$log10Area, endoz$Label, estim.mean)
sliptype <- aggregate(as.factor(paste(endoz$Type,endoz$Slip,sep=".")),by=list(endoz$Label),unique)
names(perimage)==sliptype$Group.1
sklicko <- as.factor(paste(rep(c("KO","WT"),each=60),rep(rep(1:3,each=20),2),sep="."))
boxplot(perimage~sklicko,outline=F, las=1)
abline(h=pertype["KO"],lty=1)
abline(h=pertype["WT"],lty=2)
```

5. Results

5.1. Strumpellin KO cell line generation

Polyclonal MDA strumpellin KO cell line was kindly provided by Ben Tyrrell from Beatson Institute for cancer research. This cell line was not wholly devoid of strumpellin. Therefore, we used it to establish monoclonal MDA strumpellin KO cell lines. Six MDA monoclones were tested for the presence of the strumpellin with western-blot. Three of them were completely devoid of the strumpellin (**Figure 6A**). Only MDA_monoclone_4 (MDA_Str_KO) was used further in this work.
MDA_Str_KO cell line proved hard to transfect, especially with larger constructs. Thus, to achieve further goals, easy to transfect monoclonal U2OS strumpellin KO cell line was generated with the CRISPR/Cas9 system. Three U2OS_monoclones were tested for the presence of strumpellin with wester-blot (**Figure 6B**). Two monoclones were devoid of strumpellin, and only one, U2OS_monoclone_2 (U2OS_Str_KO) was used further in this work.
Strumpellin absence in both cell lines, MDA_Str_KO and U2OS_Str_KO, was also verified by the immunofluorescence staining of endogenous strumpellin and VPS35. Despite relatively large background, upon staining with the antibody against strumpellin, colocalization between strumpellin and VPS35 was lost in both strumpellin KO cell lines (**Figure S1A and S2A**). WASH associated early endosome subdomains have been detected by retromer subunit VPS35. This, together with western-blot experiment revealed that no endogenous strumpellin was interfering with the further measurements in both strumpellin KO cell lines, even though strumpellin antibody displayed relatively large cytosolic background.

Figure 6 – Verification of monoclonal strumpellin KO cell lines with western-blot. MDA (**A**) and U2OS (**B**) cell lines. MDA_Str_KO monoclone_4 and U2OS_Str_monoclone_2 were selected for further work. The red dot indicates strumpellin.

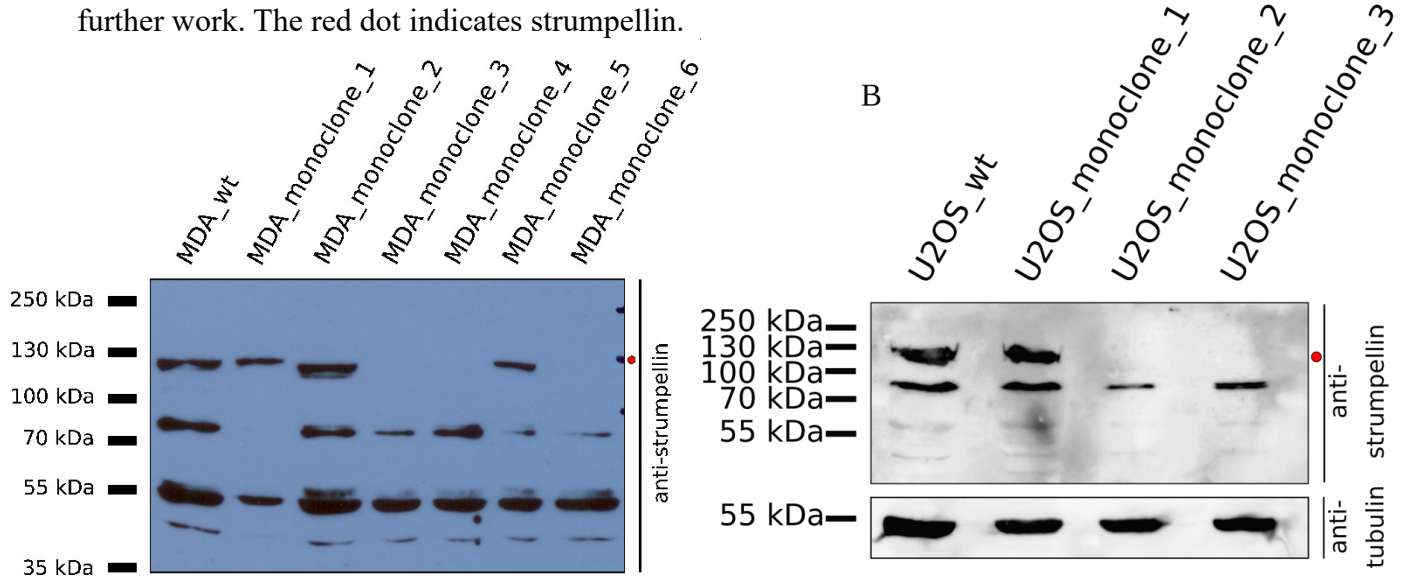

5.2. Domain analysis of strumpellin

5.2.1. In silico prediction and fragmentation of strumpellin

Strumpellin structure and function have not been adequately characterised yet. Thus, one of the major goals of this work was to divide strumpellin into fragments and observe if their localisation could elucidate strumpellin structure or function in more detail.

In silico prediction of the structure and domain organisation in the strumpellin protein body was performed with the DomPred software (data not shown)[Bryson et al., 2007]. DomPred detected eight domains. Importantly, boundaries of those domains only roughly corresponded to the already published spectrin-like domain repeat spanning from the aa 241 to 791. Therefore, the secondary structure was predicted with the PsiPred software (see methods)[Buchan et al., 2013] and schematically visualised (**Figure 7A**). The predicted structure was mostly helical with unstructured regions and few β-sheets. Two of the unstructured regions were chosen to divide strumpellin according to DomPred and PsiPred predictions into the three sections, N-terminal part (Str_N), middle part (Str_M) and C-terminal part (Str_C). All three parts were separately cloned in a mammalian expression vector. Additionally, combinations of those three sections were created, full-length strumpellin (Str_F), fragment without the C-terminal part (Str_NM) and fragment lacking the N-terminal part (Str_MC), ensuring that unidentified structural element was not impaired by the fragmentation. Moreover, all fragments were produced with the myc tag on the C-end and with the flag tag on the N-end of the respective fragment to eliminate potential deleterious effect of the tag position on the fragment function or localisation (**Figure 7A**).

Cloning procedure was verified by the sequencing (data not shown) and subsequent transfection of the constructs to the HEK293 cells followed by visualisation of expressed proteins on western blot (**Figure 7B and 7C**). Each fragment was successfully produced in the HEK293 cell line with the expected molecular mass. Expression levels were high for all fragments, except for the Str_C in the flag version. Unfortunately, the reason, which stood behind Str_C_flag low expression is currently unknown.

Figure 7 – Overview of strumpellin secondary structure. Dashed lines demarcate borders of strumpellin fragments. (**A**) Schematic representation of cloned strumpellin fragments. (**B**) Overexpression of tagged fragments in the HEK293 cells visualised with the myc/flag antibody on the western-blot. Tubulin served as a loading control (**C**).

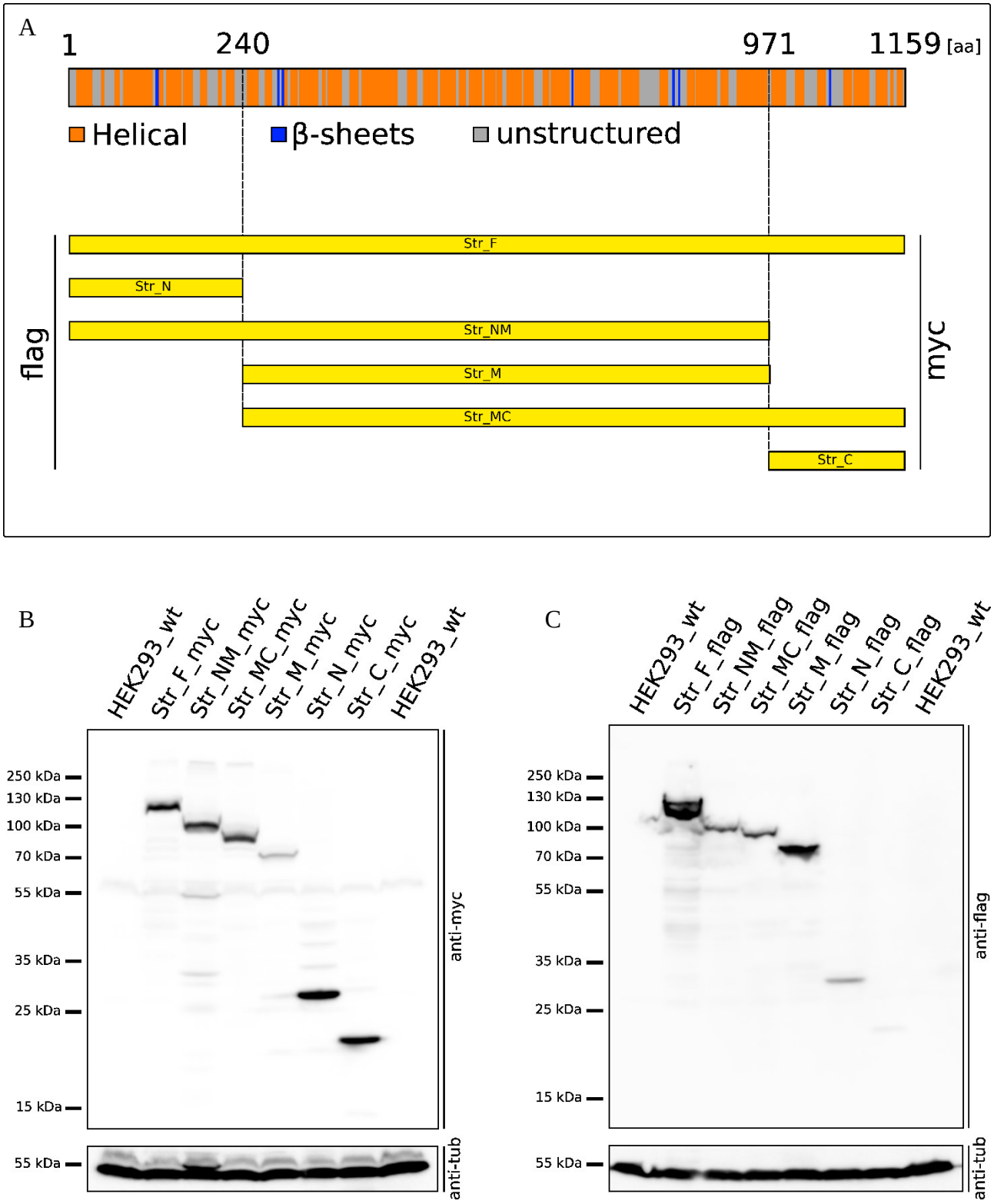

5.2.2. The localisation of strumpellin fragments in strumpellin KO cells

U2OS_Str_KO cells were transiently transfected with the fragment constructs. After 48 hours, cells were fixed and stained with the antibodies against the corresponding tag and the endogenous SWIP protein, to resolve if the expressed fragments still localised to the WASH complex (**Figure 8A, S3A, S4A and S4B**). Surprisingly, only one of the fragments, the Str_F_flag clearly colocalised with the SWIP positive spots and thus is probably incorporated into the WASH complex (**Figure 8A**). Other fragments were mostly localised dispersedly throughout the cytoplasm, except

Figure 8 – Expression of either Str_F_flag or Str_NM_flag fragments in the U2OS_Str_KO cell line, stained with the antibodies against the flag tag and endogenous SWIP (**A**), the rest of the fragments is presented in the **Figure S3B**. VPS35 positive subdomains of the early endosomes are zoomed in the insets. Image scale bar: 10 µm. Inset scale bar: 1 µm. Images were acquired using confocal microscope Zeiss LSM800.

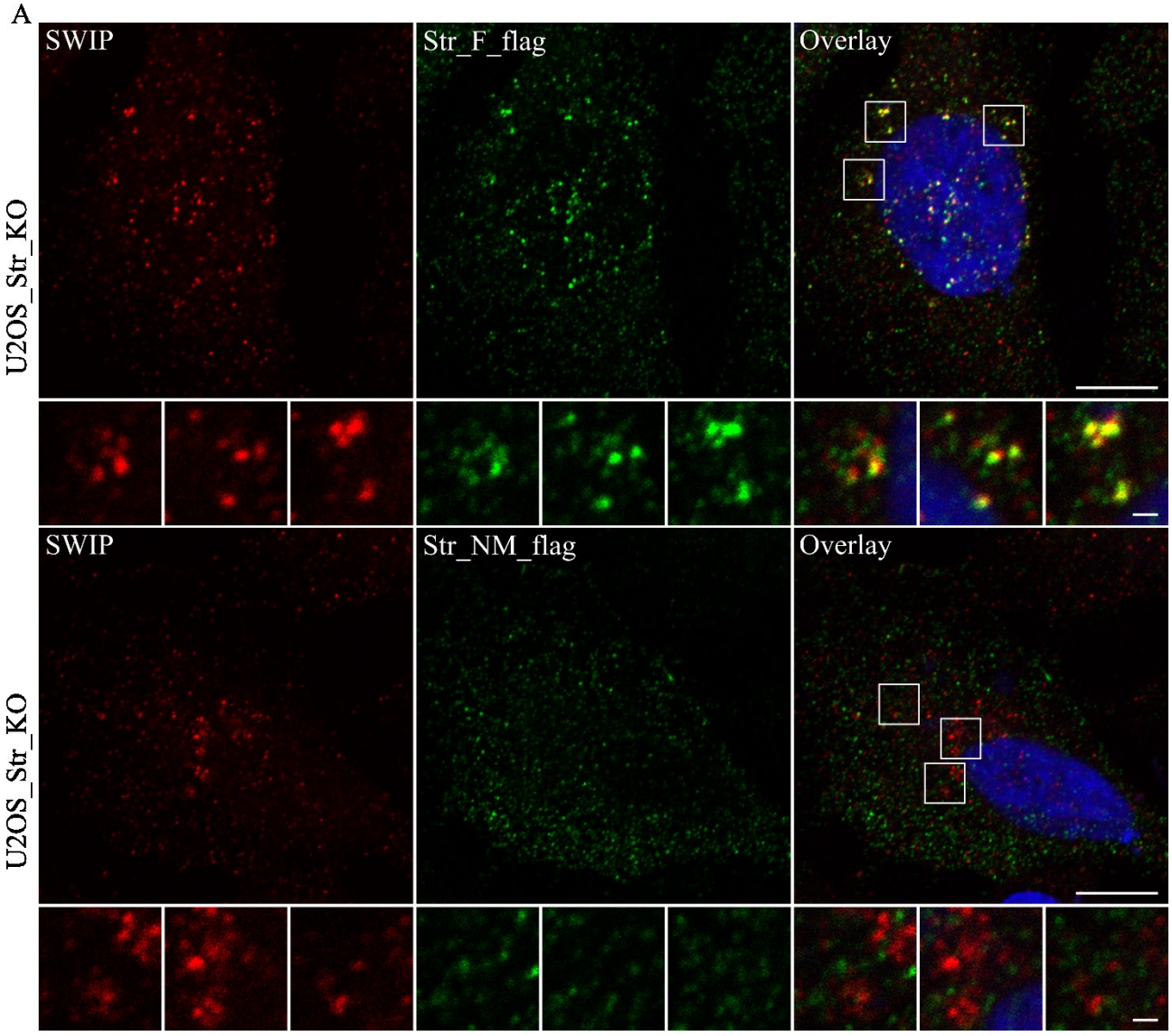

for the Str_N_myc and Str_C_myc (**Figure 8A, S3A, S4A and S4B**). The Str_N_myc, but not Str_N_flag, was enriched in the nucleus. Nuclear localization signal (NLS) prediction did not detect any new artificially formed NLS upon connecting the fragment with the linker to the tag during the molecular cloning (data not shown). Thus, data in the case of N fragment are inconsistent. On the other hand, the Str_C_myc had shown puncta localisation in the cytoplasm but did not colocalise with the endogenous SWIP. Moreover, the Str_C_myc pattern did not correspond to the endosomal localisation; rather it resembled some aggregated bodies (**Figure S4B**). Only one of the twelve fragments, the Str_C_flag, was observed to be expressed on the blot but was not detected by the immunofluorescence. This was not surprising according to the very low amount of this fragment detected with the wester-blot previously (**Figure 7C**).

Interestingly, strumpellin in the full version localised on the early endosomes with the flag tag, but not with the myc tag (**Figure 8A and S4A**). This led us to determine the hypothesis that unobscured C-terminal end of full strumpellin is needed for the proper binding into the WASH complex. To test this hypothesis, constructs with the green-fluorescent protein (GFP) tag on the C (Strumpellin_GFP) or N (GFP_strumpellin) end of the whole strumpellin were prepared and transiently expressed in the U2OS_Str_KO cell line. Strikingly, both strumpellin GFP constructs, regardless of the tag position, were localised in spots on the early endosomal subdomains stained for VPS35 (**Figure 9A**), hence able to incorporate to the WASH complex. Thus, the initial hypothesis was rejected. The disperse localisation of Str_F_myc had a most probably different cause.

Together, these observations suggest that none of designed strumpellin fragments, except full-length strumpellin was able to bind to the WASH complex.

5.3. Analysis of WASH complex function in the absence of strumpellin

5.3.1. Effect of strumpellin KO on the WASH complex subunits

Interested in the WASH complex, our laboratory was able to generate additional related KO cell lines, as U2OS SWIP KO cell line (further U2OS_SW_KO), U2OS VPS35 KO cell line (further U2OS_V35_KO). This granted us the possibility to check the stability of other WASH complex subunit upon deletion of the strumpellin, SWIP or VPS35, and further distinguish whether the effect of the particular KO was directly connected to the stability of the WASH complex subunit or whether the pleiotropic effect of the overall WASH complex loss could not be ruled out.

Figure 9 – Both variants, GFP_strumpellin and strumpellin_GFP are able to incorporate to the WASH complex. Overexpression of GFP_Strumpellin and Strumpellin_GFP constructs in the U2OS_Str_KO cell line, stained with the antibody against endogenous VPS35. VPS35 positive subdomains of the early endosomes are zoomed in the insets (**A**). Image scale bar: 10 µm. Inset scale bar: 1 µm. Images were acquired using confocal microscope Zeiss LSM800.

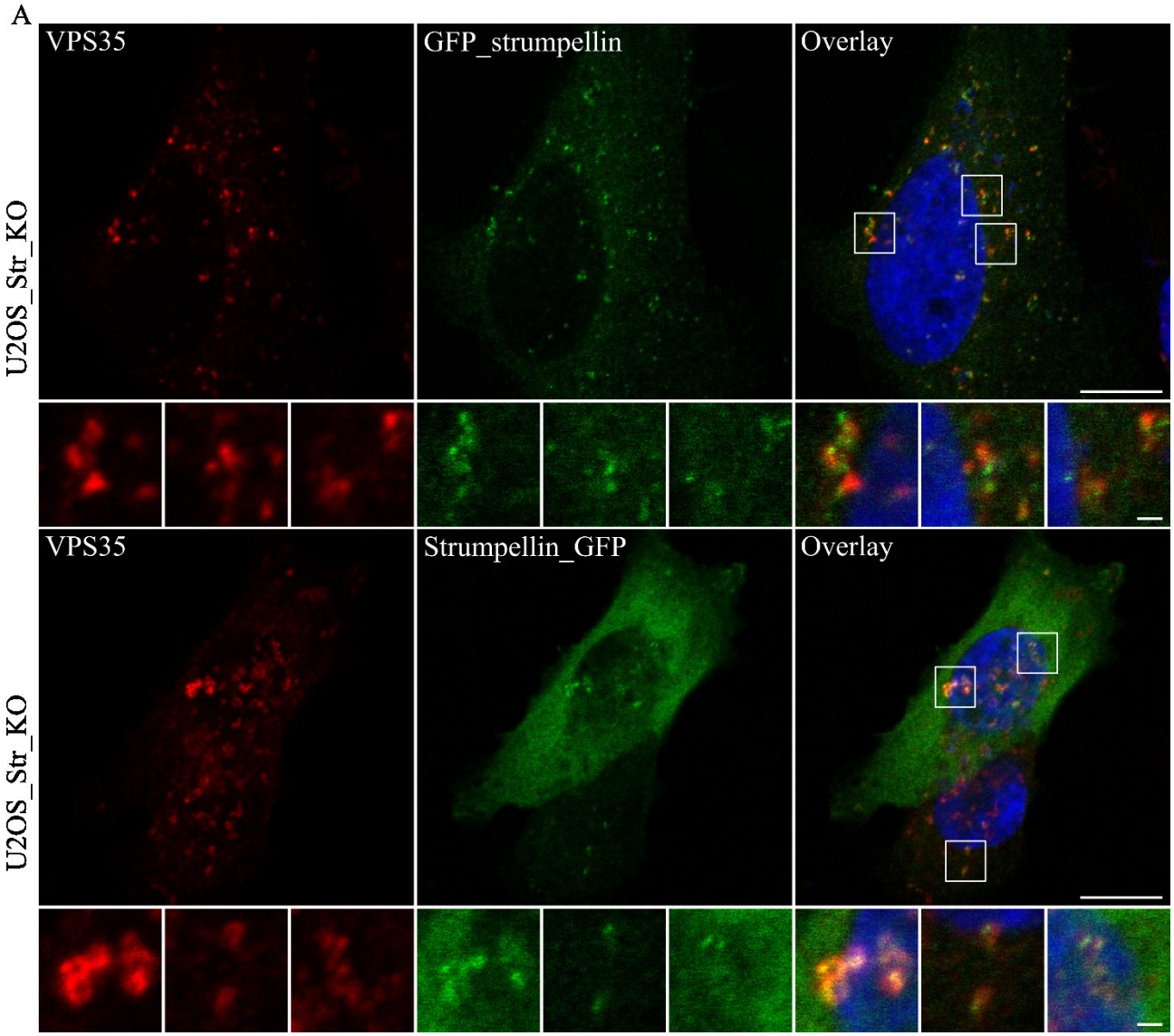

Therefore, cell lysates from the U2OS_Str/SW/V35_KO and MDA_Str_KO cell lines were examined for the amount of the WASH complex subunits and VPS35 protein by the western-blot (**Figure 10A**). Alpha-tubulin was used as loading control, and quantification of the protein of interest was done with the ImageStudio Lite software (**Figure 10B, C, D, E**). Importantly, we could do only one experiment with WASH1 staining so far. Thus, results for the WASH1 subunit need to be verified.

Figure 10 – Western-blot visualization of the amounts of the WASH complex subunits and VPS35 in the cell lines deprived of the strumpellin/SWIP or VPS35 (**A**). Amounts of the proteins in the KO cell lines were quantified relative to the control cell line from the blots, using tubulin as a loading control (**B**, **C**, **D**, **E**; for SWIP, FAM21, VPS35 **n = 3**; for WASH1 **n** = **1**).

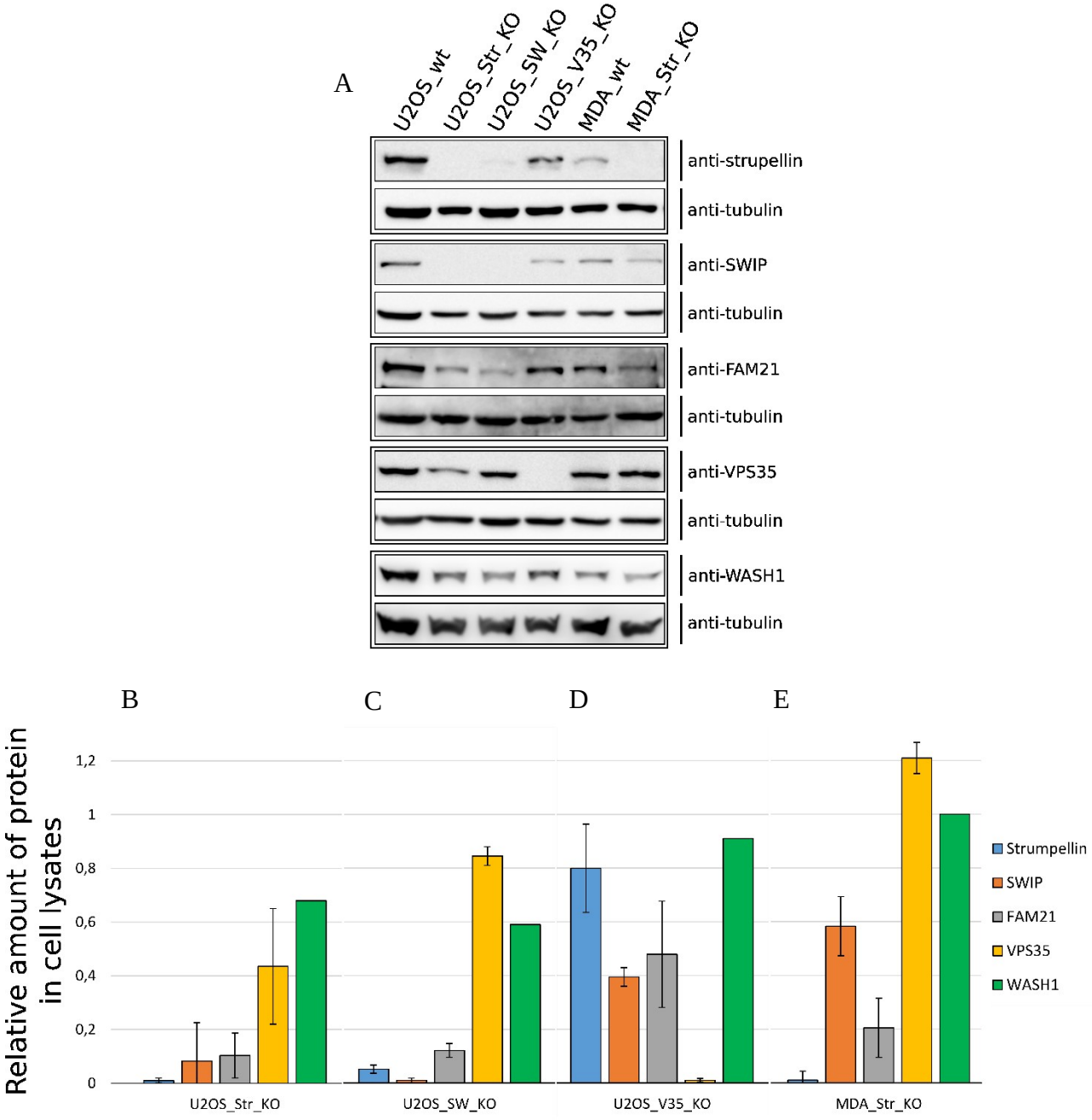

Strumpellin was, as expected, completely absent in the U2OS_Str_KO cell line. The amounts of the other WASH complex subunits, SWIP and FAM21 in this cell line were also substantially decreased. On the other hand, WASH1 levels were affected only mildly (**Figure 10B**). This means that FAM21 and SWIP proteins are more dependent with their stability on the strumpellin presence than WASH1. Still, at least small amount of SWIP/FAM21 and WASH1 persisted in the cell upon strumpellin KO.

Surprisingly, there was also a mild loss of the VPS35 amount in the U2OS_Str_KO cells, but never to the extent of FAM21 or SWIP loss. Moreover, the standard deviation is exceptionally high for VPS35 amount quantification in this cell line. Thus, results should be in this case evaluated carefully (**Figure 10B**).

Similarly, SWIP was completely absent in the U2OS_SW_KO cell line and the amounts of the other WASH complex subunits, strumpellin and FAM21, were also considerably diminished. Level of WASH1 subunit was affected only mildly. In this cell line, VPS35 amount was almost comparable to the amount of VPS35 in the control cell line (**Figure 10C**).

VPS35 was deprived of the U2OS_V35_KO cell line as expected but had no overall effect on the amount of strumpellin and WASH1. However, amounts of the other WASH complex subunits, SWIP and FAM21, were mildly decreased in the U2OS_V35_KO cell line compared to the control (**Figure 10D**).

As expected, MDA_Str_KO cell line was utterly devoid of the strumpellin. In this cell line, the FAM21 was decreased to the same extent as in the U2OS_Str_KO cell line (**Figure 10E**). This was not true for the amounts of the SWIP and WASH1. SWIP was decreased in the MDA_Str_KO cell line, but not to the same extent as in the U2OS_Str_KO cell line. Surprisingly, WASH1 was not affected at all. Additionally, the amount of the VPS35 seemed to be slightly increased in this cell line compared to the wild-type cells (**Figure 10E**).

The observed decrease in the amount of SWIP and FAM21 on the western blot was also verified using the immunofluorescent staining of the endogenous SWIP/FAM21 and VPS35 in U2OS_Str_KO cell line (**Figure 11A and S5A**).

In summary, the stability of the WASH complex subunits was clearly dependent one on each other, but overall not on the VPS35. Thus, in further experiments, the pleiotropic effect of the WASH complex loss upon strumpellin deprivation cannot be ruled out.

5.3.2. Endosomal subdomains have changed morphology in the cells lacking strumpellin

The decrease in the amount of the WASH complex subunits was observed in U2OS_Str_KO and MDA_Str_KO cell lines. This was accompanied with the clearly visible enlargement of the VPS35 positive subdomains on the early endosomes in the perinuclear region of both KO cell lines compared to the control upon immunofluorescence staining and microscopy imaging (**Figure 11A and S5A)**. To quantify this phenomenon, MDA_Str_KO and MDA_wt cells were seeded on three coverslips each, fixed and stained with the antibody against the endogenous VPS35. Wide-field fluorescence

Figure 11 – Verification of the results observed on the western-blot using the immunofluorescence staining. Amount of FAM21 seems altered upon strumpellin KO. U2OS_wt and U2OS_Str_KO cells were stained using the antibody against endogenous FAM21 and VPS35. VPS35 positive subdomains of the early endosomes are zoomed in the insets. (**A**). Image scale bar: 10 µm; inset scale bar: 1 µm. Images were acquired using confocal microscope Zeiss LSM800.

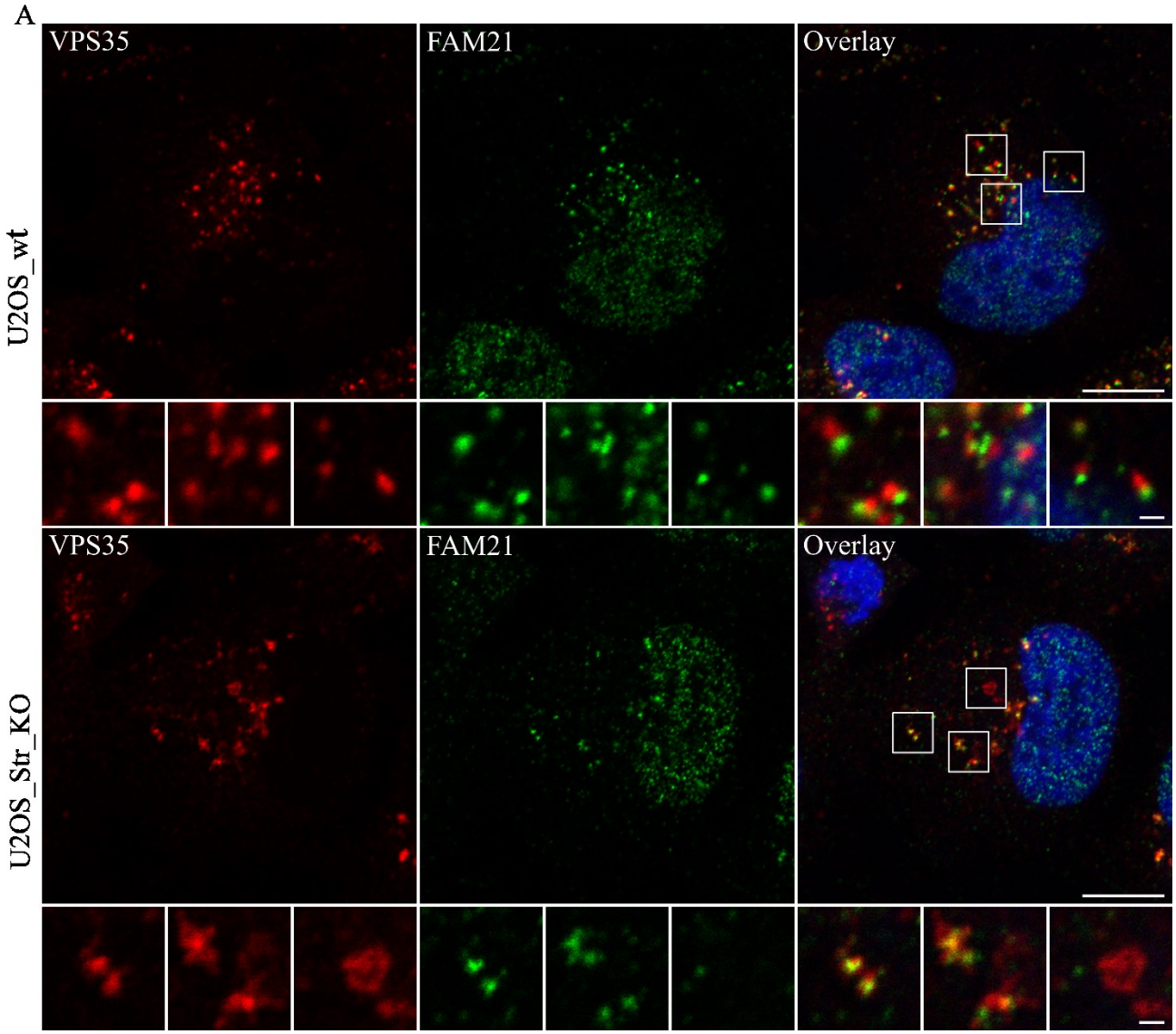

microscope was used for image acquisition. VPS35 positive subdomains and their respective area were counted as particles using the Fiji software (**Figure S6A and S6B**). Subsequent statistical analysis was done using R software. Permutation test proved that there is a difference in the area of VPS35 positive subdomains between MDA_Str_KO and MDA_wt cells (p-value ≤ 0.001). The estimated mean value of the VPS35 positive subdomain area was 1.19 times bigger for the MDA_Str_KO cell line than for the MDA_wt cell line (**Figure 12A and 12C**). Thus, MDA_Str_KO cell line has bigger VPS35 positive subdomains. Next, cells/cell nuclei were counted using Fiji software. The overall amount of VPS35 positive subdomains per cell was substantially decreased in

MDA_Str_KO cell line compared to the MDA_wt cells (**Figure 12B and 12C**). The statistical analysis remains to be done in the case of U2OS_Str_KO cells.

Figure 12 – Analysis of the VPS35 positive membrane subdomains size upon strumpellin loss. Boxplot graphs depict the distribution of the particle area size and mean value for every slip in the particular triplicate (wt/KO). The uninterrupted line represents the estimated mean value of VPS35 positive subdomain area in the MDA_Str_KO cell line. The interrupted line represents the estimated mean value of VPS35 positive subdomain area in the MDA_wt cell line. MDA_Str_KO cells have 1.19 bigger VPS35 positive subdomains than MDA_wt cells. For statistical analysis, permutation test comparing estimated mean values between two groups (wt/KO) was performed (n = 1000, ** = p-value ≤ 0.001; **A**) Additionally, number of cell nuclei and VPS35 positive subdomains per image were counted using Fiji software. MDA_Str KO cells had substantially less VPS35 positive subdomains per cell (n_{slip} = 3; **B**). A table summarising important values used for the analysis of VPS35 positive subdomains (**C**).

A

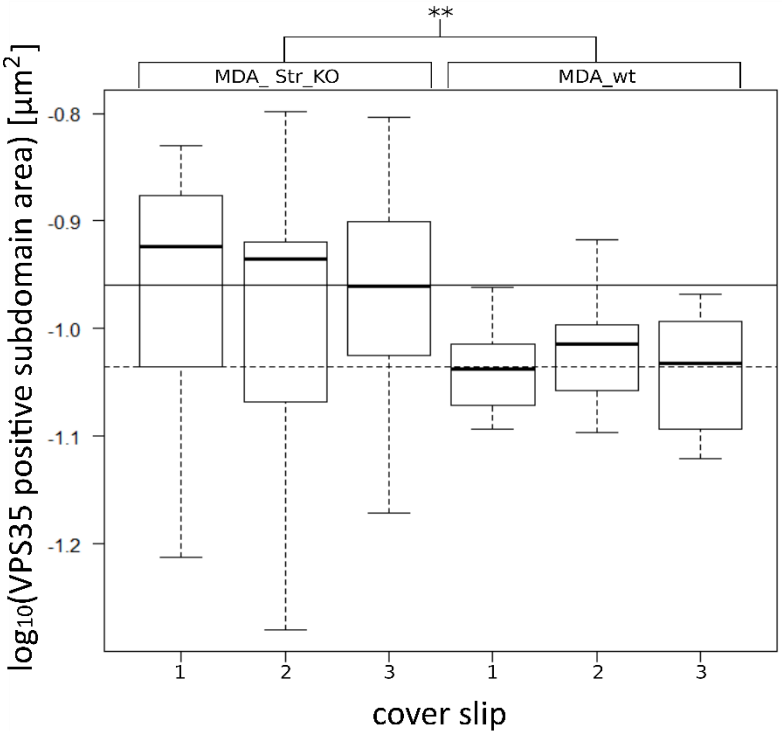

B

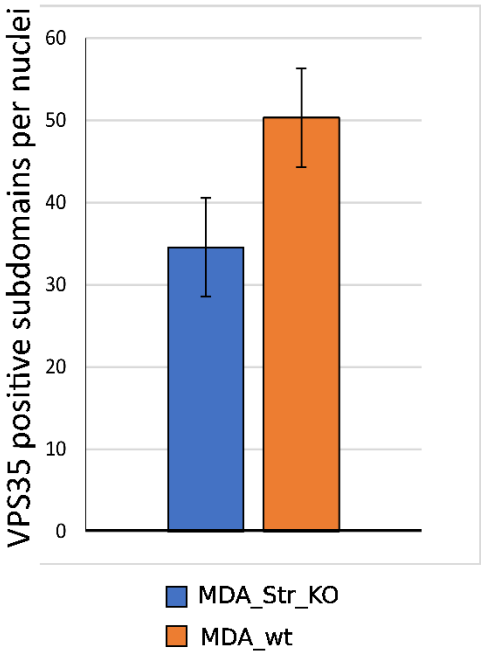

C

Type	VPS35 positive subdomains per cover slip			VPS35 positive subdomains per type	Estimated mean value of VPS35 positive subdomain area [µm²]	Nuclei per type	VPS35 positive subdomains per nuclei
	1	2	3				
MDA_Str_KO	11199	10059	10775	32033	0.1098	978	32.75
MDA_wt	14442	18314	17623	50379	0.0921	942	53.48

Additionally, in the case of U2OS_Str_KO cell line, an unusual VPS35 positive vacuolar-like structure was observed. To delineate the identity of the structure, U2OS_Str_KO cells were fixed and stained with the antibody against VPS35 and lysosomal-associated membrane glycoprotein 1 (LAMP1), marker of lysosomes (**Figure 13A**). The vacuolar-like structure was observed in 1 of every 8 U2OS_ Str_KO cells (data not shown) and was positive in both markers, VPS35 and LAMP1 (**Figure 13A**).

Altogether this indicates that the structure of the VPS35 positive subdomains is substantially altered in cells lacking strumpellin.

Figure 13 – Vacuolar-like structure, positive in endosomal and lysosomal markers appears in the perinuclear region upon strumpellin KO. U2OS_wt and U2OS_Str_KO cells were fixed and stained with the antibody against endogenous VPS35 and LAMP1 (A). VPS35 positive subdomains of the early endosomes and LAMP1 positive structures (lysosomes) are zoomed in the insets. Image scale bar: 10 µm. Inset scale bar: 1 µm. Images were acquired using confocal microscope Zeiss LSM800.

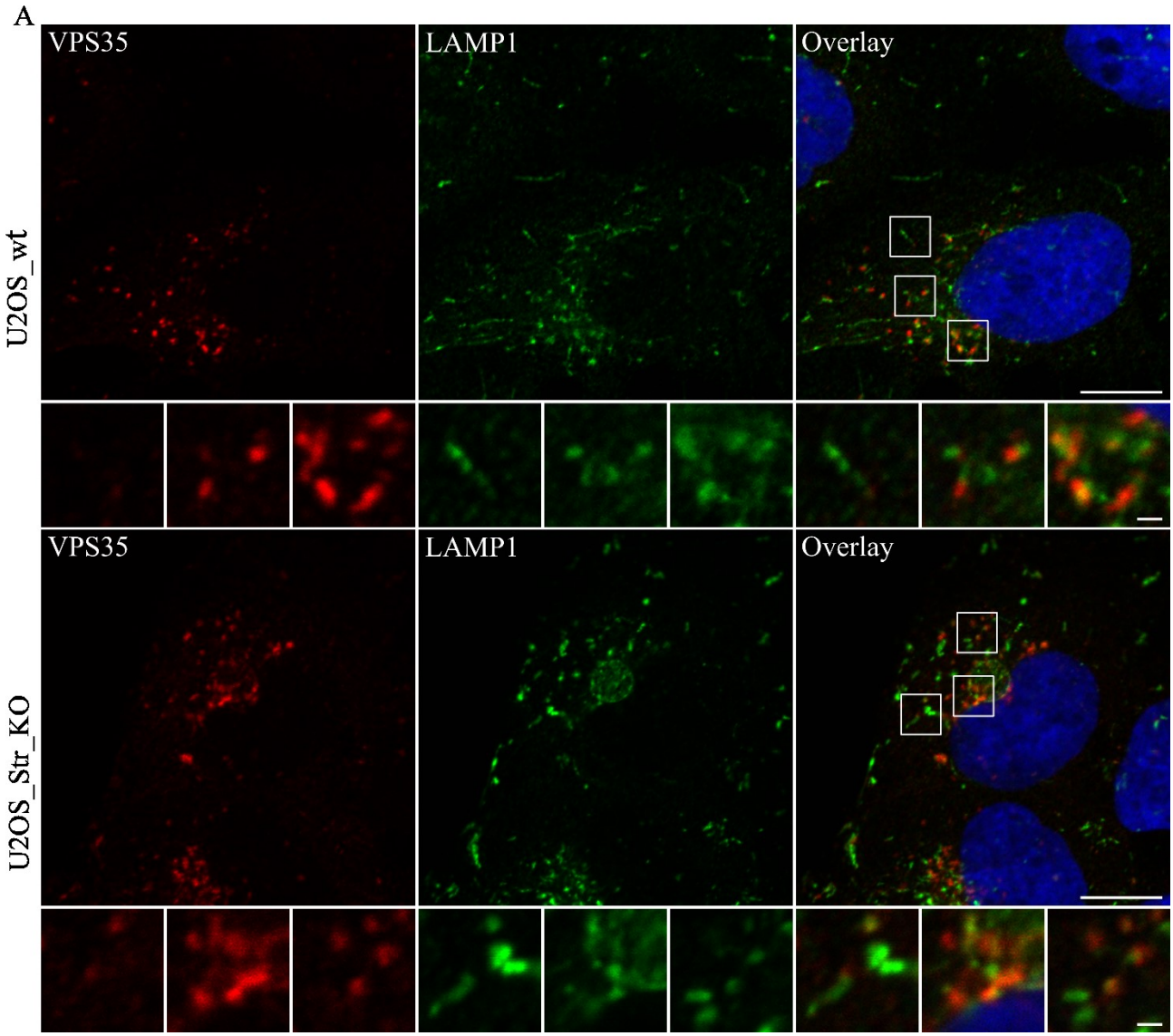

5.3.3. Nucleation of actin on the early endosomal membrane in strumpellin KO

The WASH complex is known as major endosomal NPF. As shown in previous figures, deletion of strumpellin substantially diminished the amount of FAM21 or SWIP in the cell. Importantly, residual FAM21 and SWIP were still localised to the early endosomes. This suggests that the WASH complex is still present on the membrane of the early endosome, albeit in a reduced amount. Is this residual and incomplete WASH complex still able to bind Arp2/3 complex, or is strumpellin indispensable for this bond? To answer this question, U2OS_Str_KO and U2OS_wt cells were fixed and stained with the antibody against ARP2, the subunit of the Arp2/3 complex and with the antibody against VPS35 to visualise early endosomes (**Figure 14A**). while in U2OS_Str_KO cell line ARP2 positive spots

Figure 14 – Colocalization of VPS35 with ARP2 is compromised upon strumpellin KO. U2OS_wt and U2OS_Str_KO cells were fixed and stained with the antibody against endogenous ARP2 and VPS35. VPS35 positive subdomains of the early endosomes are zoomed in the insets (**A**). Image scale bar: 10 µm. Inset scale bar: 1 µm. Images were acquired using confocal microscope Zeiss LSM800.

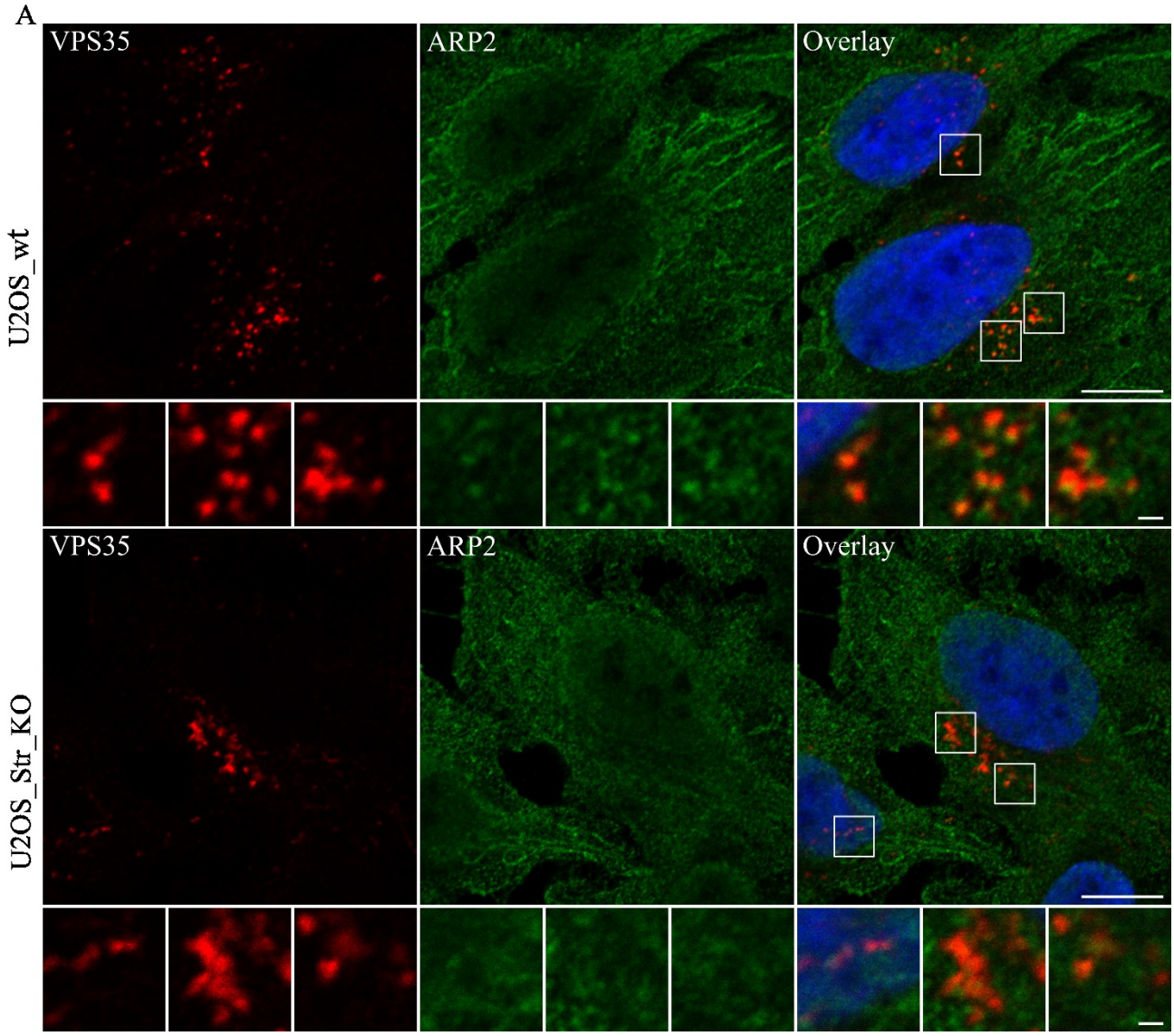

were almost, but not completely gone from the proximity of the VPS35 positive spots (**Figure 14A**). The ultimate outcome of the WASH complex activity is the nucleation of actin network on the endosomal membrane. Is the residual and truncated WASH complex able to activate Arp2/3 complex, or is strumpellin indispensable for this process?

To solve this, U2OS_Str_KO and U2OS_wt cells were fixed and stained with the antibody against VPS35 to mark early endosomes. Actin structures were labelled with the fluorescently tagged phalloidin. In wild-type cells, bright actin spots, indicating Y-branched actin, were in close proximity of VPS35 positive spots. Compared to the control cells, actin spots colocalised with VPS35 marker in U2OS_Str_KO cell line were almost, but not completely lost (**Figure 15A**).

Figure 15 – Strumpellin KO affects actin patches formation. U2OS_wt and U2OS_Str_KO cells were fixed and stained with the fluorescently labelled phalloidin488 and with the antibody against endogenous VPS35. VPS35 positive subdomains of the early endosomes are zoomed in the insets (**A**). Image scale bar: 10 µm. Inset scale bar: 1 µm. Confocal microscope Zeiss LSM880

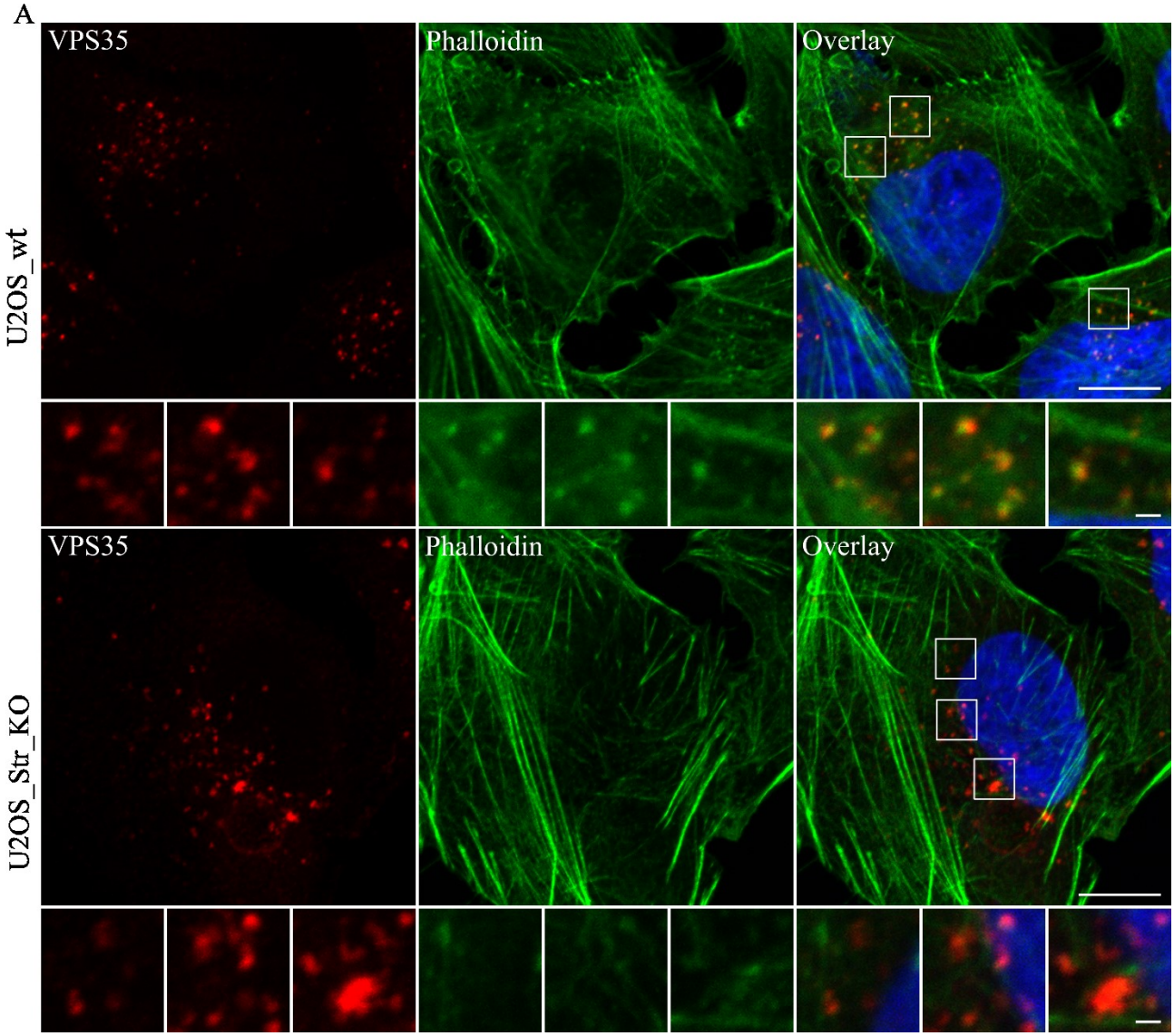

A similar phenotype was observed upon staining of MDA_Str_KO cell line with phalloidin and antibody against early endosome antigen 1 (EEA1; **Figure S7A**). Importantly, occasional, blurred and weak actin spots were still present in the area of VPS35 positive spots in U2OS_Str_KO cell line (**Figure 15A**), which is in line with the presence of the residual Arp2/3 complex at the same place.
We also performed rescue experiments. Transient overexpression rescue with full-length strumpellin proved inefficient/problematic. Therefore, we generated polyclonal U2OS_Str_KO cell line stably expressing GFP_strumpellin (U2OS_Str_KO_rescue). The expression level of GFP_strumpellin in U2OS_Str_KO_rescue cells was comparable to the expression of endogenous strumpellin in U2OS_wt cells (**Figure 16A**). We also stained U2OS_Str_KO_rescue with fluorescently tagged phalloidin. Truly, upon rescue, visible actin spots were again apparent (**Figure 16A**). Moreover, the rescue of actin spots was also accompanied with the visible rescue of VPS35 positive subdomains morphology (**Figure S8A**).

5.3.4. Recycling in the absence of strumpellin

In the previous chapter, loss of strumpellin was shown to affect the amount of the Arp2/3 complex and Y-branched actin on the membrane of the early endosome. Is this perturbation connected also to the defective cargo recycling or is the residual and truncated WASH complex still able to secure proper recycling of cargoes in the absence of the strumpellin?

To answer this question, U2OS_Str_KO and U2OS_wt cell lines were fixed and stained with the antibody against endogenous VPS35 and GLUT1. GLUT1 as it was proposed above, is cargo recycled from the early endosome back to the PM via the WASH complex dependent pathway. The clear difference between the U2OS_Str_KO and U2OS_wt cell was observed (**Figure 17A,** page 51). U2OS cells without strumpellin were prone to accumulation of GLUT1 in its early endosomes. The same phenotype was observed for the GLUT1 within the MDA_Str_KO cell line (**Figure S9A**).

TfR was proposed as another cargo recycled via the WASH dependent pathway. Thus, MDA_Str_KO cells were fixed and stained with the antibody against endogenous TfR and SWIP. In contrast to the control cells, MDA_Str_KO cells were observed with bright spots of accumulated TfR in the SWIP positive compartment (**Figure S10A**).

Together, strumpellin loss results in accumulation of GLUT1 and TfR in the early endosomal compartment. Whether the accumulation of cargo is also accompanied by the altered kinetics of the recycling remains to be uncovered.

Figure 16 – Actin patches re-appear upon rescue with GFP_strumpellin. U2OS_wt, U2OS_Str_KO and U2OS_Str_KO_rescue cells were fixed and stained with the fluorescently labelled phalloidin594 and with the antibody against endogenous strumpellin for wt and VPS35 for KO cells. Strumpellin/VPS35 positive subdomains of the early endosomes are zoomed in the insets (**A**). Image scale bar: 10 µm. Inset scale bar: 1 µm. Confocal microscope Zeiss LSM800.

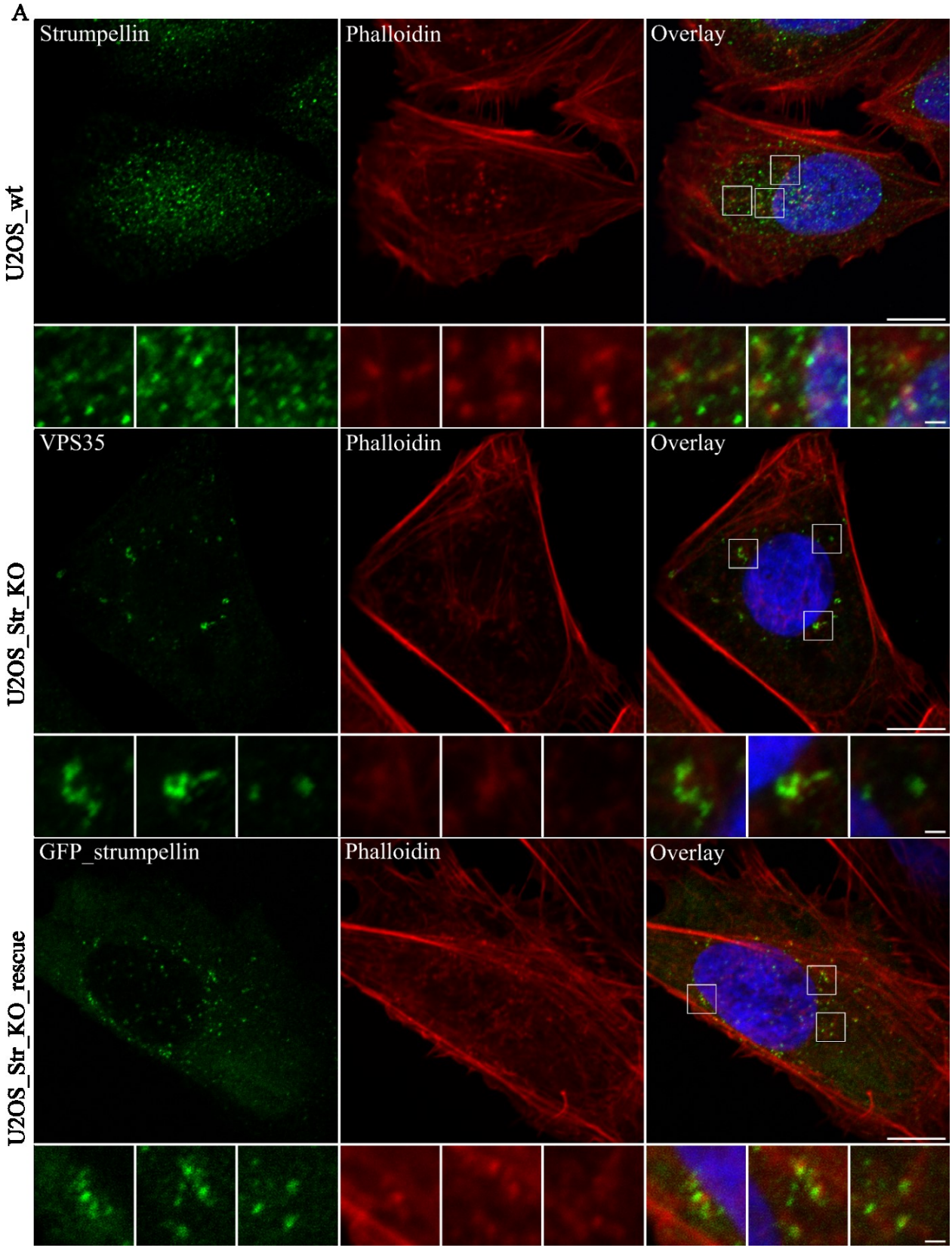

Figure 17 – GLUT1 is accumulated in the perinuclear region upon strumpellin KO. U2OS_wt and U2OS_Str_KO cells were fixed and stained with the antibody against endogenous VPS35 and GLUT1. VPS35 positive subdomains of the early endosomes are zoomed in the insets (**A**). Image scale bar: 10 µm. Inset scale bar: 1 µm. Images were acquired using confocal microscope Zeiss LSM800.

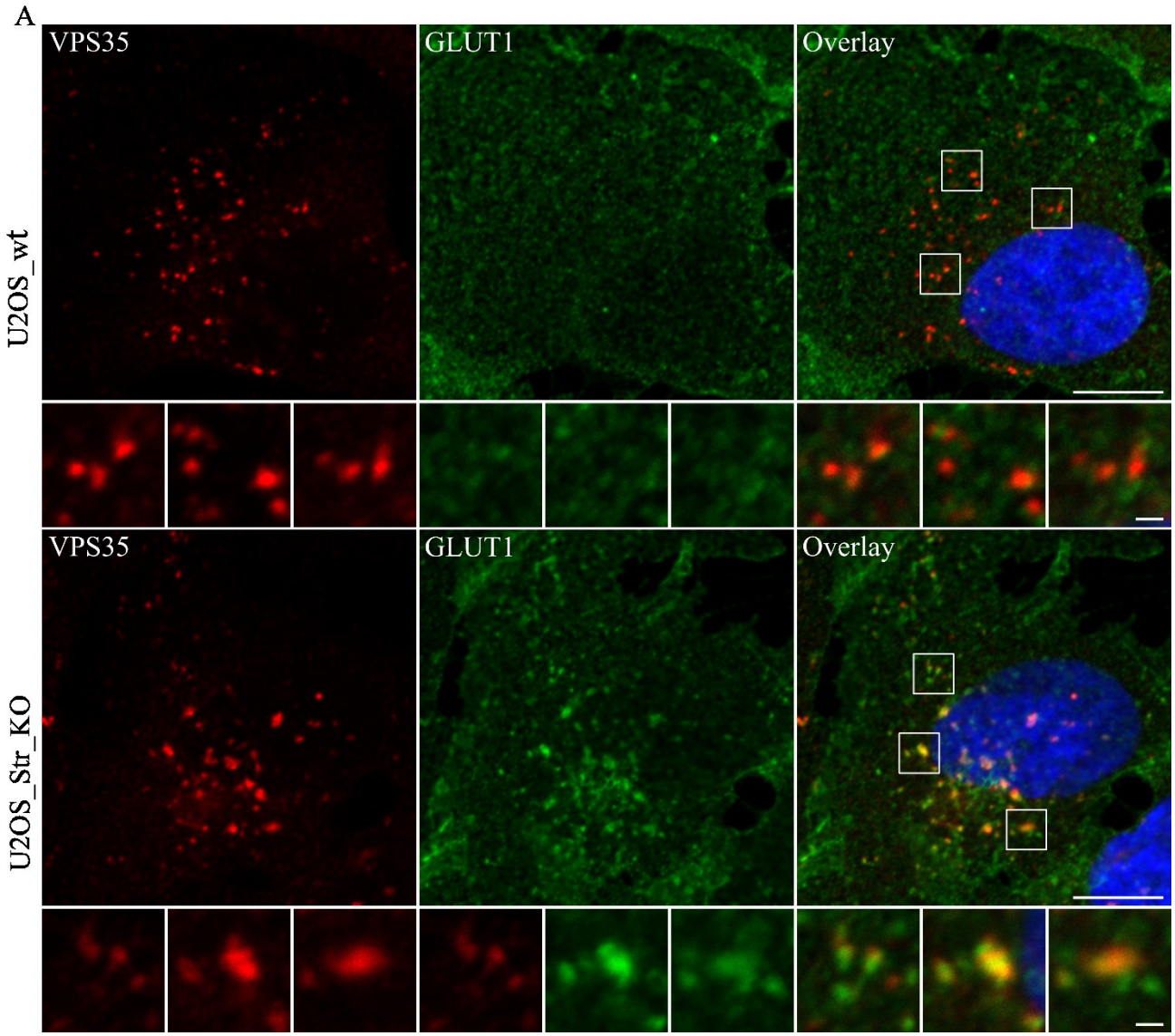

6. Discussion

6.1. Strumpellin KO cell line generation

KO cell line is a crucial tool for any study of the particular gene/protein function in the cell. Strikingly, except for two recent papers [Tyrrell et al., 2016; Song et al., 2018], researchers interested in strumpellin function used transient KD, instead of permanent KO of strumpellin, to abolish its expression in mammalian cell lines [Clemen et al., 2010; Harbour et al., 2010; Jia et al., 2010; Ryder et al., 2013]. This is of major interest, as it was shown that the KD and KO of another WASH complex member WASH1 protein have distinct effects on endosomal morphology [Derivery et al., 2009; Jia et al., 2010; Gomez et al., 2012]. Phenotypes differ probably due to the incomplete loss of WASH1 protein upon transient KD. Thus, residual activity of the WASH complex subunit targeted by KD, could still be in play and affect the observed phenotype.
Additionally, transient overexpression of recombinant full-length WASH complex subunit in wild-type cells lowered the level of its endogenous counterpart [Derivery et al., 2009; Visweshwaran et al., 2018]. This indicates, that endogenous and recombinant variants of subunits compete for the binding into the WASH complex, leading to the existence of a mixed population of WASH complexes in examined cells. In such a case, phenotype inflicted by subunit alteration is not readily identifiable, as seen in the study of Freeman [Freeman et al., 2013].
Therefore, generation of strumpellin KO cell line was an important step to avoid the above-mentioned pitfalls during the decryption of strumpellin function.

At first, we received polyclonal MDA strumpellin KO cell line from prof. Machesky laboratory (Beatson Institute for Cancer Research UK). It was used to establish our monoclonal MDA strumpellin KO cell line. MDA cells are known to be difficult to transfect. Various methods as calcium phosphate transfection or transfection with commercial reagent X-tremeGENE HP DNA Transfection Reagent were tested. None of the listed methods has proven effective for transfection of larger DNA constructs into the MDA_Str_KO cell line (data not shown). This turned out as a fundamental problem for fulfilling further goals, as the full-length strumpellin is encoded by 3480 bp cDNA.
Therefore, we were forced to employ another cell line for strumpellin elimination. We decided to use a U2OS cell line, as it was easily transfectable and the flat shape of individual cells was convenient for microscopy imaging. Hence, we established monoclonal U2OS strumpellin KO cell line.
Keeping two different strumpellin KO cell lines proved to be very useful, as we could easily verify if the observed phenotype upon strumpellin loss was cell line specific or more related to common cell physiology.

6.2. Expression of strumpellin fragments and their cellular localisation

To elucidate the function of strumpellin, we decided to divide strumpellin into parts, and subsequently express its recombinant fragments in cells lacking endogenous strumpellin. The selected approach could also reveal more precisely which part of strumpellin is indispensable for binding to the WASH complex.

6.2.1. In silico prediction and molecular cloning

According to two papers, strumpellin possess spectrin-like domain repeat, spanning from the aa 241 to 791 [Valdmanis et al., 2007; Clemen et al., 2010], with no apparent function described so far. Surprisingly, *in silico* prediction of domain organisation of strumpellin using DomPred software did not detect spectrin-like domain repeat, instead, eight shorter domains spread along the full length of strumpellin. The difference in the domain detection was most probably caused by the selected prediction tools as Valdmanis et al. used the European Bioinformatics Institute's InterProScan program, and Clemen et al. utilised the Pfam database[Valdmanis et al., 2007; Clemen et al., 2010]. Next, secondary structure prediction was done using PsiPred software. In line with previous studies, strumpellin was predicted to be mainly helical protein with few beta-sheets and many short unstructured regions [Valdmanis et al., 2007; Harbour et al., 2010]. All strumpellin fragments were successfully expressed in HEK293 cells, except for Str_C_flag which was present only in very low amounts.

6.2.2. Expression of fragments in cells deprived of strumpellin

Strumpellin fragments were expressed in U2OS_Str_KO cell line and their subcellular localisation was evaluated. From all designed fragments, only flag-tagged full length strumpellin colocalised with the endogenous SWIP positive structures, which indicated that the flag-tagged strumpellin was able to integrate into the WASH complex. Interestingly, this phenotype was not observed with myc-tagged strumpellin, which showed diffuse staining in the cytoplasm. One previously published study also reported problems with expression of strumpellin carrying myc tag on the C-terminus [Zhao et al., 2015], others mostly used the tag on the N-terminus [Jia et al., 2010; Freeman et al., 2013]. Therefore, we asked if the position or specific variant of the tag could alter strumpellin ability to be integrated into the WASH complex. Surprisingly, both GFP-strumpellin and strumpellin-GFP, localised on the same vesicular structures as the endogenous VPS35, thus were incorporated into the WASH complex. It seems that the disperse cytoplasmic pattern of full length myc-tagged strumpellin results from the combination of the particular tag sequence and its position.

Other strumpellin fragments, except for the N and C part of strumpellin coupled with myc tag, were diffusely localised in the cytoplasm lacking any apparent colocalization with the endogenous SWIP. It indicated that those fragments were not incorporated into the WASH complex. In fact, it is not surprising, that MC strumpellin fragment with myc tag had cytoplasmic localisation as a large part of the protein was similar to the full-length strumpellin with myc tag. Importantly, the same pattern was observed with flag-tagged MC strumpellin, which implies that the cytoplasmic localisation can be attributed to the MC fragment. It is possible that both selected fragmentation points disrupted structurally important region(s) and thus strumpellin fragment was no longer able to integrate into the WASH complex.

N-terminal part of the strumpellin with the myc tag localised into the nucleus. This was not in concert with the diffuse localisation of the same strumpellin fragment linked to the flag tag. Thus, it was not possible to distinguish whether the nuclear localisation is connected to the strumpellin function or it is an artefact. Nevertheless, one study described strumpellin as a part of *D. melanogaster* tata box binding factor [Valdmanis et al., 2007], which suggest nuclear localisation of strumpellin under certain conditions. Additionally, other WASH complex subunits were implicated to harbour nuclear role. FAM21 was identified as a regulator of NF-κB signalling pathway [Deng et al., 2015] and *D. melanogaster* homologue of WASH1 was described to be important for the nuclear organisation through the bond with lamins [Verboon et al., 2015]. Therefore, the N-terminal part of strumpellin could be important for the potential nuclear role of strumpellin.

Myc tagged C-terminal part of the strumpellin localised into clear dots in the cytoplasm albeit these structures were not positive for endogenous SWIP. The spots appeared to be very dense and thus resembled aggregated protein bodies rather than endosomal subdomains. Since no cells were observed to express C-terminal part of the strumpellin with the flag tag by the immunofluorescence, it was not possible to compare results of myc and flag-tagged versions.

All in all, presented results are in line with the study of Jia et al. They divided strumpellin into three roughly equivalent parts in size and tried to detect if a particular fragment of strumpellin was able to precipitate SWIP/FAM21/WASH1 or CCDC53. Only full-length strumpellin was able to precipitate members of the WASH complex [Jia et al., 2010]. On the other hand, no difference in the ability to precipitate or incorporate to the WASH complex was observed for mutated variants of strumpellin V626F, L619F or N471D, associated with HSP [Jia et al., 2010; Freeman et al., 2013]. This suggests that the effect of the strumpellin point mutations on the WASH complex assembly is too subtle to be observed or not at all connected to the WASH complex assembly and function, but rather connected to the binding of other proteins/factors. In *D. discoideum*, Song et al. showed by mass spectrometry that interactome of mutated strumpellin (N471D) is deprived off 43 proteins in comparison to wild-type strumpellin interactome [Song et al., 2018]. Among those proteins were for example COMMD1,

already described member of the CCC complex, which is important together with the WASH complex for recycling of cargoes as LDLR or ATP7A [Phillips-Krawczak et al., 2015; Bartuzi et al., 2016], V-type proton ATPase subunit d involved in the acidification/maturation of endosomes and subsequent cargo exocytosis [Marshansky et al., 2008] and myosin light chain kinase (MLCK), which is thought to be regulator of myosin coupled trafficking [Heissler et al., 2014]. Single mutation thus affected a large number of interactions connected to cargo recycling. Thus, the mechanism of HSP pathology is likely connected to the interactions of strumpellin with non-WASH complex proteins. It would be very interesting to compare results of Song et al. with interactomes of other strumpellin HSP associated variants, particularly from mammals.

Altogether, strumpellin seems to be a compact indivisible protein with no currently defined domain, connected to exclusive function. More on, recent publications imply, that strumpellin creates an important interaction platform, probably involved in fine-tuning of retrograde transport and cargoes recycling.

6.3. Analysis of the role of incomplete WASH complex in strumpellin KO cell line

6.3.1. The stability of the WASH complex subunits upon strumpellin KO

The stability of the WASH complex upon loss of one of its subunits was subject of many studies with contradictory results. In brief, KD of SWIP/strumpellin or FAM21 was published to result in the substantial, but not complete, decrease in all other WASH complex subunits. On the other hand, KD of WASH1 or CCDC53 resulted in a considerable decrease of only CCDC53 or WASH1 respectively, the amount of other subunits were altered only slightly [Derivery et al., 2009; Jia et al., 2010; unpublished results from our laboratory]. Importantly, this is not in line with another study from Gomez et al. where KO of WASH1 protein led to substantial decrease in the level of all other WASH complex subunits [Gomez et al., 2012]. Even though there are some discrepancies, it is generally accepted that each subunit of the WASH complex is stabilised by incorporation into the WASH complex, however, the existence of incomplete/partial WASH complex was not excluded. This hypothesis is further strengthened as Gomez et al. were able to detect an interaction between FAM21, SWIP and strumpellin upon WASH1 KO [Gomez et al., 2012]. It is possible that observed discrepancies between the results of research groups are caused by using different approaches of subunit alteration (KD or KO), different cell lines or different experimental setup. Notably, only one study verified the observed effects of the strumpellin KD on the stability of other WASH complex subunits within mammalian strumpellin KO cell line [Tyrrell et al., 2016].

Using a biochemical approach, we determined levels of WASH complex subunits upon strumpellin KO. Moreover, SWIP and VPS35 KO cell lines were established in our laboratory and thus effects of the complete loss of strumpellin/SWIP or major WASH complex interacting partner VPS35 could be compared.

In our cell lines, the strumpellin loss was accompanied with the substantial decrease of SWIP and FAM21 subunits. Interestingly, this was not the case for all subunits, as levels of WASH1 were affected only mildly. Same results were apparent for levels of strumpellin, FAM21 and WASH1 subunits in SWIP KO cell line. On the other hand, a large part of WASH complex subunits remained in the cells upon VPS35 KO, which indicates, that WASH complex could be efficiently assembled. Additionally, it is possible that MDA cells deprived of strumpellin somehow compensated for the accompanied loss of WASH1 and SWIP as they were held in our laboratory for a significantly longer period and thus exert elevated levels of this subunit. Importantly, the levels of the WASH1 protein should be further validated as we were able to do only one experiment. Unfortunately, CCDC53 antibody was not available in our laboratory. Therefore, we could not determine the level of CCDC53 in our KO cell lines. It remains to be established if the level of CCDC53 is affected or not.

Overall, our results are in agreement with previous studies as we saw a substantial decrease of FAM21/SWIP/strumpellin and a mild decrease of WASH1 as the other researchers [Harbour et al., 2010; Jia et al., 2010; Tyrrell et al., 2016]. WASH1 is considered to be the major subunit of the WASH complex, as it harbours WCA domain responsible for the Arp2/3 complex binding and its activation. Therefore, it is interesting that the stability of WASH1 was affected less than the stability of FAM21 or SWIP upon strumpellin KO. Thus, the mild decrease of WASH1 precludes its other possible function outside the WASH complex, for example in the nucleus [Verboon et al., 2015]. Despite numerous studies, the stoichiometry of subunits in the WASH complex is not known. Generally, it is thought, that every subunit is present in the WASH complex in one copy [Derivery et al., 2009]. Additionally, if we accept an assumption that partial WASH complex could be assembled, its overall amount should be substantially diminished upon strumpellin KO in comparison to the wild-type level, as a large part of its subunits is degraded.

6.3.2. WASH complex in the absence of strumpellin

As presented above, WASH complex subunits FAM21 and SWIP are substantially degraded in cells deprived of strumpellin. Thus, our next question was whether the residual and truncated WASH complex is still assembled. We observed that remaining SWIP and FAM21 were still localised on the VPS35 positive subdomains of the early endosomes in the strumpellin KO cells. This indicates that the WASH complex is most probably still assembled in the absence of strumpellin.
Our results are in line with a recent study, which observed assembly of partial WASH complex without strumpellin even in wild-type cells by blue native gel electrophoresis [Tyrrell et al., 2016]. Similarly, using fractionation coupled with western blot analysis, Visweshwaran and colleagues were able to identify partial WASH complex composed of FAM21, CCDC53 and WASH1 subunits [Visweshwaran et al., 2018]. Unfortunately, those data did not include any information about SWIP subunit. Therefore, it is possible that the observed partial WASH complex was the same as the one without strumpellin previously identified by Tyrrell et al. This together with the results of the yeast two-hybrid analysis of interactions between the WASH complex members [Harbour et al., 2010] and the loss of strumpellin from early endosomes upon KO of SWIP in *D. discoideum* [Park et al., 2013] suggests that strumpellin is more loosely attached to the WASH complex than other subunits and thus probably dispensable for the WASH complex assembly.

In the past, it was generally agreed that membrane association of the WASH complex is mediated by retromer. A large group of researchers claimed that interaction between FAM21 and VPS35 was the only interaction needed/responsible for the association of the WASH complex to the early endosomes [Harbour et al., 2012; Jia et al., 2012; Zavodszky et al., 2014]. The main evidence for this hypothesis was dissociation of the FAM21 protein upon KD of VPS35 [Harbour et al., 2012; Jia et al., 2012]. Interestingly, deletion of FAM21 did not result in WASH1 (or other WASH complex subunit) dissociation from the vesicular membrane in *D. discoideum* [Park et al., 2013]. Moreover, FAM21-VPS35 interaction seems to be missing in this organism, as no VPS35 was detected with mass spectrometry analysis of FAM21 interaction partners [Dostal, 2015]. In addition, purified mammalian WASH complex was shown to interact with artificially generated liposomes, which imply the existence of a retromer-independent bond between the WASH complex and liposome membrane [Derivery et al., 2009]. Therefore, we hypothesised that the FAM21-VPS35 interaction is not the only one which facilitates the binding of the WASH complex to the early endosomal membrane [Dostal, 2015; Humhalova, 2017]. This hypothesis was further underpinned by two recent findings. MacDonald et al. observed that KD of hepatocyte growth factor-regulated tyrosine kinase substrate (HRS) led to the dissociation of WASH1 from the early endosomal membrane

[MacDonald et al., 2018] and McNally et al. were able to observe endogenous FAM21 clearly localised on the endosomal membrane upon VPS35 KO [McNally et al., 2017].

Our college Humhalova already presented that FAM21 and SWIP are still apparent on the VPS35 positive subdomains in MDA strumpellin KO cell line [Humhalova, 2017]. We verified those results in another cell line and also extend it for WASH1 subunit, which exerts similar phenotype. Those results are in line with results presented by Park et al. in *D. discoideum.* Moreover, no strumpellin fragment, except for full-length flag version, was observed to be localised on structures resembling the endosomal subdomains. This suggests that strumpellin is not essential for the WASH complex membrane association. Nevertheless, we could not entirely reject the possible minor role of strumpellin in the WASH complex membrane associations, because the FAM21-VPS35 interaction was present in our strumpellin KO cell lines. Thus, partial WASH complex had still at least one major interaction, which held it at the endosomal membrane.

In summary, partial WASH complex is assembled in cells deprived of strumpellin, and strumpellin is not vital for the binding of the WASH complex to the early endosomal membrane.

6.3.3. Strumpellin loss leads to the changes in the endosomal morphology.

Set of pilot studies about the WASH complex showed that KD of its subunits led to the alteration of endosomal morphology, notably causing endosomal clustering and tubulation [Derivery et al., 2009; Gomez et al., 2009, 2012; Harbour et al., 2010]. Consequently, Gomez et al. observed, that the complete loss of WASH1 leads to the enlargement and clustering of the early endosomes in the perinuclear region [Gomez et al., 2012]. Interestingly, a similar phenotype was observed upon siRNA depletion of strumpellin or SWIP in HeLa cells [Harbour et al., 2010] and also in mouse melanocyte lineage completely deprived of strumpellin [Tyrrell et al., 2016]. In line with previous studies, our MDA_Str_KO cells had significantly larger VPS35 positive subdomains than control cells. An estimated mean for the area of VPS35 positive subdomains was 1.19 times bigger in the case of MDA_Str_KO cell line than in the control line. We noticed that U2OS cells exhibit similar phenotype upon strumpellin KO, but the statistical analysis remains to be done. Moreover, endosomes seemed to be clustered in the perinuclear region of both strumpellin KO cell lines. Importantly, it seems that upon GFP_strumpellin rescue in U2OS_Str_KO_rescue, wild-type VPS35 subdomain phenotype was restored.

It is noteworthy that the area of stained subdomains should not be addressed as a size of the whole endosome in case of immunofluorescence staining. This fact is often overlooked as well as in the case of a recent study by Tyrrell et al. [Tyrrell et al., 2016]. The size of the subdomain could be taken only as a very rough approximation of the actual endosome size. If only one protein is stained, often only one subdomain and not the whole perimeter/volume of the particular endosome is visible [Gomez et al., 2009; Duleh et al., 2010]. Thus, one could not distinguish whether the observed effect changes in the size of the whole endosome or the blurring of the endosomal subdomain/s. Here, we present our results as a difference in the size of VPS35 positive subdomains albeit we cannot exclude the potential endosome enlargement. This issue can be addressed in the future by staining endosomes with fluorescent cargo (e.g. soluble fluorescent transferrin).

The reason for VPS35 positive subdomain enlargement is currently unknown, but it is easy to imagine that WASH complex driven actin network formation provides an important scaffold for proper subdomain maintenance and/or their partition. Thus, abrogation of the WASH complex could result in the inefficient subdomain declaration followed by their enlargement, independently of the actual endosome size. Indeed, Puthenveedu et al. observed that polymerised actin is essential for particular endosomal subdomain stabilisation [Puthenveedu et al., 2010]. On the other hand, Gomez et al. did not observe global endosomal subdomain mixing upon WASH1 KO [Gomez et al., 2012]. Still, there is most probably a large number of different endosomal subdomains and Gomez et al. observed only their subset. An alternative explanation for VPS35 positive subdomain enlargement is that abrogated WASH complex cannot efficiently induce actin nucleation, which in turn disrupts tubule formation and therefore the formation of new outgoing vesicles is also substantially affected [Gomez et al., 2012]. Additionally, the WASH complex was also implied in scission of endosomal tubules [Duleh et al., 2010]. Therefore, there are two subsequent steps abrogated by WASH complex alteration connected to the new vesicle formation and its dispatch. Together, this could ultimately lead to the enlarged endosomes as no cargo, and no membrane are efficiently dispatched from the early endosome in the WASH complex dependent manner [Gomez et al., 2012]. In fact, at least two studies claimed that abrogation of the WASH complex led to the endosome enlargement [Gomez et al., 2012; Tyrrell et al., 2016]. Actually, both presented hypotheses could be proved correct in the future, as they are not in direct conflict. It is unlikely yet possible that the cause of VPS35 subdomains enlargement upon strumpellin depletion is independent of the major WASH complex function, the Arp2/3 complex activation and subsequent actin polymerisation.

In summary, strumpellin loss led to the VPS35 positive subdomain enlargement. Whether this is a result of the enlarged endosomes or only the blurring of subdomains remains to be uncovered and will require further experiments.

Besides enlarged VPS35 positive subdomains, an aberrant vacuolar-like structure was observed in a portion of U2OS_Str_KO cells. The structure was at least in one-eighth of cells, usually present in a single copy per cell in its perinuclear region. It seemed very unlikely that such a large structure was an enlarged endosome, albeit positive in VPS35 marker. Besides the VPS35, the structure was also positive in the marker of lysosomes LAMP1. In this case, the observed effect is most probably caused by the whole WASH complex deprivation as we observed the same aberrant vacuolar structures in the SWIP KO cell line (our unpublished data).
Researchers interested in WASH complex observed very similar structures upon WASH1/ SWIP or strumpellin KO in *D. discoideum* [Carnell et al., 2011; King et al., 2013; Song et al., 2018]. The structure was identified as an aberrant large lysosome [Carnell et al., 2011]. Here, the phenotype was explained by the inability to recycle V-ATPase from the lysosome back to the endosomal compartment, thus inability to neutralize lysosome, which resulted in the block of exocytosis. Strikingly, in case of WASH1 KO, phenotype was rescued by expression of wt WASH1, but not the WASH1 without VCA domain. Thus actin nucleation is important for this process [Carnell et al., 2011].
An unusual lysosomal structure was apparent also in cells lacking strumpellin. Interestingly, observed phenotype was rescued by wild-type, but ostensibly not the mutated N471D strumpellin [Song et al., 2018]. Upon N471D strumpellin rescue, structures/lysosomes were already neutralised. Thus, WASH complex was able to activate Arp2/3 complex and recycle V-ATPase away, but not able to undergo exocytosis anyway [Song et al., 2018]. This indicates that there is another step before exocytosis which is abrogated by the N471D mutation in strumpellin [Song et al., 2018]. Therefore, there needs to be an additional function for strumpellin in the WASH complex.

Still, it is not possible to address whether the observed vacuolar structure is in our case related to the lysosome stalled before exocytosis remains to be uncovered and will be the topic of further research.

6.3.4. Strumpellin is indispensable for partial WASH complex activity and proper actin patches formation

Cells lacking strumpellin displayed enlargement of VPS35 positive subdomains. Therefore, we attempted to find the reason for such a phenotype. Herein, we already discussed possible reasons behind observed VPS35 subdomain enlargement and both were tightly connected to the major WASH

complex function, the activation of Arp2/3 complex and subsequent actin network formation [Derivery et al., 2009; Gomez et al., 2009]. Hence, we tested, whether strumpellin is needed for the WASH complex ability to bind and activate Arp2/3 complex.

We were able to observe ARP2 subunit of the Arp2/3 complex localised next to the VPS35 positive spots in U2OS_wt cells. Importantly, substantial, but not complete loss of this colocalization was detected in the U2OS_Str_KO cells. This result indicated that the truncated WASH complex is still able to bind Arp2/3 complex. With this in mind, we further tested if the truncated WASH complex is able to activate Arp2/3 complex and stained cells with the phalloidin, to visualise polymerised actin. We observed substantial, but not complete decrease in the colocalization of VPS35 positive spots with bright actin patches in cells deprived of strumpellin. More precisely, it seemed, that residual actin patches were still present, although the pattern and intensity of the signal were substantially affected. Importantly, actin patches re-appeared upon strumpellin rescue. Both results are in agreement with the observation made by Tyrrell et al., as they were able to observe p34, a subunit of the Arp2/3 complex and residual polymerised actin on early endosomes in the absence of strumpellin [Tyrrell et al., 2016].

There are two possible interpretations of the observed phenotype. Firstly, the strumpellin loss itself leads to the decreased ability of the WASH complex to bind or activate the Arp2/3 complex. This suggests that strumpellin presence somehow regulate the activity of the WASH complex. However, further experiments corroborating this hypothesis are needed. It would be very interesting to address this issue in vitro. One of the possible approaches could examine the difference in the colocalization of recombinant partial (without strumpellin) and complete WASH complex with Arp2/3 complex, and factors responsible for WASH complex activation [Jia et al., 2010; Hao et al., 2013]. Alternatively, an overall outcome in the form of actin polymerisation could be measured in vitro, e.g. in the form of Pyrene-actin polymerisation assay [Linardopoulou et al., 2007; Duleh et al., 2010]. The second possible interpretation of the observed phenotype is that the overall loss of the WASH complex causes the loss of ARP2 and actin spots from the early endosomes in cells lacking strumpellin. Unfortunately, we were not able to answer this question similarly to Tyrrell et al. [Tyrrell et al., 2016]. Functional studies allowing to distinguish between both possibilities are awaited.

The WASH complex was proposed as a factor needed for the recycling of various cargoes [Derivery et al., 2009; Gomez et al., 2009; Duleh et al., 2010; Zech et al., 2011]. We were able to observe a substantial decrease in the amount of the WASH complex upon strumpellin KO. However, residual and truncated WASH complex was still present on the membrane of the early endosome. Moreover, it retained at least to some extent its ability to bind and activate Arp2/3 complex. On the

other hand, endosomal morphology seemed abrogated. Therefore, we asked, what effect does have the loss of strumpellin on cargo recycling?

One of the cargoes, which are proposed to be recycled from the endosome back to the plasma membrane in WASH dependent manner, is GLUT1 [Piotrowski et al., 2013]. The pattern of GLUT1 distribution in cells lacking strumpellin was substantially altered in comparison to the control cells. Loss of strumpellin led to the apparent shift from more ectopically localised GLUT1 in wild-type cells to the accumulation of the GLUT1 signal in the early endosomes of KO cell lines.

Another cargo, which was implied in WASH complex dependent recycling is TfR [Derivery et al., 2009; Humhalova, 2017]. In MDA cell line we observed for TfR similar phenotype as in the case of GLUT1. TfR was accumulated in the early endosomes upon strumpellin KO.

Importantly, it is not clear, whether the WASH complex is responsible for recycling of GLUT1 or TfR. Piotrowski et al. were able to see a defect in GLUT1 recycling and connected glucose uptake upon WASH1 KO in mouse T cells [Piotrowski et al., 2013], but this was not the case for all researchers [Steinberg et al., 2013; McGough et al., 2014]. McGough et al. did not observe the change in GLUT1 recycling upon expression of VPS35 with mutation D620N, which is proposed to abrogate at least partly WASH complex membrane association and thus probably its ability to recycle cargoes [McGough et al., 2014]. Additionally, Steinberg et al. presented that SNX27-retromer, another WASH complex interacting partner implicated together with the WASH complex in recycling, is vital for GLUT1 recycling. The depletion of SNX27 affected GLUT1 recycling. Re-expression of SNX27 rescued this phenotype, even though the WASH complex binding domain was deleted [Steinberg et al., 2013]. Importantly, only Piotrowski et al. from studies mentioned above interested in GLUT1 recycling used direct WASH complex abrogation [Piotrowski et al., 2013]. It is possible that in case of the other studies [Steinberg et al., 2013; McGough et al., 2014], important non-abrogated factor remained still in the cell and thus an apparent defect in GLUT1 recycling was not observed.

Similarly, there is not complete consensus, whether the WASH complex is important for TfR recycling. At least two studies observed a defect in TfR upon WASH1 KD [Derivery et al., 2009; Zech et al., 2011], but the other did not [Duleh et al., 2010; Gomez et al., 2012; Ryder et al., 2013]. Importantly, Gomez et al. presented, that altered endosomal morphology and pattern of TfR upon WASH1 KO is not necessarily connected to the defect in TfR recycling kinetics [Gomez et al., 2012]. The discrepancies mentioned above are probably caused by the different methods or cell line used for the measurement of the effect of WASH complex deprivation on TfR recycling.

Altogether, the distribution pattern of GLUT1 and TfR is altered in cell lacking strumpellin.

In general, we observed several substantial changes in the cells lacking strumpellin. However, it is crucial to bear in mind that we were not capable to distinguish, whether the observed changes in phenotype was a manifestation of the strumpellin loss or the overall loss of the whole/partial WASH complex. Additional experiments are needed to elucidate this.

7. Conclusion

During the last decade, the role of the WASH complex in the cell has been extensively studied. It was shown, that WASH complex is a major endosomal NPF and is responsible for recycling of many cargoes. Importantly, the function of strumpellin and SWIP subunits has been determined only sparsely, as most of the studies were interested in the WASH1 and FAM21 subunits. Therefore, strumpellin was selected as a main subject of this study.

In this work, cell line completely deprived of strumpellin was created as an essential tool enabling analysis of strumpellin function. Truncated fragments of strumpellin were designed and their cellular localization was examined. Importantly, only full-length strumpellin was able to colocalize with the other WASH complex subunits on the early endosomes, which imply that the intact strumpellin is needed for incorporation into the WASH complex. It suggests that strumpellin does not harbour any internal domain with a separate function and operates as one indivisible unit.

The role of strumpellin was further examined in strumpellin KO cell line. In agreement with previous studies, strumpellin absence resulted in the destabilization of the other WASH complex subunits. Interestingly, incomplete WASH complex was still assembled on the membrane of early endosomes. Finally, cells lacking strumpellin displayed enlarged VPS35 positive subdomains of early endosomes. This is very likely connected to the large loss of actin patches from the membrane of early endosomes in these cells. Additionally, WASH complex dependent cargo GLUT1 and TfR were accumulated in the early endosomal compartment.

However, it is important to keep in mind that we were not able to address, whether the observed effects were direct consequences of strumpellin loss or were rather related to the reduced level of the WASH complex.

In this work, we were able to bring further insight into the role of strumpellin in cells. The goals of this diploma work were fulfilled although the intriguing nature of strumpellin offers many further questions.

8. Acknowledgement

Firstly, I would like to thank my supervisor Lenka Libusová for valuable advice, inspiring suggestions and great patience during my Master´s studies. Her unerring guidance and knowledge helped me a lot all the time in both, experiments and thesis writing.

Besides my supervisor, I would like to thank all members of the Laboratory of Molecular Genetics of Development at Faculty of Science, Charles University, who were able to create a pleasant and inspiring environment at once. I am grateful to Tereza Humhalová for providing U2OS SWIP and VPS35 knockout cell lines and Ben Tyrrell (Beatson Institute for Cancer Research, UK) for providing polyclonal MDA strumpellin knockout cells. My thanks also go to Matthew Seaman (University of Cambridge, UK) for strumpellin_GFP construct. I would like to thank Ondřej Šebesta for help with fluorescence microscopy and image analysis and Martin Weisser for assistance with statistics. I am also grateful to Vojtěch Dostál and Nikola Sixtová for their unbiased comments on this thesis.

9. Abbreviations

ARID	autosomal recessive intellectual disability
ARP2	actin-related protein 2
Arp2/3 complex	actin-related proteins 2 and 3 complex
ATG9A	autophagy related protein 9A
ATP / ADP	adenosintriphosphate / adenosindiphosphate
ATP7A	ATPase 7A
β2AR	β2-andrenergic receptor
BAR	Bin-Amphyphisin-Rvs
BSA	bovine serum albumin
CapZα / β	capping protein Z band α / β
CCC complex	CCDC22, CCDC93, COMMD1 complex
CCDC22 / 53 / 93	coiled-coil domain containing protein 22 / 53 / 93
CIMPR	cation independent mannose-6-phosphate receptor
COMMD1	copper metabolism MURR1 domain containing protein
CSC	cargo selective complex
DNA	deoxyribonucleic acid
DMEM	Dulbecco`s Modified Eagle Medium
EDTA	ethylenediaminetetraacetic acid
EEA1	early endosome antigen 1
FAM21	family with sequence similarity 21
GFP	green-fluorescent protein
GLUT1	glucose transporter 1
HSP	hereditary spastic paraplegia
HRS	hepatocyte growth factor–regulated tyrosine kinase substrate
JMY	junction-mediating and regulatory protein
KD	knockdown
KO	knockout
LAMP1	lysosomal-associated membrane glycoprotein 1
LB	lysogeny broth
LDLR	low-density lipoprotein receptor
MAGE-L2	melanoma antigen family l2
MLCK	myosin light chain kinase
NFP	nucleation-promoting factor
NF-κB	nuclear factor kappa-light-chain-enhancer of activated B cells
NLS	nuclear localization signal
PAGE	polyacrylamide gel electrophoresis
PBS	phosphate buffer saline
PCR	polymerase chain reaction
PD	Parkinson´s disease
PM	plasmatic membrane
PX	phox homology
Rac1	Ras-related C3 botulinum toxin substrate 1
Rab7a	Ras-associated in brain 7a
RhoA	Ras homolog family member A
RING	really interesting new gene
RME-8	receptor-mediated endocytosis 8
SDS	sodium dodecyl sulphate
SHRC	WASH regulatory complex
SNARE	soluble NSF attachment protein receptor
SNX	sorting nexin
SPG8	spastic paraplegia gene 8
SWIP	strumpellin and WASH1 interacting protein
TAE	Tris-acetate EDTA
TBR	tubulin-binding region

TBST	Tris-buffer saline and tween 20
TEMED	tetramethylethylenediamine
TfR	transferrin receptor
TGN	trans-Golgi network
TRIM27	tripartite motif containing 27
VAMP7	vesicle associated membrane protein 7
VPS26 / 29 / 35	vacuolar protein sorting 26/29/35
WAFL	WASP and FKBP like protein
WAHD1 / 2	WASH homology domain 1 / 2
WASH	WASP and Scar homolog
WASP	Wiskott-Aldrich syndrome protein
WAVE	Verprolin homologous protein
WHAMM	WASP homolog associated with actin, membranes, and microtubules
wt	wild-type

10. References

Alekhina, O.; Burstein, E.; Billadeau, D. D., 2017: Cellular functions of WASP family proteins at a glance. *Journal of Cell Science*., 130, 2235–2241.

Anitei, M.; Hoflack, B., 2011: Bridging membrane and cytoskeleton dynamics in the secretory and endocytic pathways. *Nature Cell Biology*., 14, 11–19.

Bartuzi, P.; Billadeau, D. D.; Favier, R. et al., 2016: CCC- and WASH-mediated endosomal sorting of LDLR is required for normal clearance of circulating LDL. *Nature Communications*., 7.

Bateman, A.; Martin, M. J.; O'Donovan, C. et al., 2017: UniProt: The universal protein knowledge base. *Nucleic Acids Research*., 45, 158–169.

Bettencourt, C.; Morris, H. R.; Singleton, A. B. et al., 2013: Exome sequencing expands the mutational spectrum of SPG8 in a family with spasticity responsive to l-DOPA treatment. *Journal of Neurology*., 260, 2414–2416.

Blackstone, C.; Kane, C. J. O., 2011: Hereditary spastic paraplegias: membrane traffic and the motor pathway. *Nature reviews. Neuroscience*., 12, 31–42.

Bolker Ben; R Development Core Team (2016). bbmle: Tools for general maximum likelihood estimation. R package version 1.0.18.

Bryson, K.; Cozzetto, D.; Jones, D. T., 2007: Computer-Assisted Protein Domain Boundary Prediction Using the Dom-Pred Server. *Current Protein and Peptide Science*., 8, 181–188.

Buchan, D. W. A.; Minneci, F.; Nugent, T. C. O. et al., 2013: Scalable web services for the PSIPRED Protein Analysis Workbench. *Nucleic acids research*., 41, 349–357.

Campellone, K. G.; Welch, M. D., 2010: A nucleator arms race: cellular control of actin assembly. *Nature reviews. Molecular cell biology*., 11, 237–251.

Carnell, M.; Zech, T.; Calaminus, S. D. et al., 2011: Actin polymerization driven by WASH causes V-ATPase retrieval and vesicle neutralization before exocytosis. *Journal of Cell Biology*., 193, 831–839.

Clemen, C. S.; Tangavelou, K.; Strucksberg, K. H. et al., 2010: Strumpellin is a novel valosin-containing protein binding partner linking hereditary spastic paraplegia to protein aggregation diseases. *Brain*., 133, 2920–2941.

Cullen, P. J., 2008: Endosomal sorting and signalling: an emerging role for sorting nexins. *Nature reviews. Molecular cell biology*., 9, 574–582.

De Bot, S. T.; Vermeer, S.; Buijsman, W. et al., 2013: Pure adult-onset spastic paraplegia caused by a novel mutation in the KIAA0196 (SPG8) gene. *Journal of neurology*., 260, 1765–1769.

De Bot, S. T.; Schelhaas, H. J.; Kamsteeg, E. J. et al., 2012: Hereditary spastic paraplegia caused by a mutation in the VCP gene. *Brain*., 135, 1–3.

Deng, Z. H.; Gomez, T. S.; Osborne, D. G. et al., 2015: Nuclear FAM21 participates in NF-κB-dependent gene regulation in pancreatic cancer cells. *Journal of cell science*., 128, 373–384.

Derivery, E.; Sousa, C.; Gautier, J. J. et al., 2009: The Arp2/3 activator WASH controls the fission of endosomes through a large multiprotein complex. *Developmental cell*., 17, 712–723.

Derivery, E.; Gautreau, A., 2010: Evolutionary conservation of the WASH complex, an actin polymerization machine involved in endosomal fission. *Communicative & integrative biology*., 3, 227–230.

Dostal, V., 2015: Analysis of WASH complex component FAM21. *Charles University, Faculty of Science.*

Duleh, S. N.; Welch, M. D., 2010: WASH and the Arp2/3 complex regulate endosome shape and trafficking. *Cytoskeleton*., 67, 193–206.

Eden, S.; Rohatgi, R.; Podtelejnikov, A. V. et al., 2002: Mechanism of regulation of WAVE1-induced actin nucleation by Rac1 and Nck. *Nature*., 418, 790–793.

Elliott, A. M.; Simard, L. R.; Coghlan, G. et al., 2013: A novel mutation in KIAA0196: identification of a gene involved in Ritscher-Schinzel/3C syndrome in a First Nations cohort. *Journal of Medical Genetics*., 50, 819–822.

Freeman, C. L.; Seaman, M. N. J.; Reid, E., 2013: The hereditary spastic paraplegia protein strumpellin: Characterisation in neurons and of the effect of disease mutations on WASH complex assembly and function. *Biochimica et Biophysica Acta - Molecular Basis of Disease*., 1832, 160–173.

Freeman, C. L.; Hesketh, G.; Seaman, M. N. J., 2014: RME-8 coordinates the activity of the WASH complex with the function of the retromer SNX dimer to control endosomal tubulation. *Journal of cell science*., 127, 2053–2070.

Gomez, T. S.; Billadeau, D. D., 2009: A FAM21-containing WASH complex regulates retromer-dependent sorting. *Developmental cell*., 17, 699–711.

Gomez, T. S.; Gorman, J. A.; Artal-Martinez de Narvajas, A. et al., 2012: Trafficking defects in WASH-knockout fibroblasts originate from collapsed endosomal and lysosomal networks. *Molecular Biology of the Cell*., 23, 3215–3228.

Hao, Y. H.; Doyle, J. M.; Ramanathan, S. et al., 2013: Regulation of WASH-dependent actin polymerization and protein trafficking by ubiquitination. *Cell*., 152, 1051–1064.

Harbour, M. E.; Breusegem, S. Y. A.; Antrobus, R. et al., 2010: The cargo-selective retromer complex is a recruiting hub for protein complexes that regulate endosomal tubule dynamics. *Journal of cell science*., 123, 3703–3717.

Harbour, M. E.; Breusegem, S. Y.; Seaman, M. N. J., 2012: Recruitment of the endosomal WASH complex is mediated by the extended 'tail' of Fam21 binding to the retromer protein Vps35. *Biochemical Journal*., 442, 209–220.

Heissler, S. M.; Sellers, J. R., 2014: Myosin light chains: Teaching old dogs new tricks. *Bioarchitecture*., 4, 169–188.

Helfer, E.; Harbour, M. E.; Henriot, V. et al., 2013: Endosomal recruitment of the WASH complex: Active sequences and mutations impairing interaction with the retromer. *Biology of the Cell*., 105, 191–207.

Humhalova, T., 2017: Characterization of WASH complex member protein SWIP. *Charles University, Faculty of Science.*

Ichinose, Y.; Koh, K.; Fukumoto, M. et al., 2016: Exome sequencing reveals a novel missense mutation in the KIAA0196 gene in a Japanese patient with SPG8. *Clinical Neurology and Neurosurgery*., 144, 36–38.

Insall, R. H.; Veltman, D. M., 2010: WASP family proteins: their evolution and its physiological implications. *Molecular biology of the cell*., 21, 2880–2893.

Ishiura, H.; Takahashi, Y.; Hayashi, T. et al., 2014: Molecular epidemiology and clinical spectrum of hereditary spastic paraplegia in the Japanese population based on comprehensive mutational analyses. *Journal of human genetics*., 59, 163–172.

Jahic, A.; Kreuz, F.; Zacher, P. et al., 2014: A novel strumpellin mutation and potential pitfalls in the molecular diagnosis of hereditary spastic paraplegia type SPG8. *Journal of the Neurological Sciences*., 347, 372–374.

Jahic, A.; Khundadze, M.; Jaenisch, N. et al., 2015: The spectrum of KIAA0196 variants, and characterization of a murine knockout: implications for the mutational mechanism in hereditary spastic paraplegia type SPG8. *Orphanet Journal of Rare Diseases*., 10, 147–157.

Jia, D.; Gomez, T. S.; Billadeau, D. D. et al., 2012: Multiple repeat elements within the FAM21 tail link the WASH actin regulatory complex to the retromer. *Molecular Biology of the Cell*., 23, 2352–2361.

Jia, D.; Gomez, T. S.; Metlagel, Z. et al., 2010: WASH and WAVE actin regulators of the Wiskott-Aldrich syndrome protein (WASP) family are controlled by analogous structurally related complexes. *Proceedings of the National Academy of Sciences*., 107, 10442–10447.

Jovic, M.; Sharma, M.; Rahajeng, J. et al., 2010: The early endosome: A busy sorting station for proteins at the crossroads. *Histology and Histopathology*., 25, 99–112.

King, J. S.; Gueho, A.; Hagedorn, M. et al., 2013: WASH is required for lysosomal recycling and efficient autophagic and phagocytic digestion. *Molecular Biology of the Cell*., 24, 2714–2726.

Linardopoulou, E. V; Parghi, S. S.; Friedman, C. et al., 2007: Human subtelomeric WASH genes encode a new subclass of the WASP family. *PLoS genetics*., 3, 2478-2485.

Liu, R.; Abreu-Blanco, M. T.; Barry, K. C. et al., 2009: Wash functions downstream of Rho and links linear and branched actin nucleation factors. *Development.*, 136, 2849–2860.

MacDonald, E.; Brown, L.; Selvais, A. et al., 2018: HRS-WASH axis governs actin-mediated endosomal recycling and cell invasion. *Journal of Cell Biology*., 217, 2549–2564.

Marshansky, V.; Futai, M., 2008: The V-type H+-ATPase in vesicular trafficking: targeting, regulation and function. *Current Opinion in Cell Biology*., 20, 415–426.

McGough, I. J.; Steinberg, F.; Jia, D. et al., 2014: Retromer binding to FAM21 and the WASH complex is perturbed by the Parkinson disease-linked VPS35(D620N) mutation. *Current Biology*., 24, 1670–1676.

McNally, K. E.; Faulkner, R.; Steinberg, F. et al., 2017: Retriever is a multiprotein complex for retromer-independent endosomal cargo recycling. *Nature Cell Biology*., 19, 1214–1225.

Mutterer, J.; Zinck, E., 2013: Quick-and-clean article figures with FigureJ. *Journal of Microscopy*., 252, 89–91.

Nagel, B. M.; Bechtold, M.; Rodriguez, L. G. et al., 2017: *Drosophila* WASH is required for integrin-mediated cell adhesion, cell motility and lysosomal neutralization. *Journal of Cell Science*., 130, 344–359.

Neveling, K.; Feenstra, I.; Gilissen, C. et al., 2013: A post-hoc comparison of the utility of Sanger sequencing and exome sequencing for the diagnosis of heterogeneous diseases. *Human Mutation*., 34, 1721–1726.

Park, L.; Thomason, P. A.; Zech, T. et al. 2013: Cyclical action of the WASH Complex: FAM21 and Capping protein drive WASH recycling, not initial recruitment. *Developmental Cell*., 24, 169–181.

Phillips-Krawczak, C. A.; Singla, A.; Starokadomskyy, P. et al., 2015: COMMD1 is linked to the WASH complex and regulates endosomal trafficking of the copper transporter ATP7A. *Molecular biology of the cell*., 26, 91–103.

Piotrowski, J. T.; Gomez, T. S.; Schoon, R. A. et al., 2013: WASH knockout T cells demonstrate defective receptor trafficking, proliferation, and effector function. *Molecular and Cellular Biology*., 33, 958–973.

Pollard, T. D., 2016: Actin and Actin-binding proteins. *Cold Spring Harbor perspectives in biology*., 8, 1–18.

Puthenveedu, M. A.; Lauffer, B.; Temkin, P. et al. 2010: Sequence-dependent sorting of recycling proteins by actin-stabilized endosomal microdomains. *Cell*., 143, 761–773.

R Core Team (2014). R: A language and environment for statistical computing. *R Foundation for Statistical Computing, Vienna, Austria*.

Ropers, F.; Derivery, E.; Hu, H. et al., 2011: Identification of a novel candidate gene for non-syndromic autosomal recessive intellectual disability: the WASH complex member SWIP. *Human Molecular Genetics*., 20, 2585–2590.

Rottner, K.; Hanisch, J.; Campellone, K. G., 2010: WASH, WHAMM and JMY: Regulation of Arp2/3 complex and beyond. *Trends in Cell Biology*., 20, 650–661.

Ryder, P. V.; Vistein, R.; Gokhale, A. et al. 2013: The WASH complex, an endosomal Arp2/3 activator, interacts with the Hermansky-Pudlak syndrome complex BLOC-1 and its cargo phosphatidylinositol-4-kinase type II . *Molecular Biology of the Cell*., 24, 2269–2284.

Salinas, S.; Proukakis, C.; Crosby, A. et al., 2008: Hereditary spastic paraplegia: clinical features and pathogenetic mechanisms. *The Lancet Neurology*., 7, 1127–1138.

Schindelin, J.; Arganda-Carreras, I.; Frise, E. et al. 2012: Fiji: An open-source platform for biological-image analysis. *Nature Methods*., 9, 676–682.

Schindelin, J.; Rueden, C. T.; Hiner, M. C. et al., 2015: The ImageJ ecosystem: An open platform for biomedical image analysis. *Molecular Reproduction and Development*., 82, 518–529.

Seaman, M. N. J., 2012: The retromer complex - endosomal protein recycling and beyond. *Journal of cell science*., 125, 4693–4702.

Seaman, M. N. J.; Gautreau, A.; Billadeau, D. D., 2013: Retromer-mediated endosomal protein sorting: All WASHed up! *Trends in Cell Biology*., 23, 522–528.

Song, L.; Rijal, R.; Karow, M. et al., 2018: Expression of N471D strumpellin leads to defects in the endolysosomal system. *Disease Models & Mechanisms*., 10.

Steinberg, F.; Gallon, M.; Winfield, M. et al., 2013: A global analysis of SNX27-retromer assembly and cargo specificity reveals a function in glucose and metal ion transport. *Nature cell biology*., 15, 461–471.

Temkin, P.; Lauffer, B.; Jäger, S. et al., 2011: SNX27 mediates retromer tubule entry and endosome-to-plasma membrane trafficking of signalling receptors. *Nature Cell Biology*., 13, 717–723.

Trautmann Heike; Steuer Detlef; Mersmann Olaf; Bornkamp Björn (2014). truncnorm: Truncated normal distribution. R package version 1.0-7.

Tyrrell, B. J.; Woodham, E. F.; Spence, H. J. et al., 2016: Loss of strumpellin in the melanocytic lineage impairs the WASH Complex but does not affect coat colour. *Pigment Cell & Melanoma Research*., 29, 559-571.

Valdmanis, P. N.; Meijer, I. A.; Reynolds, A. et al., 2007: Mutations in the KIAA0196 gene at the SPG8 locus cause hereditary spastic paraplegia. *American journal of human genetics*., 80, 152–161.

Verboon, J. M.; Rincon-Arano, H.; Werwie, T. R. et al., 2015: Wash interacts with lamin and affects global nuclear organization. *Current Biology*., 25, 804–810.

Visweshwaran, S. P.; Thomason, P. A.; Guerois, R. et al., 2018: The trimeric coiled-coil HSBP1 protein promotes WASH complex assembly at centrosomes. *The EMBO Journal*., 37

Wang, X. L. B.; Yang, Y. H.; Li, C. J. et al., 2014: A novel KIAA0196 (SPG8) mutation in a Chinese family with spastic paraplegia. *Chinese Medical Journal*., 127, 1987–1989.

Zavodszky, E.; Seaman, M. N. J.; Moreau, K. et al., 2014: Mutation in VPS35 associated with Parkinson's disease impairs WASH complex association and inhibits autophagy. *Nature Communications*., 5, 3828.

Zech, T.; Calaminus, S. D. J.; Caswell, P. et al., 2011: The Arp2/3 activator WASH regulates α5β1-integrin-mediated invasive migration. *Journal of cell science*., 124, 3753–3759.

Zhao, J.; Hedera, P., 2015: Strumpellin and Spartin, Hereditary spastic paraplegia proteins, are binding partners. *Journal of Experimental Neuroscience*., 9, 15.

11. Supplementary materials

Supplementary figure 1 – Verification of the absence of strumpellin in U2OS cell line by the immunofluorescence staining. U2OS_wt and U2OS_Str_KO cells were stained using the antibody against endogenous strumpellin and VPS35. VPS35 positive subdomains of the early endosomes are zoomed in the insets. (**A**). Image scale bar: 10 µm; inset scale bar: 1 µm. Images were acquired using confocal microscope Zeiss LSM800.

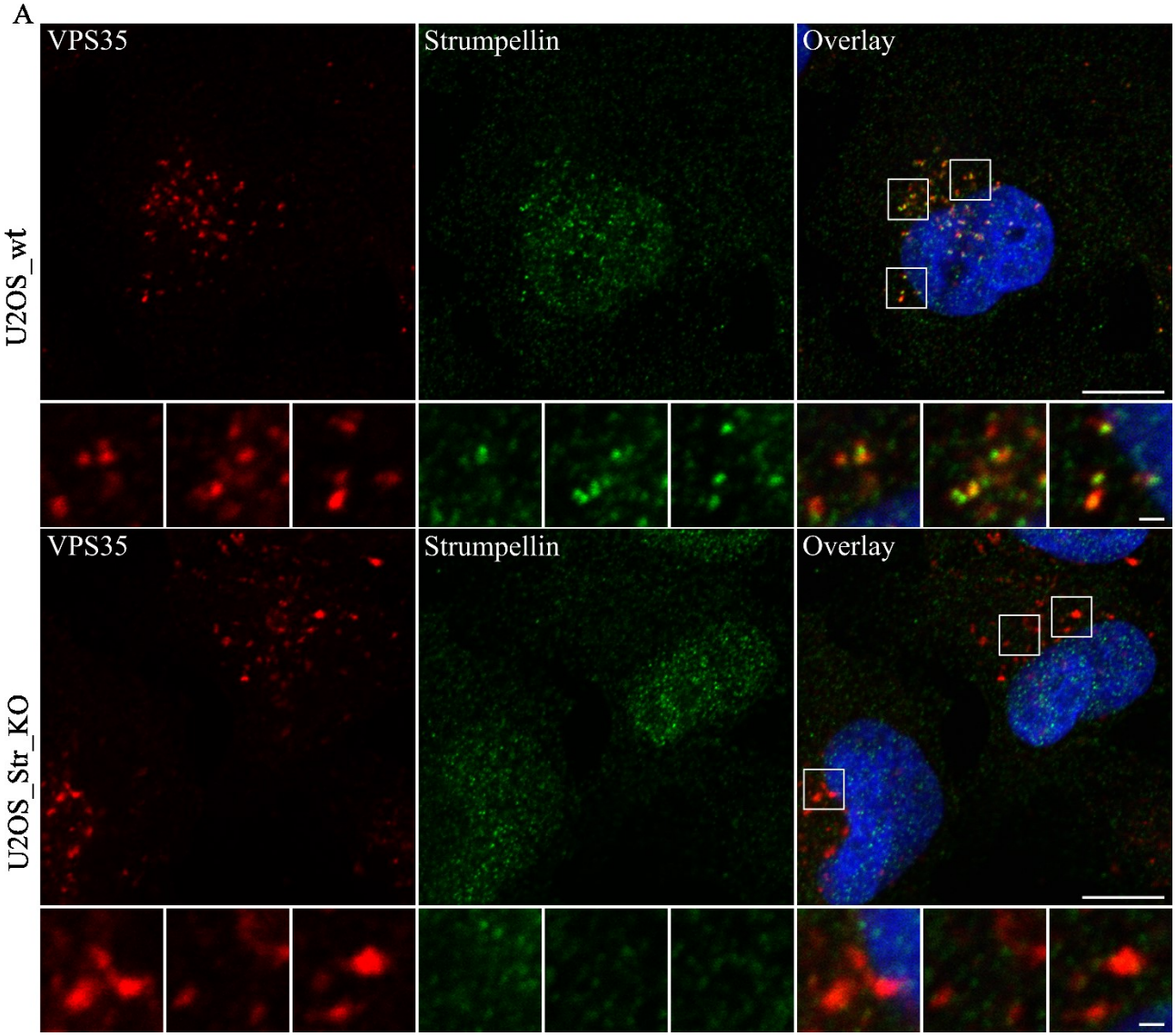

Supplementary figure 2 – Verification of the strumpellin deletion in MDA cell line by the immunofluorescence staining. MDA_wt and MDA_Str_KO cells were stained using the antibody against endogenous strumpellin and VPS35. VPS35 positive subdomains of the early endosomes are zoomed in the insets. (**A**). Image scale bar: 10 µm; inset scale bar: 1 µm. Images were acquired using confocal microscope Zeiss LSM800.

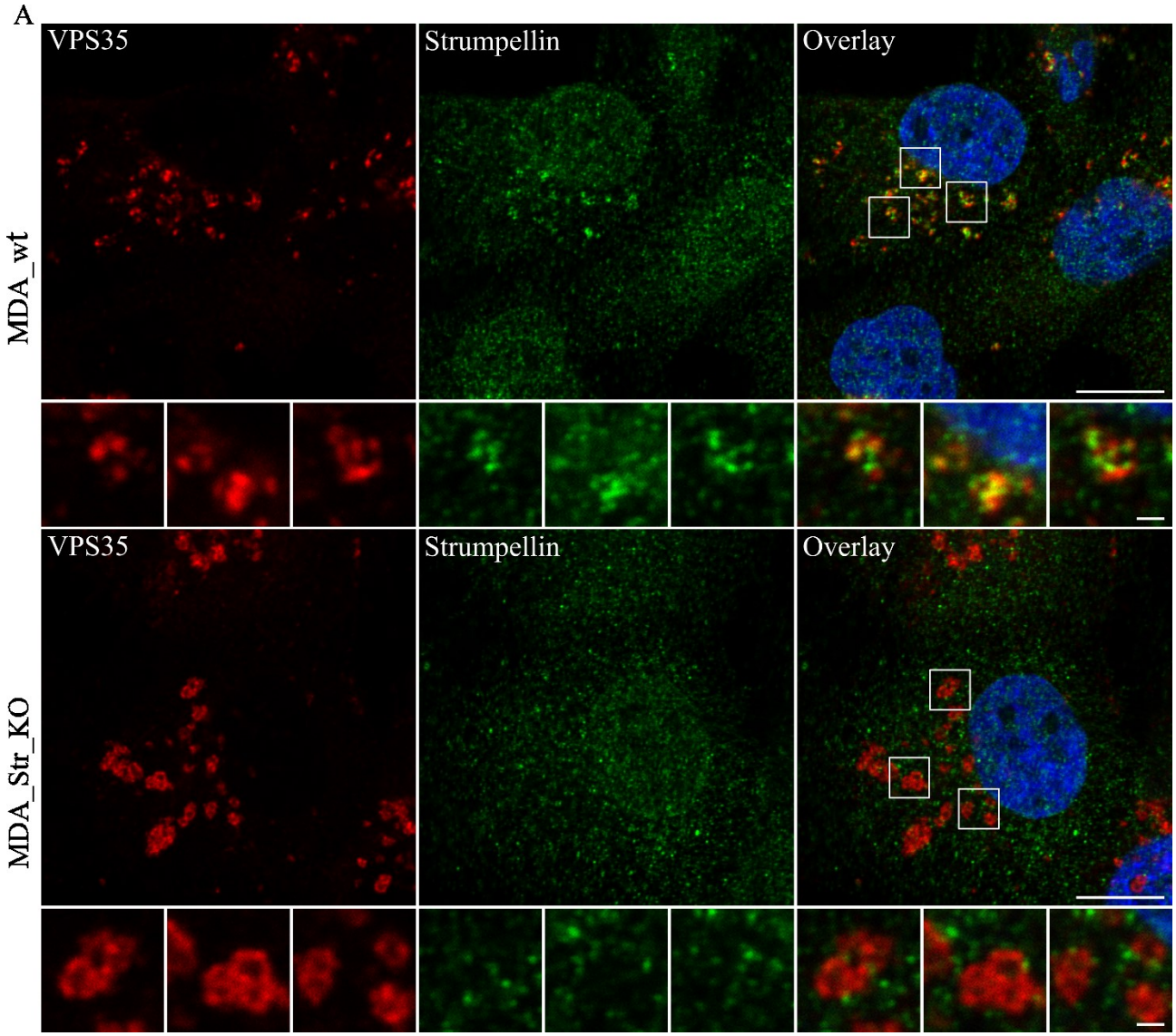

Supplementary figure 3 – Expression of Str_MC/M/N_flag fragments in the U2OS_Str_KO cell line, stained with the antibodies against the flag tag and endogenous SWIP (**A**), the rest of the fragments is presented in the **Figure 8A**. VPS35 positive subdomains of the early endosomes are zoomed in the insets. Image scale bar: 10 µm. Inset scale bar: 1 µm. Images were acquired using confocal microscope Zeiss LSM800.

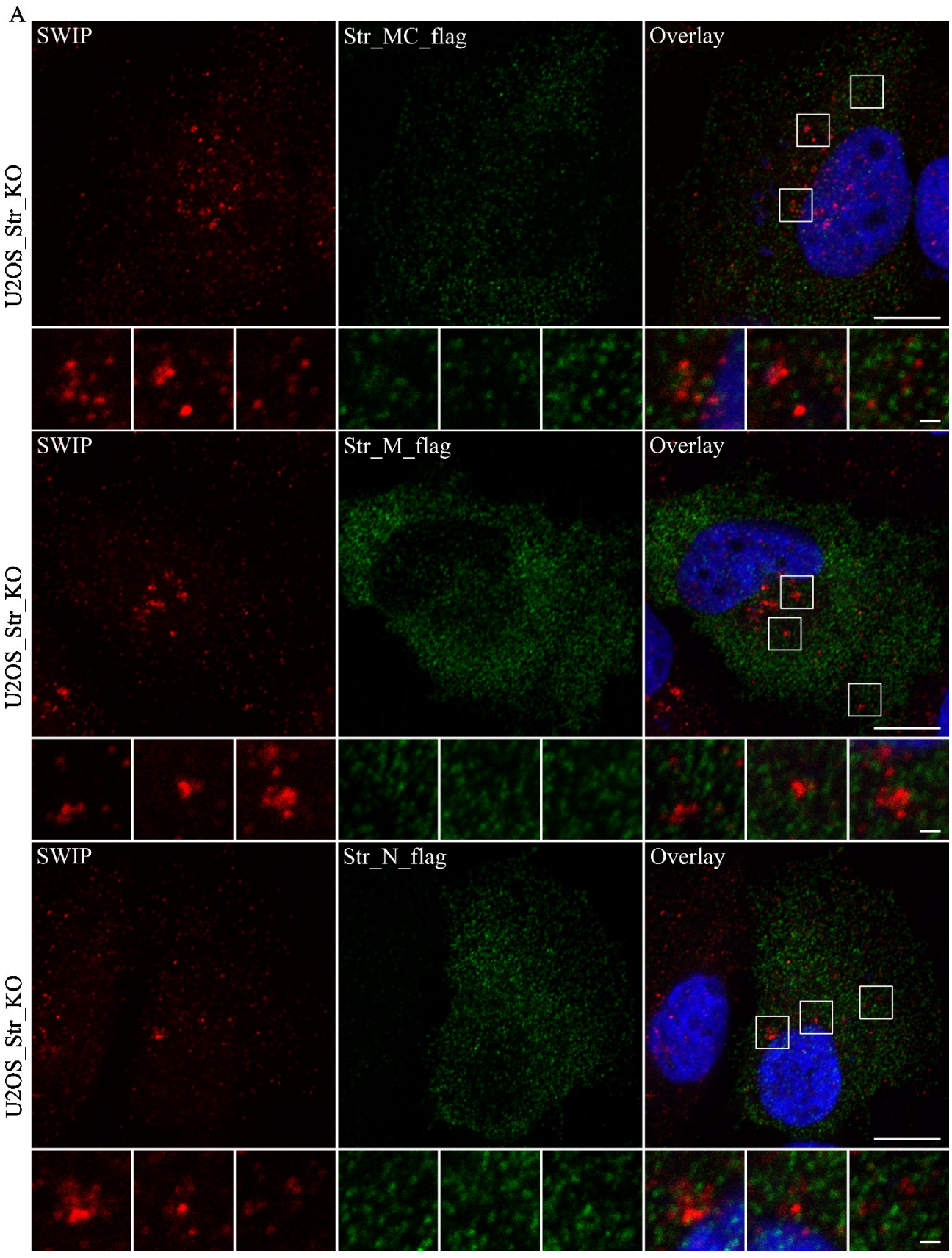

Supplementary figure 4 – Expression of Str_F/NM/MC/M/N_myc fragments in the U2OS_Str_KO cell line, stained with the antibodies against the flag tag and endogenous SWIP (**A**), the rest of the fragments is presented in the **Figure S4B**. VPS35 positive subdomains of the early endosomes are zoomed in the insets. Images were acquired using confocal microscope Zeiss LSM800. Image scale bar: 10 µm. Inset scale bar: 1 µm.

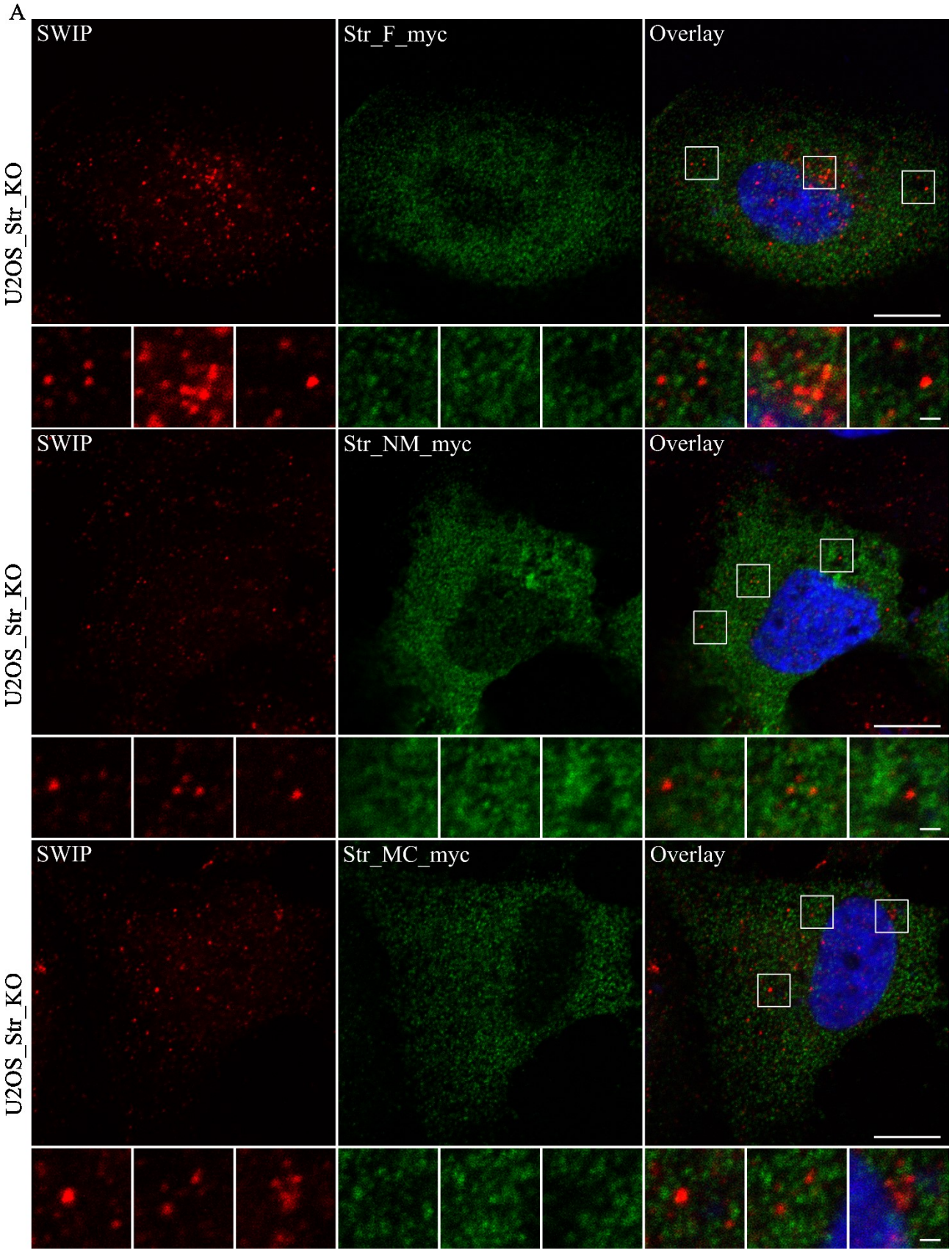

Supplementary figure 4 – Second part (**B**), for legend see previous page.

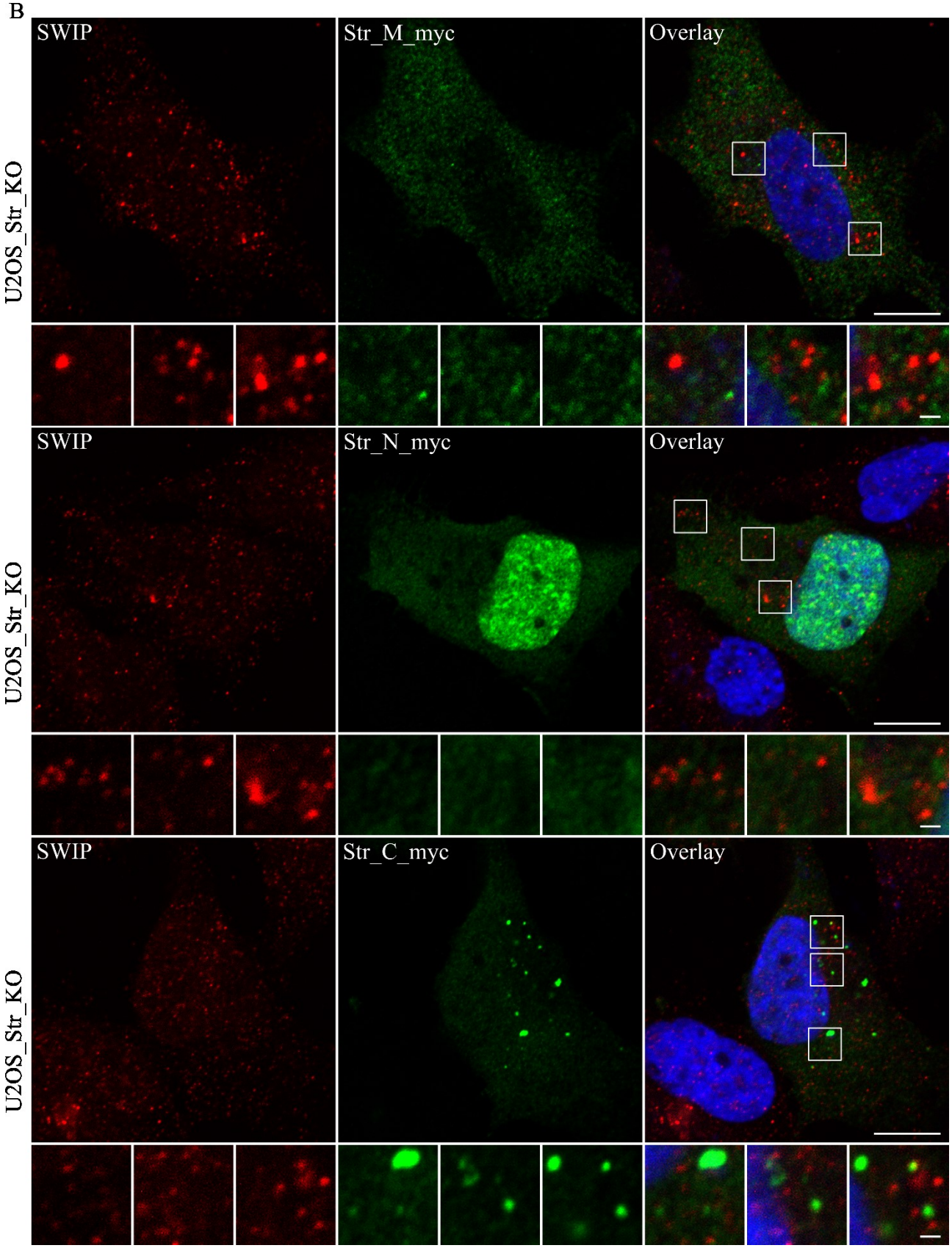

Supplementary figure 5 – Verification of the results observed on the western-blot with the immunofluorescence staining. Amount of FAM21 seems altered upon strumpellin KO. U2OS_wt and U2OS_Str_KO cells were stained using the antibody against endogenous SWIP and VPS35. VPS35 positive subdomains of the early endosomes are zoomed in the insets. (**A**). Image scale bar: 10 µm; inset scale bar: 1 µm. Images were acquired using confocal microscope Zeiss LSM800.

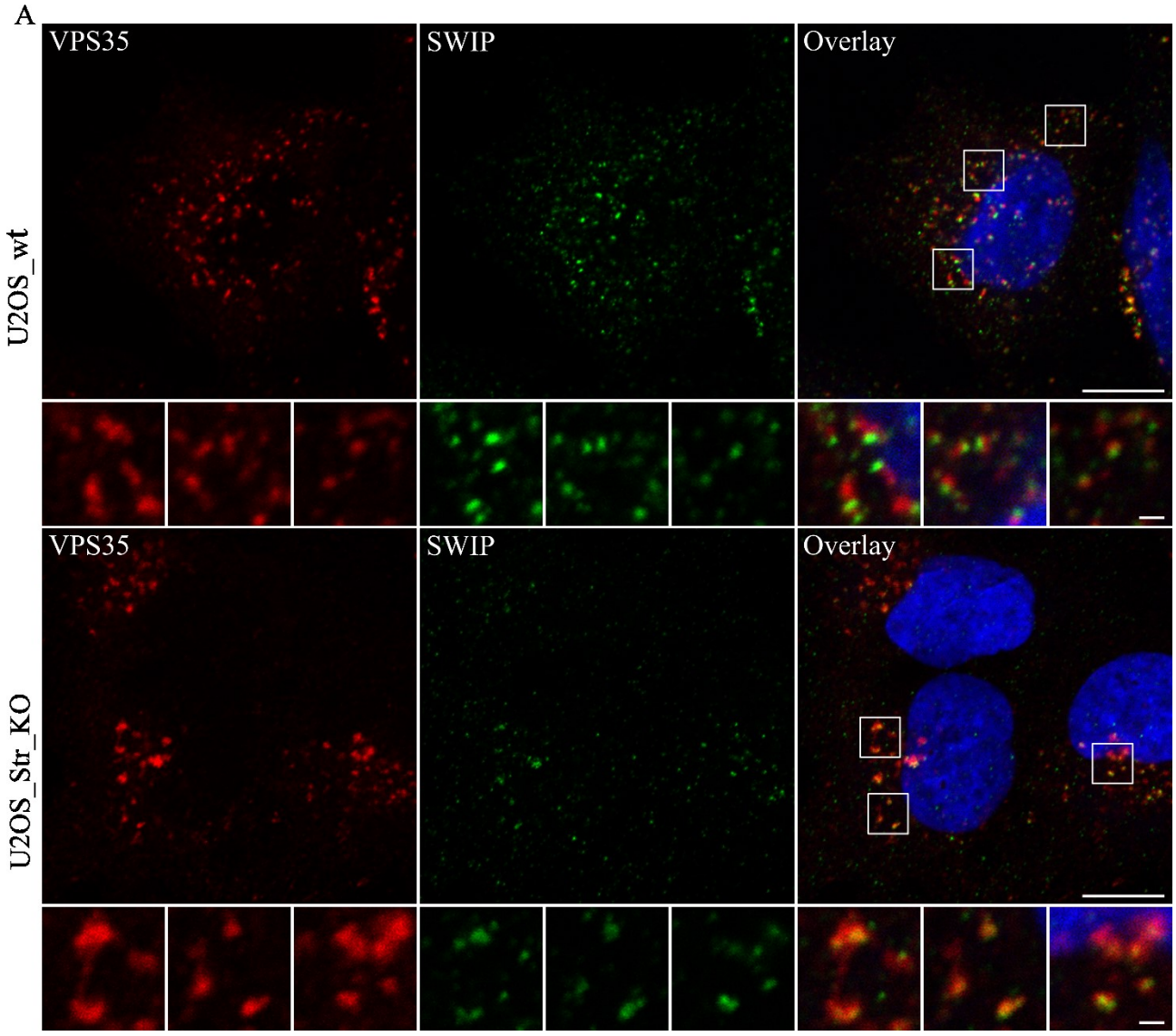

Supplementary figure 6 – Visualization of VPS35 positive subdomains (particle) area counting procedure. MDA_Str_KO and MDA_wt cells were stained with the antibody against endogenous VPS35. Images were deconvolved, and maximum intensity projection from z-stack (33 planes) was used for further particle and nuclei counting (**A**). Automatic threshold "Otsu dark" was set and "Analyze particle" function of Fiji software automatically distinguished and counted VPS35 positive particles. The representation of this procedure is depicted here (**B**). Image scale bar = 10 µm. Images were acquired using inverted fluorescence microscope Cell-R.

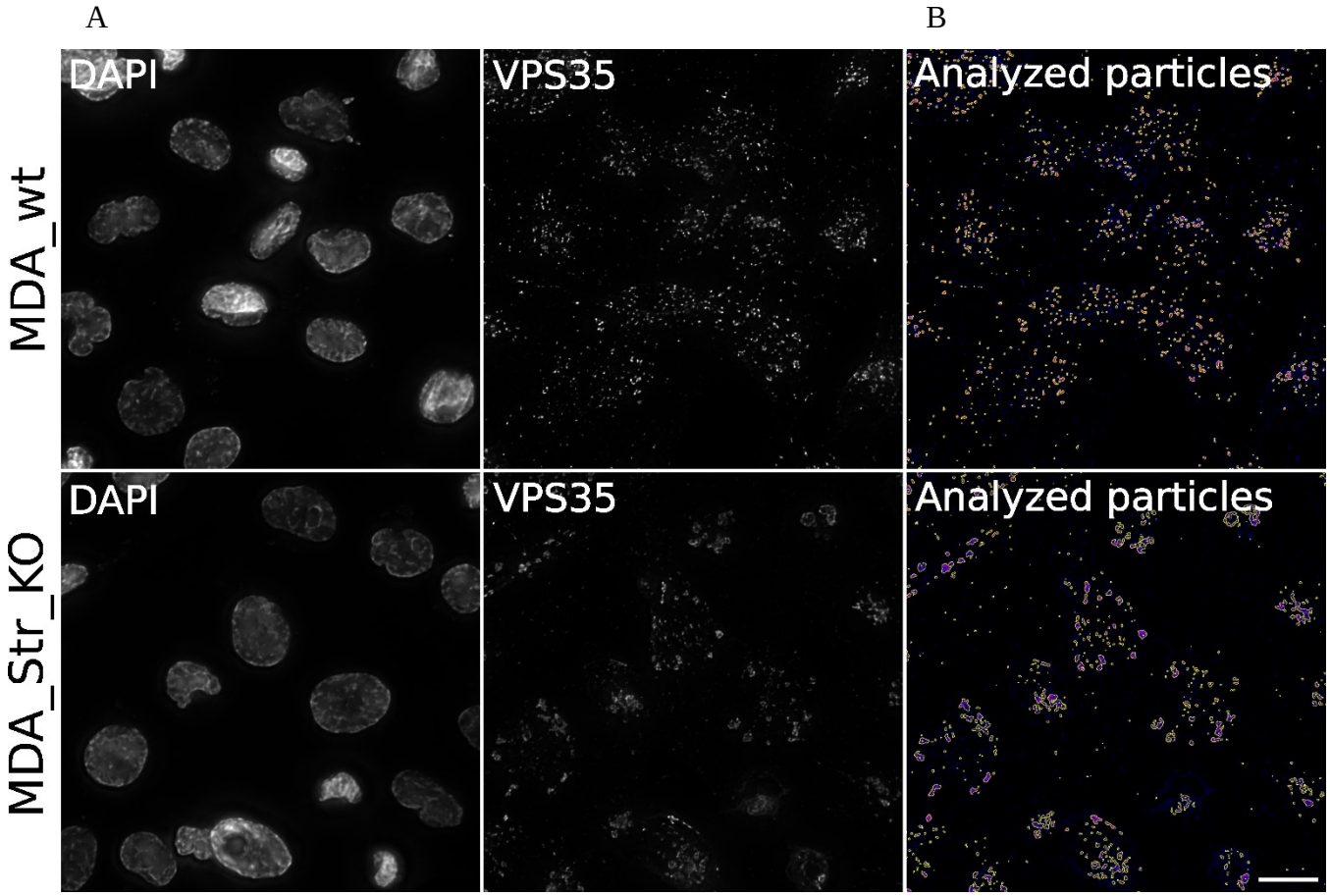

Supplementary figure 7 – Strumpellin KO affects actin patches formation. MDA_wt and MDA_Str_KO cells were stained with the fluorescently labelled phalloidin488 and with the antibody against endogenous EEA1. EEA1 positive subdomains of the early endosomes are zoomed in the insets (**A**). Image scale bar: 10 µm. Inset scale bar: 1 µm. Images were acquired using confocal microscope Leica SP2.

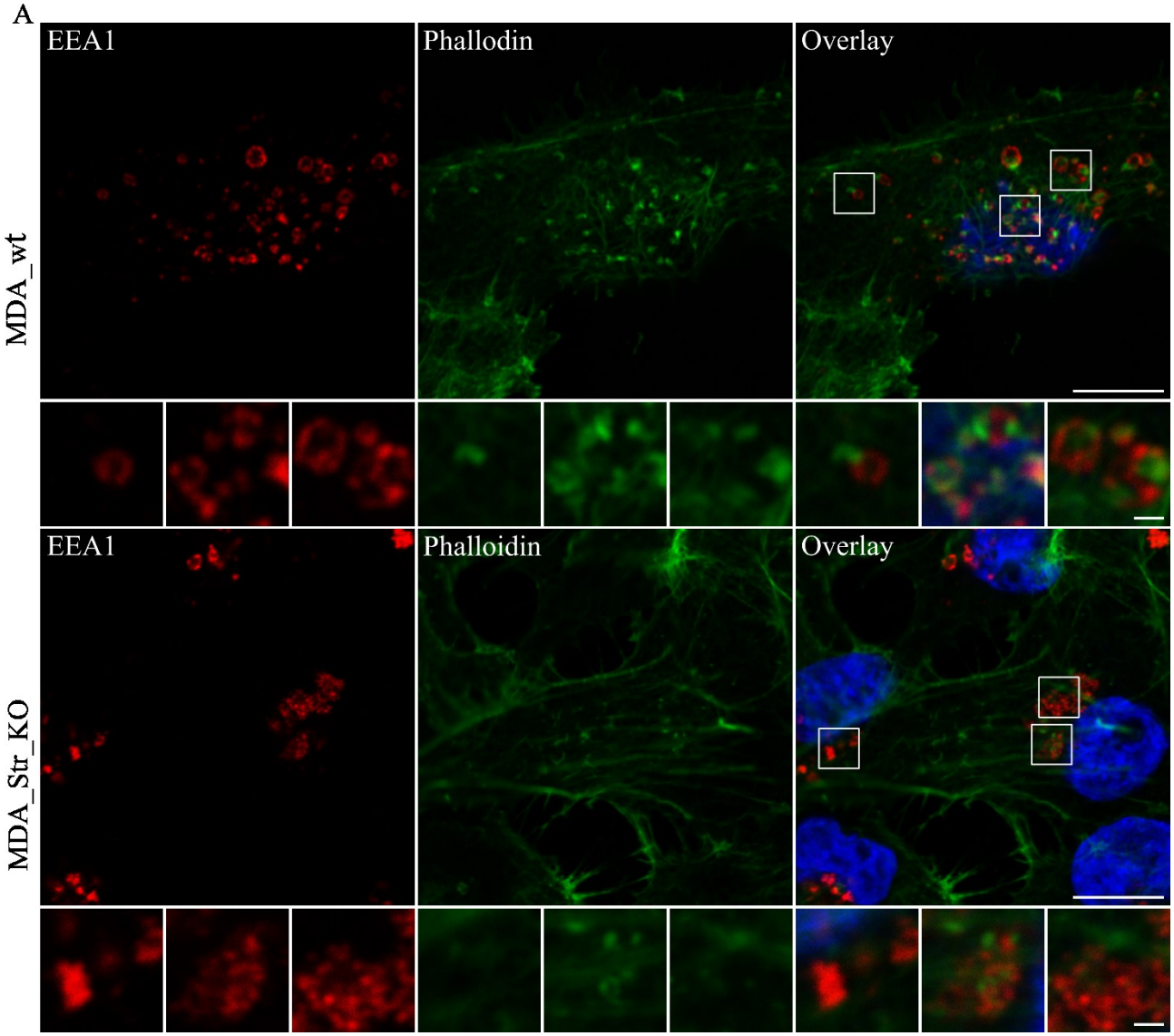

Supplementary figure 8 – Morphology of VPS35 positive subdomains is rescued in cells stably expressing GFP_strumpellin. U2OS_wt, U2OS_Str_KO cells were stained with the antibody against endogenous strumpellin and VPS35. U2OS_Str_KO_rescue cells were stained with the antibody against endogenous VPS35. Strumpellin/VPS35 positive subdomains of the early endosomes are zoomed in the insets (**A**). Image scale bar: 10 µm. Inset scale bar: 1 µm. Images were acquired using confocal microscope Zeiss LSM800.

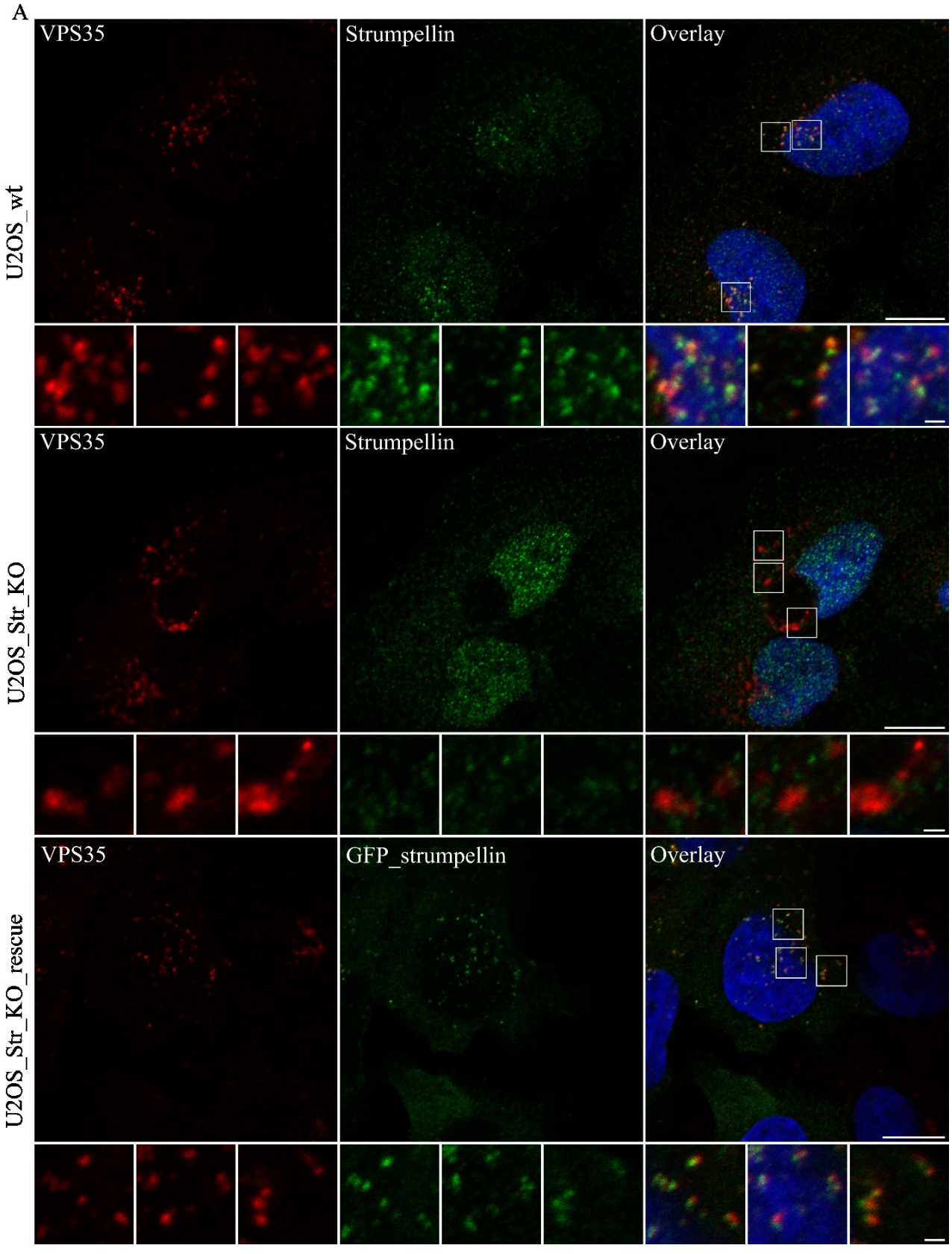

Supplementary figure 9 – GLUT1 is accumulated in the perinuclear region in strumpellin KO. MDA_wt and MDA_Str_KO cells were stained with the antibody against endogenous VPS35 and GLUT1. VPS35 positive subdomains of the early endosomes are zoomed in the insets (**A**). Image scale bar: 10 µm. Inset scale bar: 1 µm. Images were acquired using confocal microscope Leica SP2.

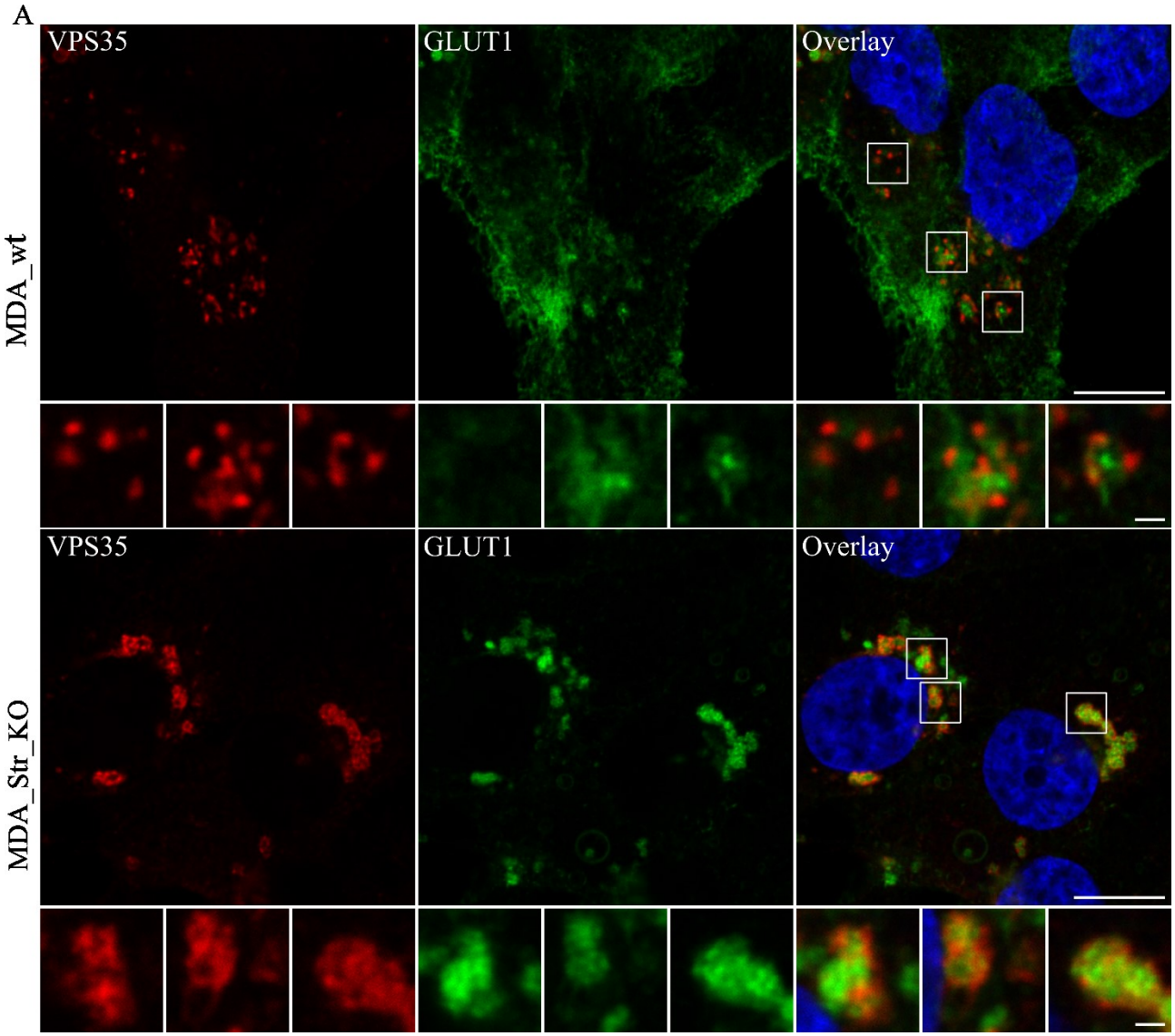

Supplementary figure 10 – TfR is accumulated in the early endosomes upon strumpellin KO. MDA_wt and MDA_Str_KO cells were fixed and stained with the antibody against endogenous SWIP and TfR. TfR positive subdomains of the early endosomes are zoomed in the insets (**A**). Image scale bar: 10 µm. Inset scale bar: 1 µm. Images were acquired using confocal microscope Leica SP2.